MODIFICATION OF POLYPROPYLENE BY FREE RADICAL GRAFTING

by
Gülizar Kaya
B.S., Chemistry, Boğaziçi University, 2018

Submitted to the Institute for Graduate Studies in
Science and Engineering in partial fulfillment of
the requirements for the degree of
Master of Science

Graduate Program in Chemistry
Boğaziçi University
2021

Dedicated to my family

ACKNOWLEDGEMENTS

First of all, I would like to thank my supervisor Assoc. Prof. A. Ersin Acar for giving me the opportunity to be part of his research group and work on this project. It is a pleasure to express my sincere gratitude to him for his academic guidance, encouragement and wise advices throughout my master's studies.

I would like to thank my committee members Prof. Duygu Avcı Semiz and Assoc. Prof. Uğur Ünal for allocating their precious time and reviewing my thesis.

Also, I would like to thank all Acar Lab members for providing friendly and delightful environment. I am grateful to Ayşenur, Ayşe Zeyneb, Banu, Göknil, Halenur, Işıl, Melike, Refia, Sedef and Şule for sharing knowledge and experiences, and for the good time we spent together. Especially, I would like to express my immense gratitude to Işıl for her help and guidance. I am also thankful to Ferid and Fatma for their help and friendship. I feel blissful to work with and meet these amazing people.

I would like to thank my dear friend Gonca for her encouragement and trust in me. Also, I am profoundly grateful to Kenzo for his endless support and love.

As a recipient of 2210/E National MSc/MA Scholarship for Former Undergraduate Students, I am very thankful to TÜBİTAK for providing financial assistance during my graduate education.

Lastly, I owe a deep debt of gratitude to my family for their love and support. Particularly, I would like to thank my mother Aysel and my brother Kurtuluş for their encouragement during my education. This thesis study would not have been accomplished without them.

ABSTRACT

MODIFICATION OF POLYPROPYLENE BY FREE RADICAL GRAFTING

Polypropylene (PP) market forms the second largest polymer business worldwide owing to its good mechanical properties, excellent chemical resistance and low-cost production. These attractive properties of PP are mainly dependent on its stereospecificity. Isotactic polypropylene (iPP), which can be produced by Ziegler-Natta catalysts with high isotacticity indices, has a commercial significance. However, atactic polypropylene (aPP) which has a lack of order is produced as a byproduct during iPP manufacturing. In general, aPP obtained as a byproduct has a low molecular weight, and it is essentially amorphous. Since aPP has low thermal stability and poor mechanical properties, it is considered an industrial waste, and application fields are limited. In this study, aPP was modified by free radical grafting technique to obtain value-added material from this industrial waste. Free radical grafting of functional monomers onto polyolefins is a widely practiced method for modification of polyolefins. The functionalization of polyolefins can improve their compatibility with engineering polymers. In this way, the incorporation of modified polyolefins into polymer blends and composites can be achieved. However, during free radical grafting, the desired grafting reaction competes against side reactions including homopolymerization of the monomer, chain scission and crosslinking. Within the scope of this study, grafting reactions of maleic anhydride and its derivative onto aPP were carried out in both solution and melt. The effect of reaction parameters and conditions on grafting yield and its effect on final polymer properties were investigated.

ÖZET

POLİPROPİLENİN SERBEST RADİKALER AŞILAMA YÖNTEMİ İLE MODİFİKASYONU

Polipropilen (PP) pazarı, iyi mekanik özellikleri, mükemmel kimyasal direnci ve düşük maliyetli üretimi sayesinde dünya çapında ikinci en büyük polimer işini oluşturmaktadır. Polipropilenin cazip özellikleri temel olarak onun sterospesifikliğine bağlıdır. Ziegler-Natta katalizörleri ile yüksek izotaktisite indeksleri ile üretilebilen izotaktik polipropilen (iPP), ticari bir öneme sahiptir. Ancak iPP üretimi sırasında yan ürün olarak düzensiz yapıdaki ataktik polipropilen (aPP) üretilir. Yan ürün olarak elde edilen aPP, genellikle düşük moleküler ağırlığa sahiptir ve büyük ölçüde amorftur. aPP'nin düşük termal kararlılığa ve zayıf mekanik özelliklere sahip olması onun endüstriyel atık olarak görülmesine neden olmaktadır ve uygulama alanları oldukça sınırlıdır. Bu çalışma kapsamında, bu endüstriyel atığı katma değerli bir ürüne dönüştürmek için aPP serbest radikaler aşılama yöntemi ile modifiye edilmiştir. Poliolefinler üzerine fonksiyonel monomerlerin serbest radikaler aşılama yöntemi ile eklenmesi, poliolefinlerin modifikasyonu için yaygın olarak uygulanan bir yöntemdir. Poliolefinlerin fonksiyonelleştirilmesi onların mühendislik polimerleriyle uyumluluklarını iyileştirebilir. Böylece, modifiye edilmiş poliolefinlerin polimer karışımlarına ve kompozitlerine katılımları sağlanabilir. Bununla birlikte, serbest radikal aşılama sırasında, amaçlanan aşılama reaksiyonu, zincir kırılımı, çapraz bağlanma ve monomerin homopolimerizasyonu gibi yan reaksiyonlar ile yarışmaktadır. Bu çalışma kapsamında, maleik anhidritin ve bir türevinin aPP üzerine aşılama reaksiyonları gerçekleştirilmiştir. Reaksiyon parametrelerinin ve koşullarının aşılama verimine etkisi ve nihai polimer özelliklerine etkisi araştırılmıştır.

TABLE OF CONTENTS

ACKNOWLEDGEMENTS iii

ABSTRACT iv

ÖZET v

LIST OF FIGURES ix

LIST OF TABLES xiv

LIST OF ACRONYMS/ABBREVIATIONS xv

1. INTRODUCTION 1

1.1. Polypropylene at a Glance 1

1.2. Polypropylene Structures and Analyses 2

1.3. Industrial Polymerization of Propylene 7

1.3.1. Polypropylene Copolymers 10

1.4. Atactic Polypropylene 11

1.5. Post-Reactor Modifications of Polypropylene 12

1.5.1. Free Radical Grafting of Monomers onto Polypropylene 13

1.5.1.1. The Significance of Peroxides in Free Radical Grafting 15

1.5.1.2. The Significance of Polyolefin Structure in Free Radical Graffting 17

1.5.1.3. The Significance of Reaction Conditions in Free Radical Grafting 20

1.5.1.4. Applications of PP-based Graft Copolymers.....22

2. AIM OF THE STUDY.....24

3. EXPERIMENTAL.....25

3.1. Synthesis.....25

3.1.1. Free Radical Grafting of MAH onto aPP in Solution.....25

3.1.2. Free Radical Grafting in Melt.....28

3.1.2.1. Maleic Anhydride Grafting onto aPP in Melt.....28

3.1.2.2. Modified MAH Grafting onto aPP in Melt.....29

3.2. Analysis.....32

3.2.1. FTIR Analysis.....32

3.2.2. DSC Analysis.....32

3.2.3. Volumetric Titration.....33

3.2.4. NMR Analysis.....34

4. RESULTS AND DISCUSSION.....35

4.1. Analyses of Pristine Atactic Polypropylene Used in the Thesis.....36

4.2. Free Radical Grafting of MAH onto aPP in Solution.....40

4.2.1. Control Experiments in Solution.....40

4.2.2. Maleic Anhydride Grafting Experiments in Solution.....45

4.3. Free Radical Grafting of MAH onto aPP in Melt.....50

4.4. Free Radical Grafting of mMAH onto aPP in Melt.....53

4.4.1. Control Experiments for mMAH Grafting in Melt.....54

4.4.2. Effect of Time on mMAH Grafting in Melt 58

4.4.3. Effect of Initiator Concentration on mMAH Grafting in Melt 59

4.4.4. Effect of mMAH concentration on mMAH Grafting in Melt 61

5. CONCLUSION 63

REFERENCES 65

APPENDIX A: SPECTROSCOPY DATA 69

LIST OF FIGURES

Figure 1.1. Polymerization of propene. 1

Figure 1.2. The structures of a) linear PP and b) branched PP. 2

Figure 1.3. a) Regioregular and b) regioirregular insertions of propylene [5]. 2

Figure 1.4. Saw horse (top) and modified Fisher projections (bottom) of a) m-diad and b) r-diad [1]. 3

Figure 1.5. Stereostructures of PP. 4

Figure 1.6. Change in specific volume during glass transition and melting of amorphous, semicrystalline and crystalline polymers [4]. 5

Figure 1.7. The mechanism of oxidative degradation of PP [7]. 7

Figure 1.8. Mechanism of ethylene polymerization with ZN catalysts [9]. 9

Figure 1.9. The scheme of free radical grafting onto a polymer backbone [12]. 14

Figure 1.10. The states of homogeneity during melt free radical grafting: a) microfluid, b) partially segregated fluid, c) macrofluid [12]. 21

Figure 3.1. Hydrolysis of grafted MAH in titration conditions. 34

Figure 4.1. Possible free radical grafting mechanism and competing side reactions. 35

Figure 4.2. FTIR spectra of pristine aPP (top) and xylene insoluble fraction of aPP (bottom). 37

Figure 4.3. ^{1}H-NMR spectrum of aPP used in the study in toluene-d_8. 38

Figure 4.4. ^{13}C-NMR spectrum of aPP used in the study in toluene-d_8. 39

Figure 4.5. ^{1}H- NMR spectrum of acetone washed, xylene soluble aPP in toluene-d_8 39

Figure 4.6. FTIR spectra of pristine aPP (top), Blank_aPP (middle) and Blank_aPP+BPO (bottom). 41

Figure 4.7. FTIR spectrum of MAH. 42

Figure 4.8. FTIR spectra of Blank_aPP+MAH (top), its ethanol wash (middle) and Blank_aPP (bottom). 43

Figure 4.9. Mono-ester formation from MAH during the precipitation into ethanol. 43

Figure 4.10. FTIR spectra of Blank_MAH+BPO (top) and its aged sample (bottom). 44

Figure 4.11. FTIR spectra of ethanol precipitate of BIG_0.70/0.037 (top) and its ethanol wash (bottom). 46

Figure 4.12. Possible structures of MAH grafted onto aPP. 47

Figure 4.13. FTIR spectrum of commercial PP-g-MAH. 47

Figure 4.14. FTIR spectra of BIG_0.70/0.037 ethanol filtrate and Blank_MAH+BPO aged form. 48

Figure 4.15. Mechanism of BPO decomposition. 52

Figure 4.16. FTIR spectra of ethanol precipitate (top), ethanol filtrate (middle) of MAG_10/0.5 and itself (bottom). 53

Figure 4.17. Reactive locations of MAH. 54

Figure 4.18. FTIR spectra of purified (top) and unpurified (bottom) Blank_ aPP_T_1. 54

Figure 4.19. FTIR spectra of purified (top) and unpurified (bottom) samples of Blank_DCP_T_1 56

Figure 4.20. FTIR spectra of purified (top) and unpurified (bottom) samples of Blank_mMAH_T_1. 57

Figure 4.21. FTIR spectra of MEG_10/3_t_0+60_T_1 (top), MEG_10/3_t_0+30_T_1 (middle), MEG_10/3_t_0+_T_1 (bottom). 58

Figure 4.22. FTIR spectra of MEG_10/3_t_0+60_T_1+5 (top), MEG_10/3_t_0+30_T_1+5 (middle), MEG_10/3_t_0+10_T_1+5 (bottom). 59

Figure 4.23. FTIR spectra of MEG_10/5_t_0+30_T_1 (top), MEG_10/3_t_0+30_T_1 (middle), MEG_10/1_t_0+30_T_1 (bottom). 60

Figure 4.24. FTIR spectra of MEG_10/5_t_0+30_T_1+5 (top), MEG_10/3_t_0+30_T_1+5 (middle), MEG_10/1_t_0+30_T_1+5 (bottom). 61

Figure 4.25. FTIR spectra of MEG_5/3_t_0+30_T_1 (top), MEG_10/3_t_0+30_T_1 (middle), MEG_15/3_t_0+30_T_1 (bottom). 62

Figure 4.26. FTIR spectra of MEG_5/1_t_0+30_T_1+5 (top), MEG_10/1_t_0+30_T_1+5 (middle), MEG_15/1_t_0+30_T_1+5 (bottom). 62

Figure A.1. FTIR spectra of 1st batch (top) and 2nd batch of pristine aPP. 69

Figure A.2. FTIR spectrum of BPO. 69

Figure A.3. FTIR spectra of EtOH washes of BIG_0.30/0.037 (top), BIG_0.50/0.037 (middle), BIG_0.90/0.037 (bottom). 70

Figure A.4. FTIR spectra of EtOH filtrates of BIG_0.30/0.037 (top), BIG_0.50/0.037 (middle), BIG_0.90/0.037 (bottom). 70

Figure A.5. FTIR spectra of EtOH washes of BIG_0.30/0.075 (pale green), BIG_0.49/0.074 (pink), BIG_0.70/0.075 (blue), BIG_0.90/0.075 (red). 71

Figure A.6. FTIR spectra of EtOH filtrates of BIG_0.30/0.075 (pale green), BIG_0.49/0.074 (dark green), BIG_0.70/0.075 (blue), BIG_0.90/0.075 (red). 71

Figure A.7. FTIR spectrum of DCP. 72

Figure A.8. FTIR spectra of purified MAG_10/1 (red), MAG_10/2 (blue), MAG_10/3 (yellow), MAG_20/1 (purple). 72

Figure A.9. FTIR spectra of filtrates of MAG reactions. 73

Figure A.10. FTIR spectra of purified (top) and unpurified (bottom) Blank_aPP_T_1+5. ..73

Figure A.11. FTIR spectra of purified (top) and unpurified (bottom) Blank_DCP_T_1+5..74

Figure A.12. FTIR spectra of MEG_10/3_45_T_1 (top) and MEG_10/3_20_T_1 (bottom)..74

Figure A.13. FTIR spectra of MEG_5/5_30_T_1 (top) and MEG_5/1_30_T_1 (bottom).....75

Figure A.14. FTIR spectra of MEG_10/5_60_T_1 (top) and MEG_10/5_45_T_1 (bottom)...75

Figure A.15. FTIR spectra of MEG_15/5_30_T_1 (top) and MEG_15/1_30_T_1 (bottom)..76

Figure A.16. FTIR spectra of MEG_5/5_30_T_1+5 (top) and MEG_5/3_30_T_1+5 (bottom). 76

Figure A.17. FTIR spectra of MEG_10/3_45_T_1+5 (top) and MEG_10/3_20_T_1+5 (bottom). 77

Figure A.18. FTIR spectra of MEG_15/5_30_T_1+5 (top) and MEG_15/3_30_T_1+5 (bottom). 77

Figure A.19. DSC thermogram of pristine aPP used in the study.....78

Figure A.20. DSC thermogram of Blank_aPP. 78

Figure A.21. DSC thermogram of Blank_aPP+BPO. 79

Figure A.22. DSC thermogram of Blank_aPP+MAH. 79

Figure A.23. DSC thermogram of BIG_0.30/0.037_EtOH_wash. 80

Figure A.24. DSC thermogram of BIG_0.50/0.037_EtOH_wash. 80

Figure A.25. DSC thermogram of BIG_0.70/0.037_EtOH_wash. 81

Figure A.26. DSC thermogram of BIG_0.90/0.037_EtOH_wash. 81

Figure A.27. DSC thermogram of BIG_0.30/0.075_EtOH_wash. 82

Figure A.28. DSC thermogram of BIG_0.49/0.074_EtOH_wash. 82

Figure A.29. DSC thermogram of BIG_0.70/0.075_EtOH_wash. 83

Figure A.30. DSC thermogram of BIG_0.90/0.075_EtOH_wash. 83

Figure A.31. DSC thermogram of aPP_2nd batch..... 84

Figure A.32. DSC thermogram of purified Blank_aPP_T_1..... 84

Figure A.33. DSC thermogram of purified Blank_DCP_T_1. 85

Figure A.34. DSC thermogram of purified Blank_aPP_T_1+5. 85

Figure A.35. DSC thermogram of purified Blank_DCP_T_1+5. 86

Figure A.36. DSC thermogram of purified Blank_mMAH_T_1. 86

LIST OF TABLES

Table 1.1. Properties of various catalyst generations [5]. 8

Table 1.2. Features of byproduct aPP and synthesized aPP [7]. 11

Table 1.3. Reactivities of radical-monomer combinations with respect to the homopropagation of the radical [12]. 19

Table 3.1. Varying amounts of reactants for control and grafting reactions in solution. 26

Table 3.2. Varying amounts of reactants for grafting reactions in melt. 29

Table 3.3. Reaction conditions to graft mMAH onto aPP in melt. 31

Table 4.1. Thermal properties of aPP used in the study. 36

Table 4.2. Thermal transition values of purified control samples. 41

Table 4.3. Grafted MAH amounts in purified samples determined by hot titration method. 46

Table 4.4. Thermal properties of purified samples determined by DSC. 50

Table 4.5. Details of melt reactions and grafted MAH amounts determined by hot titration..... 52

Table 4.6. Thermal properties of purified control samples. 55

LIST OF ACRONYMS/ABBREVIATIONS

aPP	Atactic polypropylene
BPO	Benzoyl peroxide
DEAC	Diethylaluminum chloride
DSC	Differential scanning calorimetry
DCP	Dicumyl peroxide
EPDM	Ethylene-propylene-diene monomer
EPM	Ethylene-propylene monomer rubber
EPR	Ethylene-propylene rubber
EtOH	Ethanol
EVOH	Ethylene/vinyl alcohol copolymer
FRR	Flow rate ratio
FTIR	Fourier-transform infrared spectroscopy
GMA	Glycidyl methacrylate
GPC	Gel permeation chromatography
HBDE	Hydrogen bond dissociation energy
HDPE	High-density polyethylene
iPP	Isotactic polypropylene
IR	Infrared

LDPE	Low-density polyethylene
m	Meso
MAH	Maleic anhydride
MAO	Methylaluminoxane
MeOH	Methanol
MFR	Melt Flow Rate
mMAH	Modified maleic anhydride
MWD	Molecular weight distribution
NMR	Nuclear magnetic resonance spectroscopy
PE	Polyethylene
PP-g-MAH	Maleic anhydride grafted polypropylene
phr	Parts per hundred resin
PP	Polypropylene
ppt	Precipitate
PTFE	Polytetrafluoroethylene
r	Racemo
sPP	Syndiotactic polypropylene
TEA	Triethylamine
T_m	Crystalline melting temperature
T_g	Glass transition temperature
T_c	Crystallization temperature, or ceiling temperature

UV	Ultraviolet
ZN	Ziegler-Natta
ΔE	Activation energy
ΔH_p	Enthalpy of polymerization
ΔS_p	Entropy of polymerization
k	Rate constant
k_0	Pre-exponential factor
R	Gas constant
$t_{1/2}$	Half-life

1. INTRODUCTION

1.1. Polypropylene at a Glance

Polypropylene, henceforward called PP, is a commodity thermoplastic manufactured in the second largest quantity in the world and makes up about 25 % of global polymer demand. The combination of low cost production and outstanding chemical and mechanical properties explains the popularity of PP. It is commercially available as homopolymer and copolymer, and homopolymer surpassed the market with 83.3 % share of the global revenue in 2019. It is mainly used in packaging, automotive, healthcare, construction, electronics and textile [1], [2].

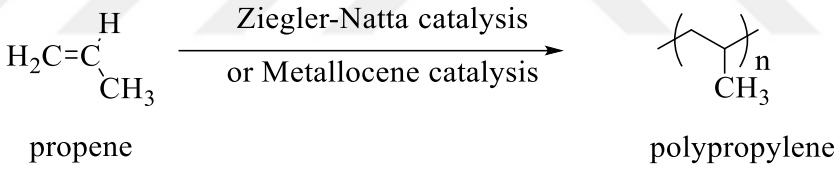


Figure 1.1. Polymerization of propene.

Polypropylene as a member of polyolefins is produced by the polymerization of propylene, also called propene, *via* chain-growth mechanism in the presence of Ziegler-Natta catalysts or metallocene catalysts (Figure 1.1). Since PP is a prochiral molecule, the repeating unit of PP contains a stereogenic carbon. Isotactic polypropylene (iPP) is commercially important kind of PP, which has high stereoregularity. It is a semicrystalline polymer with high temperature stability, high tensile strength, optical clarity and flexibility. Owing to its semicrystalline morphology iPP can be molded. Also, PP has excellent resistance to many solvents, acids, bases and moisture because of its hydrocarbon nature.

1.2. Polypropylene Structures and Analyses

Polymer characteristics are not only governed by the chemical structure of polymers but also by polymer morphology. The term of polymer morphology expresses crystallinity and its extend, orientation, distribution and shape of the crystallites [1]. Crystallinity of polymers differs from that of small molecules since a small segments of the polymeric chain can attain a three-dimensional order when a polymer crystallizes from its melt [3] . Polymers can possess different morphologies ranging from completely amorphous to highly crystalline. Complete crystallinity is seldomly seen in polymers. Polymers which are partially crystalline are referred as semicrystalline. The degree of crystallinity is controlled by the magnitude of the secondary attractive forces between chains, the structural regularity of the chains, compactness and the degree of flexibility [3], [4].

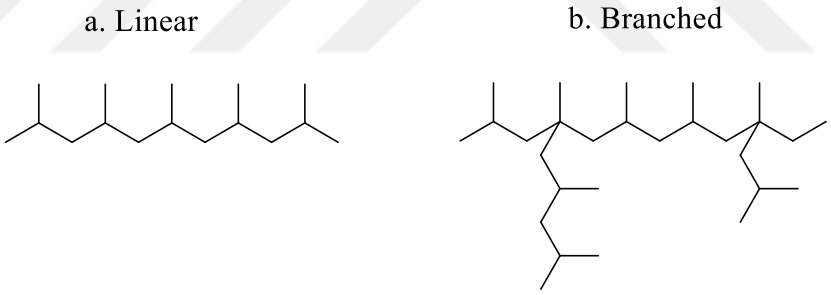


Figure 1.2. The structures of a) linear PP and b) branched PP.

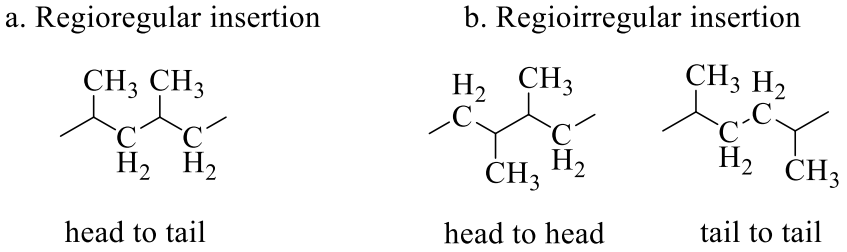


Figure 1.3. a) Regioregular and b) regioirregular insertions of propylene [5].

Even though the magnitude of secondary forces is relatively small in polyolefins due to the absence of dipole interactions, the structural regularity of polymer chains assists the progress of crystallization. In case of polyethylene, the linearity of the polymer chains is the only criterion that must be fulfilled for higher crystallinity since ethylene monomer is symmetrical. Contrarily, polymerization of the unsymmetrical monosubstituted ethylene, CH2=CHR (where R is any group different from H), brings about a polymer chain with stereogenic tertiary carbon atoms [4]. Unlike PE, the stereoregularity of polymer chains is required, together with the structural regularity, to obtain crystalline PP. As long as propene monomer is added at growing polymer chain end and not the backbone to form branches, linear PP can be attained. In Figure 1.2, the structures of linear PP and branched PP are shown. Furthermore, monomer addition must be head-to-tail to ensure the structural regularity. Resultant structures of regioregular and regioirregular insertions are shown in Figure 1.3. Two propene insertions with the same enantioface bear a sequence with the same configuration of the stereogenic carbons, while the insertions of alternate enantiofaces bear a sequence with opposite configurations. This is said to formation of steric diad which can be labelled as *meso* (m) or *racemo* (r), respectively (Figure 1.4) [1]. The term of tacticity is used to define the arrangement of stereogenic centers in macromolecules. Polypropylene chain with a succession of m diads is called isotactic PP (iPP), whereas PP chain with a succession of r diads is called syndiotactic PP (sPP). The absence of configurational order brings about atactic PP (aPP), and the lack of linearity and regiospecificity would result in atactic PP [6]. On the other hand, hemiisotactic PP (hPP) has a partial order with the same configuration of even monomeric units and random configuration of all odd monomeric units (Figure 1.5). Although real PP microstructures are more complex, the recommended nomenclature reflects the prevailing features of real macromolecules [1].

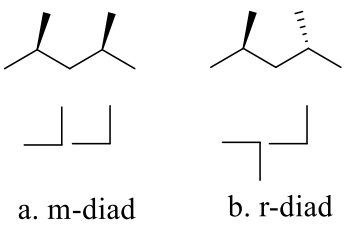


Figure 1.4. Saw horse (top) and modified Fisher projections (bottom) of a) m-diad and b) r-diad [1].

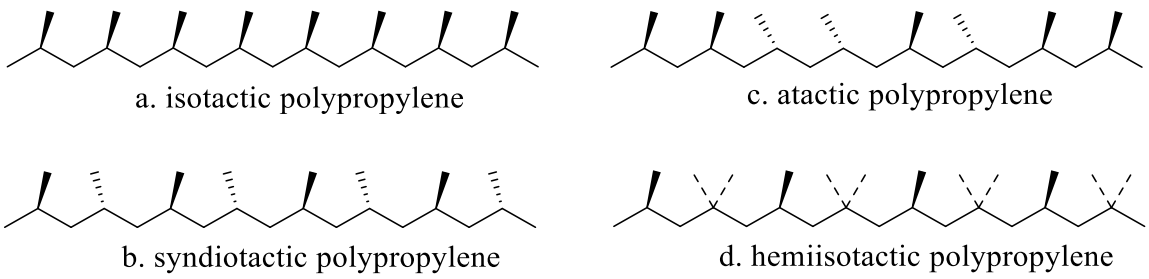


Figure 1.5. Stereostructures of PP.

Stereoregularity of PP is ascertained by microstructural measurements and physical measurements. ^{13}C-NMR spectroscopy is a powerful technique for microtacticity analysis of PP. In ^{13}C-NMR spectrum, the intense peak at δ=21.84 ppm corresponding to mmmm pentad configuration infers highly isotactic PP homopolymer [7]. Apart from ^{13}C-NMR analysis, infrared (IR) and Raman spectroscopy can be used to investigate the configuration, tacticity and conformation of polymer chains as complementary techniques. The calibration of absorption bands based on ^{13}C-NMR permits them using for fast quantitative analysis. The formation of regular isotactic helices is confirmed by the presence of IR bands at 1168, 998, 973 and 841 cm^{-1}. The peaks at 998 and 841 cm^{-1} are widely utilized to determine isotacticity [1]. On the other side, solubility difference between aPP and iPP allows determining stereoregularity by physical means. In contrast to completely atactic PP, iPP is not soluble in any organic solvent at ambient temperatures. Heptane is recommended to perform some fractionation, since it is more selective extractant than octane and xylene for aPP. The insoluble fraction in boiling heptane gives the isotacticity index of the analyzed PP [5].

Both iPP and sPP can crystallize owing to the presence of stereoregularity, and they are polymorphic polymers. Several crystallographic forms observed in iPP are monoclinic α-phase, trigonal β-phase, orthorhombic γ-phase and smectic mesophase. The monoclinic α-phase which is thermodynamically stable phase predominates under traditional industrial circumstances. Special thermal conditions or special nucleating agents are required to form β-phase [1]. In addition, most iPPs are semicrystalline because of random defects in tacticity. Attainable crystallinity in commercial iPP is commonly around 70 % [5]. Attractive properties of iPP such as stiffness, high tensile strength and lightweight arise from its

capability to crystallize. Atactic PP is usually obtained as a byproduct during the polymerization of propene to produce iPP. The amount of aPP could be between 2 and 10 wt. % depending upon the target iPP grade and the catalyst type used [7]. Physical properties of the polymer vary according to aPP content in iPP. The impact strength, clarity and ductility increase with the increasing aPP content where melting temperature, tensile strength and stiffness decrease [5].

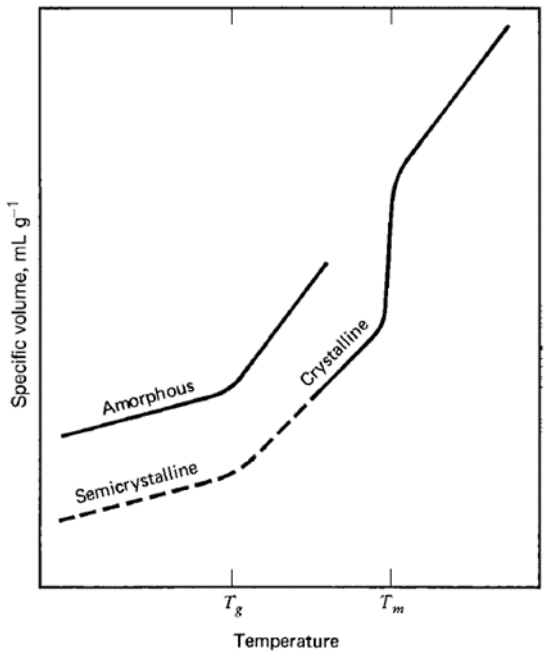


Figure 1.6. Change in specific volume during glass transition and melting of amorphous, semicrystalline and crystalline polymers [4].

Thermal transitions characterizing polymeric materials depend on polymer morphology. The melting of the crystalline domains in a polymeric material occurs at crystalline melting temperature (T_m), which is a first-order thermal transition with a discontinuous change in the specific volume. Unlike small organic molecules, melting of polymers occurs over a range, and in general, the onset temperature of melting is recorded as T_m. The glass transition temperature (T_g) identifies the temperature where the segmental motion of polymer chains starts. Upon segmental motions, the transition from brittle, stiff and glass state to rubbery state occurs [3]. In contrast to T_m, T_g is a second-order transition,

and discontinuous change in the specific volume does not take place (Figure 1.6). Fully amorphous polymers exhibit solely a T_g, while fully crystalline polymers exhibit solely a T_m. Both T_g and T_m are observed in semicrystalline polymers. Glass transition temperature and crystalline melting temperature are affected in the same manner but not in the same quantitative manner by secondary forces, molecular symmetry and chain rigidity. Molecular symmetry is more effective on T_m, secondary forces and chain flexibility are more effective on T_g. Both T_g and T_m are increased by high secondary forces owing to high polarity or hydrogen bonding. Decrease in chain mobility and increase in chain rigidity, due to the presence of bulky substituents, increase T_g and T_m. The values of T_g and T_m influence mechanical properties and service temperatures of polymers [4]. Depending on iPP grade, the melting point of iPP ranges from 100 to 180 °C [1].

The molecular weight and the molecular weight distribution (MWD/polydispersity) are other crucial factors influencing processing and product performance. The processability of PP is directly connected to melt viscosity, and melt viscosity of iPP depends on molecular weight and its distribution. Melt viscosity decreases as molecular weight decreases, and hence injection and extrusion of molten polymer become easier. Yet, melt strength of iPP may decrease upon reduction of the molecular weight. The increase in molecular weight increases the interlamellar entanglements which increases impact strength. On the other hand, crystallinity impinging on hardness can diminish with higher molecular weight. High-temperature gel permeation chromatography, colligative property, light scattering and viscometry measurements can be used to determine actual molecular weights of polymers [5]. Melt flow rate (MFR) measurement is performed industrially to determine the molecular weight of PP. The molecular weight of a polymer is inversely proportional to its melt flow rate. Melt flow rate can be measured under different loads of 21.6 kg and 2.16 kg. Flow rate ratio (FRR) as an indicator of broadness of the MWD is afforded by dividing the MFR measured at high load by the MFR at low load [5].

Polypropylene is prone to oxidative degradation induced by thermal energy and/or ultraviolet (UV) light. The oxidative degradation mechanism is shown in Figure 1.7. The rate of oxidation is slow in the beginning, but its rate increases in catalytic manner, and this process is called autooxidation. Intrinsic resistance to oxidation depends on chemical structure, physical and morphological properties of polymers. Since 3° carbon atom has the lowest bond dissociation energies for C-H, 3° C-H bond is more susceptible to attack by

molecular oxygen than 1° or 2° C-H bonds. When compared to PE, PP has lower oxidative stability. Also, oxidative stability increases with crystallinity but decreases with chain branching. Apart from temperature and UV light, mechanical stress, atmospheric pollutants and metal contaminants can accelerate the oxidative degradation process. Thermo- and photo-oxidation lead to irreversible deterioration of useful properties of PP, so antioxidants minimizing oxidative degradation are incorporated during the fabrication process [5], [7].

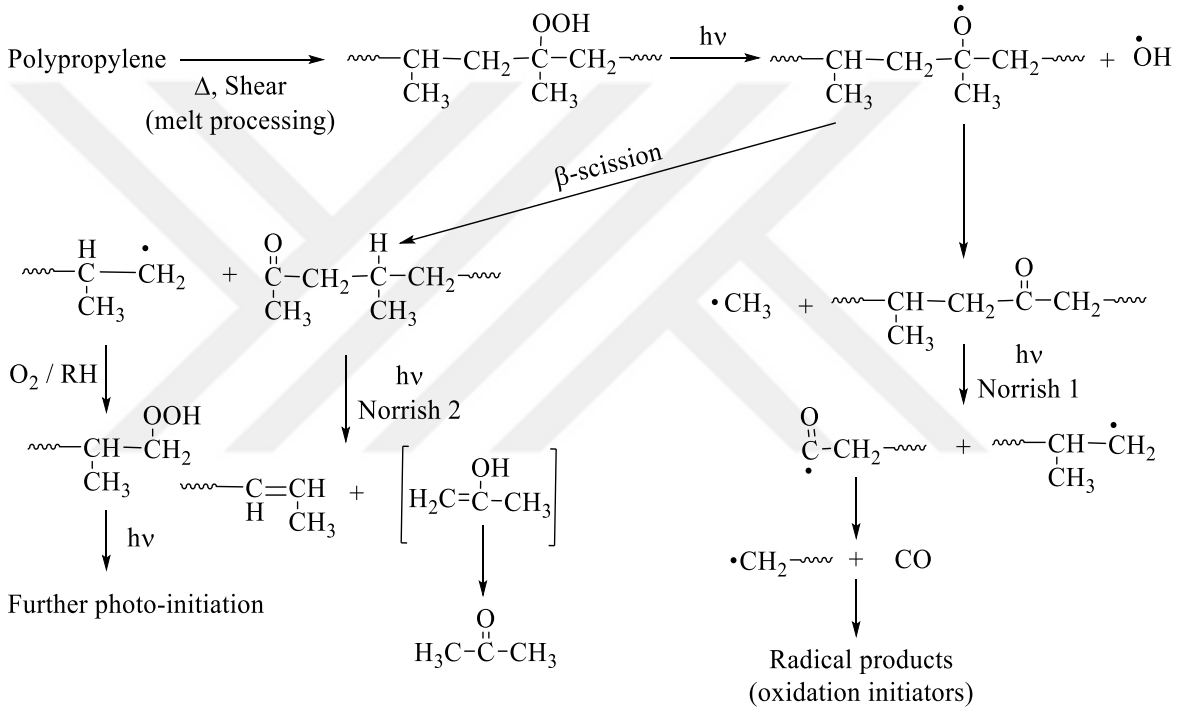


Figure 1.7. The mechanism of oxidative degradation of PP [7].

1.3. Industrial Polymerization of Propylene

Polyolefin production was not commercialized by 1950s [6]. LDPE produced *via* free radical ethylene polymerization patented by Imperial Chemical Industries (ICI) in 1937, which was requiring high temperature (200-300 °C) and high pressure (1000-4000 bars) process, was commercialized by ICI in 1939 [6], [8]. Propene was not polymerized using this method. Hogan and Banks at Philips Petroleum Company succeeded in producing HDPE

and crystalline PP *via* chromium oxides supported on silica in 1951. Phillips catalysts are employed today to produce 40 to 50 % of global demand of HDPE. However, they are not satisfactory to produce PP commercially [5].

Table 1.1. Properties of various catalyst generations [5].

Generation	Composition	Productivity (kg PP/g catalyst)	Isotactic index (wt. %)	Process requirements
1st	δ-$TiCl_3$ + $AlCl_3$ +DEAC	0.8-1.2	90-94	Deashing + aPP removal
2nd	δ-$TiCl_3$ + DEAC	3-5 (10-15)	94-97	Deashing
3rd	$TiCl_4$/Ester/$MgCl_2$ + AlR_3/Ester	5-10 (15-30)	90-95	aPP removal
4th	$TiCl_4$/Diester/$MgCl_2$ + TEA/Silane	10-25 (30-60)	95-99	
5th	$TiCl_4$/Diether/$MgCl_2$ + TEA	25-35 (70-120)	95-99	
6th	Zirconocene + MAO	5-9x103 (on Zr)	90-99	

In 1953, Karl Ziegler at the Mülheim Max Planck Institute patented his invention about the polymerization of ethylene at lower temperatures and pressure *via* a catalyst system based on titanium tetrachloride and triethylaluminum, but Ziegler failed to polymerize propene. In 1954, Giulio Natta at Milan Polytechnic succeeded in polymerizing propene by using $TiCl_4$/AlR_3 Ziegler catalyst, and isotactic content was around 40 %. Soon after, he synthesized PP with higher isotactic content (80 % to 90%) by using crystalline $TiCl_3$ instead of soluble $TiCl_4$. Ziegler-Natta (ZN) catalysts are described as a transition metal compound able to realize a repeated insertion of olefin units [6]. The catalysts generally contain two components which are a transition metal salt as a catalyst and a main group organometallic compound as a co-catalyst (activator). These catalysts are heterogeneous and insoluble in

hydrocarbons so the recycle process of ZN catalysts is not feasible. The catalyst system consisting of $TiCl_3$/ $AlEt_2Cl$ are known as the first generation ZN catalysts. Since they had low productivity and stereospecificity, both removal of catalytic residues (deashing) and separation of aPP were needed. In 1957, iPP *via* a slurry process in inert hydrocarbons was produced commercially in Ferrara plant of Montecatini by using the first generation catalysts. In 1963, G. Natta and K. Ziegler were awarded the Nobel Prize in chemistry for olefin polymerization. Propene polymerization processes have been substantially simplified by progresses in catalyst development, and environmental pollution is reduced considerably. The developments in the catalyst systems are summarized in Table 1.2. The polymerization medium can be liquid, gaseous propylene or an inert hydrocarbon diluent. Also, metallocenes provide outstanding control of polymer structure and polymer morphology. Today, majority of commercial PP is produced via ZN catalysts since metallocene catalysts are not cost-effective [5-7].

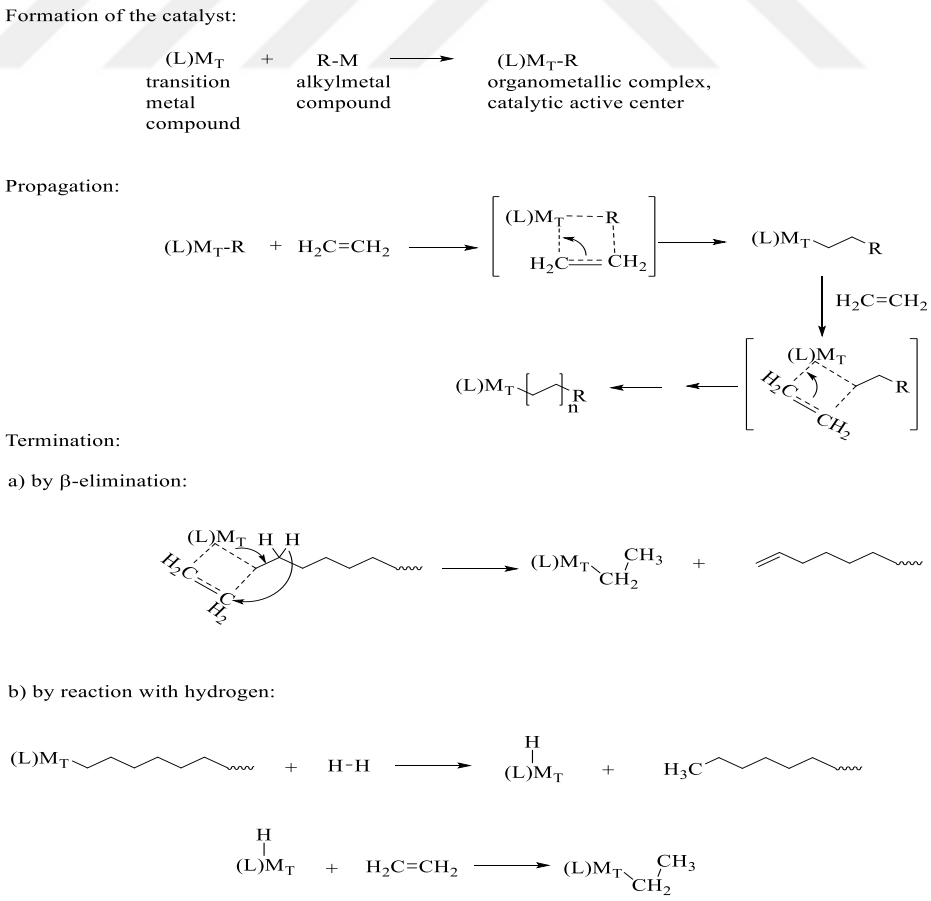


Figure 1.8. Mechanism of ethylene polymerization with ZN catalysts [9].

Olefin polymerization with ZN catalysts is a chain-growth mechanism involving initiation, propagation and termination steps. Migratory alkyl transfer mechanism proposed by Cossee and Arlman is the most widely cited mechanism. In Figure 1.8, the mechanism of ethylene polymerization with ZN catalysts is shown. Firstly, catalytic active center is generated upon alkylation of transition metal compound, and then ethylene monomer forms π-complex with this catalytic center. This complexed ethylene monomer is then inserted into the metal-carbon bond, and subsequent addition of the monomer leads to the propagation reaction. The reaction by hydrogen or β-elimination can result in termination [5], [9].

1.3.1. Polypropylene Copolymers

In addition to homopolymer, random copolymers and impact copolymers are essential kinds of PP. Propene can be copolymerized with various olefins including ethene, 1-butene, 2-hexene. However, oxygen-containing polar comonomers cannot be copolymerized with propene *via* Ziegler-Natta catalysts due to catalyst poisoning. Copolymers containing propylene and polar comonomers can be producible *via* single-site catalysts. Copolymers produced from copolymerization of propene with up to 6 % by weight of ethylene or other comonomers are called random copolymers because of random insertion of comonomer within the chain. These irregularities decrease crystallinity and melting point, and hence random copolymers are used in applications requiring clarity, lower melting point or lower modulus are preferable. Elastomeric copolymer known as ethylene-propylene rubber (EPR) or ethylene-propylene monomer rubber (EPM) is obtained as a result of copolymerization of propylene with large amounts (> 25%) of ethylene. Incorporation of diene such as dicyclopentadiene leads to terpolymer known as ethylene-propylene-diene monomer (EPDM) rubber. Contrary to iPP, EPR and EPDM are amorphous. Polypropylene impact copolymers, or heterophasic copolymers, are obtained by dispersing EPR within PP homopolymer. Impact copolymers are useful in applications where impact strength is crucial, particularly at low temperatures [1], [5], [6].

1.4. Atactic Polypropylene

Since the topic of the present study is the modification of aPP, more details about aPP will be given in this section. It is worth to mention that aPP obtained as a byproduct of iPP manufacturing is not completely amorphous, because this kind of aPP is a mixture of PPs with different tacticities and molecular weights. As mentioned above, aPP differs from iPP in terms of solubility, and in this way, aPP can be separated from iPP. by a post-polymerization process. If not, aPP deteriorates mechanical properties of iPP. For instance, the decrease in yield strength of iPP/aPP blend from 40 to 20 MPa was observed by increasing aPP content from 5 to 20 wt. % [10]. Depending on the polymerization and aPP/iPP separation methods, the crystalline content of aPP might attain 15 wt. %.

Table 1.2. Features of byproduct aPP and synthesized aPP [7].

Property	Test Method or ASTM standard	Unit	Commercial by product	Metallocene-synthesized HMW-aPP
Density	D1505	gcm-3	>0.86	≈0.85
Intrinsic viscosity	D2857	dL/g	0.4-0.6	1.5-3.5
Molecular weight	GPC	kg/mol	20-80	400-700
Polydispersity	GPC	-	5-7	2.3-3.3
Melt flow index	D1238	dg/min	>500	<5
Tg	DSC	°C	-25 ±5	≈0
Tm	DSC	°C	>140	-
Tensile strength	D638	MPa	<0.7	>1.0
Elongation at break	D638	%	<50	>1000

In general, aPP obtained as a byproduct is low in molecular weight, but high molecular weight aPP (HMW-aPP) may be attainable *via* metallocene catalysts where rubber elasticity may be gained. Features of byproduct aPP and synthesized aPP are tabulated in Table 1.2.

Owing to its tackiness, aPP-based additives are used in paper lamination, and these additives impart good adhesion as well as good barrier properties. Moreover, aPP is very compatible with rubbers, and incorporation of aPP into EPR and EPDM lowers the Mooney viscosity, improves the extrudability and enables high uptake of inert and reinforcing fillers. Additionally, aPP is used as butyl rubber replacement in caulking and sealants. Also, aPP is used as release agents for concretes, viscosity modifier for lubricants, oil, inks and dispersing additives for masterbatches [7].

1.5. Post-Reactor Modifications of Polypropylene

Polypropylene like other polyolefins is highly inert due to the absence of functional groups. The lack of chemical functionalities results in poor adhesion properties, so the use of PP in high value added applications, particularly in polymer composites and blends, is restricted. Thus, modification of PP is necessary to extend the utilization areas of PP [11], [12].

As mentioned above, ZN catalysts are the primary choice for commercial PP production and direct copolymerization of propene with other functional monomers is not possible *via* ZN catalysts. Transition metal salts of the catalytic system acts like Lewis acids. During the copolymerization, they are likely to complex with non-bonded electron pairs on heteroatoms of the polar comonomers. Active polymerization sites are deactivated upon complexation, and this phenomenon is known as catalyst poisoning [12]. This fact necessitates post-reactor modifications to introduce polarity and reactivity to PP Copolymerization of propene with polar monomers *via* other catalytic systems can be found in the literature, but this subject is beyond the scope of the present study. Controlled oxidation and grafting of functional monomers are the mainly adopted postmodification approaches to functionalize PP.

In controlled oxidation method, nonpolar PP surface is oxidized to create polar and reactive groups including carbonyl, carboxyl and hydroxyl groups by chemical or physical treatments. The etching process in very concentrated chromic acid is an effective surface

treatment. However, this process is not favored today because the etching solution contains carcinogenic chromium (IV). Corona discharge and flame treatments are industrially applied methods to achive good adhesion in PP surfaces. Corona discharge creates plasma which is a very reactive gas containing radicals, ions and ozone [13]. Polymer surfaces react with corono discharge by forming radicals. These radicals react with atmospheric oxygen to generate polar groups such as carbonyl and carboxyl groups. The functionalization of the polymer surface by corona treatment might be accompanied by crosslinking and chain scission. High flame temperatures (1000-2000 °C) or excited species in the flame induce the oxidation of polymer surfaces. Addition of peroxides into PP without any other component is another oxidation method. PP peroxides and hydroperoxides are generated upon thermal and UV decomposition, and in this way sufficienct polarity can be gained [7].

In grafting method, reactive monomers are incorporated onto PP backbone to form side chains by a radical addition mechanism. The active radical sites can be generated through ion radiation, UV radiation, plasma or chemical initiators. If the grafts are long, original polymer properties can be changed drastically. When the grafts are short, physical and/or mechanical properties are retained, but chemical properties of the modified polymer can be different, which is usually the ultimate purpose [12]. In the scope of the present study, aPP is modified by peroxide initiated free radical grafting of maleic anhydride (MAH). The details of free radical grafting will be covered in the next section.

1.5.1. Free Radical Grafting of Monomers onto Polypropylene

Free radical grafting is an extensively used method to modify polymers, especially polyolefins or polymers with a polyolefinic substructure [14]. A variety of monomers including acrylic acid, glycidyl methacrylate, maleic anhydride, hydroxymethyl methacrylate, itaconic acid have been studied to graft onto PP by free-radical chemistry [14]. Grafting reactions can be carried out in melt, in solid state, in solution and in emulsions or suspensions [12].

A free radical grafting system consists of a polymer to be modified, an unsaturated monomer such as vinyl monomer and free-radical initiator.The most proposed free-radical grafting mechanism is illustrated in Figure 1.9. In the first place, primary free radicals (R*) are created upon decomposition of initiator. Then, R* may initiate monomer to form monomer radical (RM*), which is not desired during grafting. If RM* continues to react with more monomers, oligomer of homopolymer will be produced. The grafting of this oligomer or homopolymer onto polyolefin backbone hardly takes place since hydrogen abstracting capacity of a propagating monomer is quite low. Yet, some radicals such as vinyl acetate are highly reactive to abstract hydrogen. On the other hand, R* can abstract hydrogen from the polymer backbone to form a macroradical, which is the favored pathway during the grafting process. This macroradical can undergo chain scission, crosslinking or grafting. The reaction of the macroradical with the monomer bears a branched macroradical. Longer grafts can be formed from the reaction of the branched macroradical with more monomers. Or, this branched macroradical may can transfer its reactivity to the same or another polymer backbone to form new macroradicals.

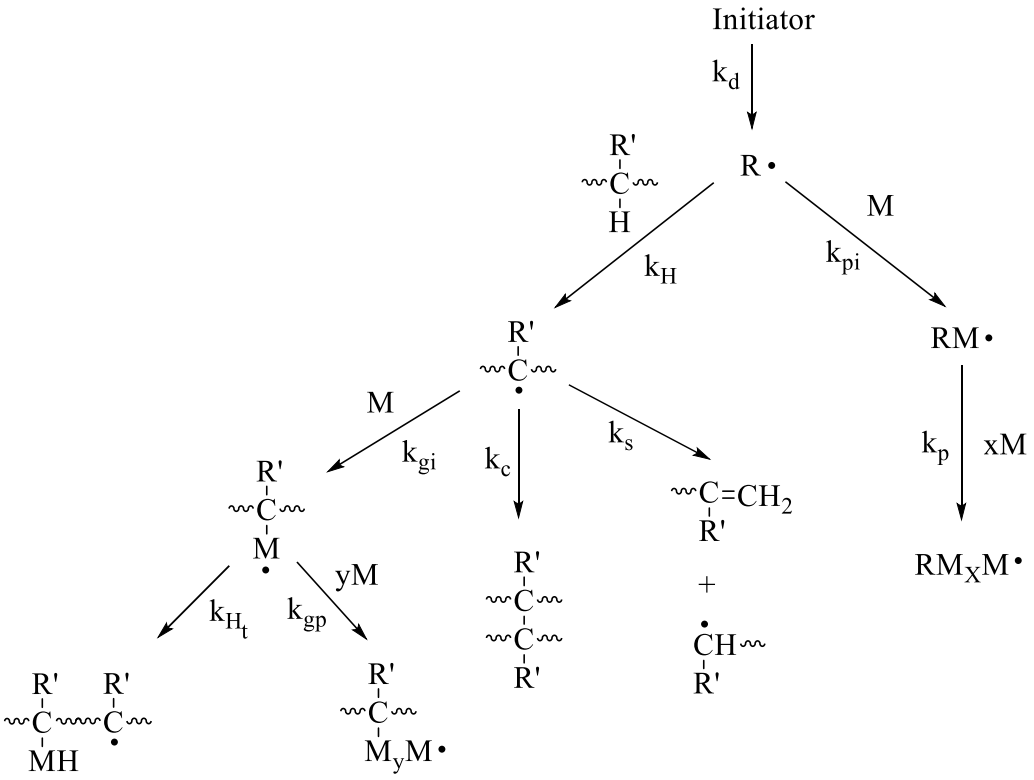


Figure 1.9. The scheme of free radical grafting onto a polymer backbone [12].

According to the proposed reaction scheme, desired grafting reaction competes with the undesired homopolymerization. In addition, free radical grafting can be accompanied by crosslinking and chain-scission. The choice of reactants and reaction conditions are important parameters to promote grafting.

1.5.1.1. The Significance of Peroxides in Free Radical Grafting. Free-radical initiators are the main sources of free radicals in the free-radical grafting process. The creation of radicals by pure thermal or mechanical means might be possible but they are not adequate to reach desired grafting degrees. Organic peroxides are the most efficient sources and can be used in small amounts.

Organic peroxides decompose at proper temperatures to supply free radicals upon the homolytic dissociation of the labile oxygen-oxygen bond. The rate of peroxide decomposition at particular conditions can be expressed as its half-life, $t_{1/2}$. As decomposition rate increases, $t_{1/2}$ decreases. The thermal decomposition of organic peroxides follows first-order kinetics under suitable conditions. The distinctive $t_{1/2}$value is just dependent on the intrinsic rate constant k as follows:

$$t_{1/2} = ln\left(\frac{2}{k}\right). \tag{1.1}$$

The value of k is determined by the relative stability of the radicals formed, steric effects and electronic effects. If the radical is more stable, the peroxide is less stable. Highly strained peroxides are less stable since steric strain energy decreases upon decomposition. Whereas electron-withdrawing groups stabilize peroxides, they are destabilized by electron-donating groups. These factors are demonstrated in the Arrhenius equation:

$$k = k_0 exp\left(-\frac{\Delta E}{RT}\right) \tag{1.2}$$

where ΔE is the activation energy and k_0 is pre-factor.

Temperature dependence of $t_{1/2}$ is shown as follows:

$$t_{1/2} = ln\left(\frac{2}{k_0}\right) exp\left(\frac{\Delta E}{RT}\right) \quad (1.3)$$

where R is gas constant and T is temperature in Kelvin.

The activation energy of organic peroxides varies from 100 to 150 kJ/mol, and so the $t_{1/2}$ will be doubled with a decrease in temperature by 5-10 °C. In addition to temperature, pressure also influences the $t_{1/2}$, but the effect of pressure is not much pronounced as temperature.

Decomposition of organic peroxides obeys first-order kinetics at highly diluted conditions. Apart from temperature and pressure, kinetics of the decomposition might be affected by peroxide concentration, the presence of solvents and other substances in the medium. Decomposition may result from not only thermal energy but also the attack of free radicals originating from the peroxide itself, the solvent or the reactive substances. This situation is known as induced decomposition. Organic peroxide molecules may be attacked by primary radicals to break oxygen-oxygen bonds at high concentration of the peroxides. In this way, decomposition is accelerated but the radical concentration decreases because of induced decomposition. Polarity of the solvent greatly influences the half-life. Certain solvents can attack and decompose peroxides. Or, primary free radicals resulted from the peroxide may react with some solvents to yield secondary radicals which are capable of attacking the peroxide molecules. These induced decompositions follow second-order kinetics, and they are faster than the first-order thermal decomposition of the peroxides.

The suitable peroxide should bear free radicals reactive enough to abstract hydrogen from polymer backbone to form the corresponding macroradical. Hydrogen-abstracting capacity of primary radicals are not only governed by the nature of primary radicals but also the kind of C-H bonds in polyolefins. As hydrogen bond dissociation energy (HBDE) lowers, hydrogen abstraction becomes easier, and activation energy for hydrogen abstraction decreases. On the other hand, as HDBE lowers, the reactivity of the radicals generated decreases as well, since the stability of the generated radical is higher.

The convenient peroxide should have low toxicity and volatility, suitable half-life and yield primary radicals with an enough hydrogen-abstracting capacity. Since organic peroxides with short half-lives produce free radicals in a short time, they can favor chain scission. On the other hand, organic peroxides with long half-lives may not completely decompose to bring about enough free radical concentration required for grafting [15]. Azo-initiators are not suggested in free radical grafting due to their short half-lives and low hydrogen abstracting capacities [12]. Alkoxy radicals are viewed as proper hydrogen abstracting radicals [16].

1.5.1.2. The Significance of Polyolefin Structure in Free Radical Grafting. During free radical grafting, the occurrence of grafting, chain scission or crosslinking is also affected by the nature of macroradical, and hence the kind of the equivalent polymer backbone.

The reduction in molecular weight takes place upon β-scission. Polymer chains with higher molecular weight have more C-C bonds, so the probability of chain scission increases. The reduction in molecular weight may cause worsening mechanical properties of original polymer. Radical scavengers like sterically hindered phenolic antioxidants (i.e. available under the name Irganox and its derivatives) were incorporated during free radical grafting of MAH onto PP to control chain scission [17], [18]. F. Kučera et al. has observed that the addition of Irganox 1010 (0.2-0.8 wt. %) enabled suppression of β-scission of PP, and the grafting kinetics and yield were not greatly influenced up to 0.4 wt. % [18]. Additionally, any strategy favoring faster grafting of monomer onto macroradical can suppress the chain scission during free radical grafting.

On the other hand, macroradicals can yield long chain branching or crosslinked network when bimolecular termination by combination happens. Crosslinking is usually believed to be undesired, but it might also give rise to various property improvements such as elevated service temperature, solvent resistance, flexural modulus and dimension stability. In case of PP, the probability of bimolecular termination is low. Polypropylene macroradicals are mainly tertiary, so they have low reactivity for combination. Also, steric hindrance of tertiary macroradicals lowers the probability of crosslinking [12].

The attack of the macroradical to double bond of a selected monomer is generally the only desired pathway for the macroradical. As mentioned above, upon this attack, branched macroradical is formed, and this branched macroradical can bring about longer grafts. The degree of grafting significantly depends on the reactivity of monomer and macroradical. Yet, direct information about such combinations is very limited. Nonetheless, similar copolymerization systems may contribute to predict the reactivity of such combinations. Copolymerization systems are controlled by reactivity ratios. When a monomer A copolymerizes with a monomer B, the reactivity of A and B monomers towards the radical A* is represented by the reciprocal of the ratio, $^1/_{r_a}$. $^1/_{r_a}$ is calculated as follows:

$$\frac{1}{r_a} = \frac{k_p^{ab}}{k_p^{aa}} = \frac{specific\ rate\ of\ (A^* + B)}{specific\ rate\ of\ (A^* + A)} \ . \tag{1.4}$$

Broadly speaking, the inherent reactivity of radicals is inversely proportional to the reactivity of its precursor. That is, the most reactive radicals are supplied from the least reactive monomers and *vice versa*. The reactivities of various radical-monomer combinations in respect to homopropagation of the radical are shown in Table 1.3. If the magnitude of $^1/_{r_a}$ is greater than unity, the free radical favors reacting with other monomers instead of its double bond precursor. For example, the MAH radical reacts violently with the styrene monomer, and also styryl radical chooses to react with the MAH radical. Thus, alternating copolymer results from MAH and styrene combination.

Above discussion about reactivity ratios of monomers for the classical copolymerization can be useful to improve grafting of unreactive monomers onto polymer backbones. For example, GMA exhibits low free radical reactivity towards PP in melt. Cartier *et al.* showed that the addition of styrene as a comonomer during melt free radical grafting of GMA on PP improved the grafting degree of GMA and diminished the chain scission. Since styrene possesses higher free radical reactivity, PP macroradical can react faster with styrene before they undergo chain scission, and the resulting styryl radical is able to copolymerize with GMA. The addition of α-methyl styrene was also checked, and there was no improvement in GMA grafting since α-methyl styrene is not capable of copolymerizing with GMA [19].

Table 1.3. Reactivities of radical-monomer combinations with respect to the homopropagation of the radical [12].

Radical	Monomer					
	Vinyl acetate	Acrylonitrile	Methyl methacrylate	Glycidyl methacrylate	Styrene	Maleic anhydride
Vinyl acetate	1.00	20.0	21.4	-	15.6	52.6
Acrylonitrile	0.21	1.00	7.25	0.92	14.0	0.17
Methyl methacrylate	0.039	0.76	1.00	1.37	2.25	0.234
Glycidyl methacrylate	-	0.92	1.33	1.00	1.78	-
Styrene	0.005	2.64	1.99	2.41	1.00	29.0
Maleic anhydride	$+\infty$	$+\infty$	38.5	-	93.0	1.00

Apart from free radical reactivity of monomer, the reactivity of macroradical depends on polyolefin structure. While there are mainly methylene groups in HDPE, iPP contains methyl, methylene and methine groups. In general, PE is more reactive than PP in free radical grafting process [12]. It has been shown that the grafting degree of MAH onto polyolefin decreases with increase in propene content [20]. However, the fundamental reason for low free-radical reactivity of PP relative to PE is not the kind of hydrogens in the structure. There are one 3°, two 2° and three 1° hydrogens in one repeating unit of PP, while four 2° hydrogens are present in one repeating unit of PE. Hence, while total reactivity of PE repeat unit toward t-butoxyl radical corresponds to 40, that of PP repeat unit corresponds to 73. From this starting point, PP should have had higher free radical reactivity. This situation proves that the effect of steric factors on the reactivity is more pronounced in free-radical grafting relative to classical copolymerization [12]. Furthermore, the effect of tacticity in modification of PP was investigated by comparing metallocene-synthesized polypropylenes with different tacticities and similar molecular weights. The degree of modification of low crystalline PP was easier than that of highly crystalline PP due to random rearrangement of methyl groups [21].

1.5.1.3. The Significance of Reaction Conditions in Free Radical Grafting. Melt free radical grafting is industrially favored because these systems allow fast grafting reactions with economic advantages such as the lack of solvent recovery [20]. Melt free radical grafting can be conducted using extruders in continous reactors or internal batch mixers in discontinuous reactors [18]. As an alternative method to melt grafting, solid state grafting can be carried out. Unlike melt system, this system as a batch process necessitates long reaction times but milder conditions. Although it is not as common as the melt grafting, industrial applications of solid state grafting exist. Since grafting reactions are realized below the melting temperatures of polymers, the grafting take places only at the amorphous phase, and the likelihood of chain scission is diminished [14].

On the other hand, performing grafting in solution is advantageous in terms of homogeneity of the medium and the uniformity of the grafting. However, grafting in solution cannot be carried out at elevated temperatures due the boiling point of used solvents. Moreover, decrease in grafting efficiency is likely due to the solvent-free radical interactions [17]. The temperature range of melt free radical grafting can extend from 150 to 300 °C. While elevated temperatures speed up the free radical grafting, they can promote undesired side reactions. Previously mentioned induced decomposition of peroxides may become more pronounced at elevated temperatures, and lead to decrease in initiator grafting efficiency. Another effect of elevated temperature is associated with the ceiling temperature. The critical temperature where the rates of polymer propagation is equal to that of polymer degradation is called ceiling temperature (T_c) of polymerization. Since the grafts and homopolymers involve the same monomer, T_c for grafting and for polymerization is anticipated to be equal. The ceiling temperature is determined as follows:

$$T_c = \frac{\Delta H_p}{\Delta S_p} = \frac{\Delta H_p}{\Delta S_p^\circ + R\ ln[M]} \tag{1.5}$$

where ΔH_p is enthalpy change of polymerization, ΔS_p is entropy change of polymerization and ΔS_p^0 is standard entropy change for $[M]$ monomer concentration. When free-radical grafting reactions are conducted at temperatures close to T_c, the lengths of grafts and homopolymerization by products will be shorter [12].

It has been questioned whether ceiling temperature is effective on the length of grafts. Upon increase in monomer concentration, decrease in T_c should induce a significant alteration in the microstructure of the grafts. In the grafting of MAH onto model low molecular weight hydrocarbons (n-eicosane and squalene), they concluded that in the absence of model hydrocarbon substrates, the formation of homopolymer was governed by T_c. On the other hand, in the presence of model hydrocarbon structures, the relative rates of intramolecular hydrogen abstraction and monomer addition to MAH radical was predominant factor determining the graft length [22].

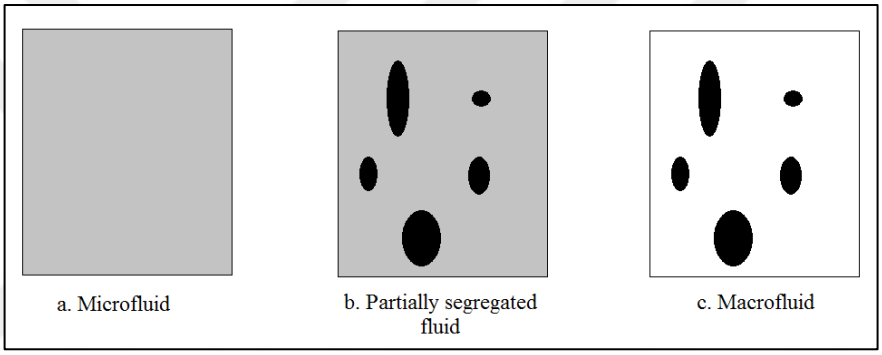


Figure 1.10. The states of homogeneity during melt free radical grafting: a) microfluid, b) partially segregated fluid, c) macrofluid [12].

Another critical issue associated with melt systems is the higher viscosity of the reaction medium. The diffusion of reacting species may be hampered in the highly viscous medium. Homogenous dispersion of peroxides and monomers into highly viscous polymer melt may not be always possible. Most of the monomers selected for grafting are liquid at grafting temperatures, and they are able to dissolve organic peroxides. When the whole system is homogeneous, this type of system is called microfluid. Grafting and homopolymerization will take place over the whole system in microfluids, so the most uniform grafted polyolefins in terms of grafting yield, molecular weight, etc. can be obtained in such systems. When the monomer and the organic peroxide are not completely miscible with the polyolefin melt, then this system is called partially segregated fluid. In partially segregated systems, grafting will take place in the polymeric phase, but homopolymerization

will occur in the aggregates. The solubility of the organic peroxide and the monomer in the polymer melt is significant to increase grafting yield and uniformity. On the other hand, when the monomer and organic peroxides is completely immiscible with the polymer melt, this system is called macrofluid. In such system, grafting will take place only at the interface and homopolymerization will occur in the aggregates. These systems are illustrated in Figure 1.10.

1.5.1.4. Applications of PP-based Graft Copolymers. Polymer blending permits producing tailor-made polymeric materials integrating attractive features of polymer components [23]. Additionally, it is a very valuable method in industrial practice because it is an economically viable way to obtain new macromolecular materials from existing polymers [1], [23]. However, the majority of PP blends are not thermodynamically compatible. Polypropylene-based graft copolymers can function as an interfacial agent and a compatibilizer in PP blends [11]. Maleic anhydride grafted PP, often written as PP-g-MAH, is a very famous example of grafted polymers. It is commercially available as Bynel 5000 (DuPont), Admer (Mitsui), Tymor (Rohm&Haas) [24]. Maleic anhydride is not only polymerizable due to the presence of the double bond in its structure but also reactive toward many functional groups thanks to its cyclic anhydride in the structure. Upon grafting onto PP, it becomes substituted succinic anhydride (SA), it makes PP greatly reactive towards diverse nucleophilic groups such as amines, alcohols, thiols or electrophilic groups like epoxies in the presence of a catalyst. It has been showed that incompatibility of the blend of polyamide 12 (PA 12) and PP due to polarity difference was improved by addition of either PP-g-MAH or acrylic acid grafted PP (PP-g-AA). Interfacial adhesion is enhanced upon reaction of reactive groups on PP-g-MAH and PP-g-AA with terminal amine groups of PA 12 to bring about copolymers locating at the interface [25]. Similarly, PP/poly (ethylene terephthalate) blend is compatibilized by the addition of PP-g-MAH [26].

On the other hand, PP-based graft copolymers can be incorporated into laminate composites as a tie layer. Lamination of several polymers exploits the specific functions of each layer in order to gain improved or complementary properties in the final product. For example, ethylene/vinyl alcohol copolymer (EVOH) possesses outstanding gas barrier properties while it is not much moisture and solvent resistant as polyolefins. Packaging

materials demanding excellent gas barrier property and solvent/moisture resistance can be obtained by lamination of PP on EVOH. Since they are thermodynamically incompatible, multilayered film with desired properties can be produced by inserting PP-g-MAH as a tie layer [24], [27]. Likely, in wood-plastic composites, PP-based graft copolymers can be used as coupling agent between highly nonpolar PP and hygroscopic wood fiber [7], [28].

2. AIM OF THE STUDY

Atactic polypropylene (aPP) is considered as an industrial waste originating from isotactic polypropylene (iPP) production, and its utilization fields are quite limited. The present study aims to synthesize a high value added material from this industrial byproduct. For this purpose, atactic polypropylene is modified by grafting maleic anhydride (MAH) onto polymer backbone in the presence of free radical initiators. When compared to the grafting conditions of iPP, the lower melting temperature and amorphous nature of aPP allow to carry out grafting reactions under milder conditions. Thus, inevitable chain scission of original polymer can be minimized. In the scope of this study, the modification of aPP by free radical grafting was carried out in both solution and melt. The influence of grafting was examined mainly *via* FTIR spectroscopy and DSC.

3. EXPERIMENTAL

3.1. Synthesis

All chemicals were used as received from manufacturers. Benzoyl peroxide (BPO) supplied by Park Scientific contains 25 % water, molar calculations were done accordingly. The molar mass of atactic polypropylene (aPP) supplied by Petkim Petrokimya Holding A.Ş. as a byproduct of iPP manufacturing process was not known so mole calculations were done with respect to the repeating unit. That is to say, the molar mass of aPP is 42.08 g/mol.

3.1.1. Free Radical Grafting of MAH onto aPP in Solution

In the first part of the study, grafting reactions were conducted in solution. In a typical experimental procedure, aPP (2.0 g, 0.048 mol) and a stir bar were placed in a 2-neck round-bottom flask, and 40 mL toluene was poured onto them. One neck was stoppered with a rubber septum, and the other neck was connected to a condenser. The round bottom flask was then immersed into a silicone oil bath at 110 °C. The reaction flask was purged with nitrogen gas for 10 minutes. Maleic anhydride (MAH) (1.4 g, 0.014 mol) and BPO (0.58 g, 0.0018 mol) were added to the medium in turn by removing the septum. Any accumulating solid particles on the neck were washed with a small amount of toluene. The moment when all BPO had been added was accepted as the reaction start time. Nitrogen gas flow was maintained for 10 minutes after the addition of BPO. Then, an inert atmosphere was provided with a balloon filled with N_2 gas. Once 4 h had elapsed, the mixture was precipitated into ethanol. The solutions containing precipitates were placed aside and filtered next day. The products obtained were dried under vacuum for 24 h at room temperature to analyze with an FTIR spectrometer. After first ethanol precipitation, products were washed with ethanol. Benzoyl peroxide initiated maleic anhdride grafting reactions were abbreviated as BIG. The numbers following “BIG_” specify the used mole ratios (relative to aPP) of MAH and BPO

in that particular reaction, respectively. For instance, BIG_0.30/0.037 means that 1 mole ratio of aPP was reacted with 0.30 mole ratio MAH in the presence of 0.037 mole ratio BPO. Varying ratios of reactants used in solution reactions were given in Table 3.1.

Table 3.1. Varying ratios of reactants for control and grafting reactions in solution.

Experiment Code	aPP: MAH: BPO (mole ratio wrt aPP)
Blank_aPP	1: -: -
Blank_aPP+BPO	1: -: 0.037
Blank_aPP+MAH	1: 0.90: -
Blank_MAH+BPO	-: 0.70: 0.037
BIG_0.30/0.037	1: 0.30: 0.037
BIG_0.50/0.037	1: 0.50: 0.037
BIG_0.70/0.037	1: 0.70: 0.037
BIG_0.90/0.037	1: 0.90: 0.037
BIG_0.30/0.075	1: 0.30: 0.075
BIG_0.49/0.074	1: 0.49: 0.074
BIG_0.70/0.075	1: 0.70: 0.075
BIG-0.90/0.075	1: 0.90: 0.075

Control Experiments: Four different control experiments were carried.

The control experiment coded as Blank_aPP and was carried out to investigate the behavior of aPP at 110 °C in toluene. Atactic PP (2 g, 0.048 mol) and a stir bar were placed in a 2-neck round-bottom flask, and 40 mL toluene was poured onto them. One neck of the bottom was stoppered with a rubber septum, and the other neck was connected to a condenser. The round bottom flask was immersed in a silicone oil bath at 110 °C. The reaction flask was purged with nitrogen gas for 10 minutes. Then, an inert atmosphere was provided with a balloon filled with N_2 gas. Once 4 h had elapsed, the mixture was precipitated in ethanol. The solution containing the precipitate was placed aside and filtered

next day. The product obtained was dried under vacuum for 24 h at room temperature to analyze with an FTIR spectrometer.

The control experiment coded as Blank_aPP+BPO was carried out to investigate the magnitude of degradation in the presence of BPO at 110 °C in toluene. Atactic PP (2.0 g, 0.048 mol) and a stir bar were placed in a 2-neck round-bottom flask, and 40 mL toluene was poured onto them. One neck of the bottom was stoppered with a rubber septum, and the other neck was connected to a condenser. The round bottom flask was immersed in a silicone oil bath at 110 °C. The reaction flask was purged with nitrogen gas for 10 minutes. Benzoyl peroxide (0.58 g, 0.018 mol) was added to the medium by removing the septum. Any accumulating solid particles onto the neck were washed with a little amount of toluene. The moment when all BPO had been added was accepted as the reaction start time. Nitrogen gas flow was maintained for 10 minutes after the addition of BPO. Then, an inert atmosphere was provided with a balloon filled with N_2 gas. Once 4 h had elapsed, the mixture was precipitated in ethanol. The solution containing the precipitate was placed aside and filtered next day. The product obtained was dried under vacuum for 24 h at room temperature to analyze with an FTIR spectrometer.

The control experiment coded as Blank_aPP+MAH was carried out to evaluate whether the grafting reaction happens without a radical initiator. Atactic PP (2.0 g, 0.048 mol) and MAH (4.2 g, 0.043 mol) with a stir bar were placed in a 2-neck round-bottom flask, and 40 mL toluene was poured onto them. One neck of the bottom was stoppered with a rubber septum, and the other neck was connected to a condenser. The round bottom flask was immersed in a silicone oil bath at 110 °C. This moment was accepted as the reaction start time. The reaction flask was purged with nitrogen gas for 10 minutes. Then, an inert atmosphere was provided with a balloon filled with N_2 gas. Once 4 h had elapsed, the mixture was precipitated in ethanol. The solution containing the precipitate was placed aside and filtered next day. The product obtained was dried under vacuum for 24 h at room temperature to analyze with an FTIR spectrometer. After first ethanol precipitation, the product was washed with ethanol further.

The control experiment coded as Blank_MAH+BPO was carried out to investigate homopolymerization of MAH in the presence of BPO. Firstly, MAH (4.0 g, 0.41 mol) and a stir bar were placed in a 2-neck round-bottom flask, and 40 mL toluene was poured onto

them. One neck of the bottom was stoppered with a rubber septum, and the other neck was connected to a condenser. The round bottom flask was immersed in a silicone oil bath at 110 °C. The reaction flask was purged with nitrogen gas for 10 minutes. Afterwards, BPO (0.57 g, 0.0018 mol) was added to the medium by removing the septum. Any accumulating solid particles onto the neck were washed with a little amount of toluene. The moment when all BPO had been added was accepted as the reaction start time. Nitrogen gas flow was maintained for 10 minutes after the addition of BPO. Then, an inert atmosphere was provided with a balloon filled with N_2 gas. Once 4 h had elapsed, the mixture was not precipitated in ethanol, because it was miscible with ethanol. The burgundy solid particles adhered to inner wall of the flask were collected by dissolving in acetone, and then the acetone was discarded via rotary evaporator at 30 °C. The remaining solid was dried under vacuum for 24 h at room temperature to analyze with an FTIR spectrometer.

3.1.2. Free Radical Grafting in Melt

In the second part of the study, the grafting reactions were conducted in the absence of solvents.

3.1.2.1. Maleic Anhydride Grafting onto aPP in Melt. Maleic anhydride grafting reactions were carried out at 130 °C in the presence of dicumyl peroxide (DCP) as an initiator. In a typical experimental procedure, aPP (15 g, 0.36 mol) was placed in a glass reactor equipped with a mechanical stirrer, and immersed into a silicone oil bath at 130 °C. The mechanical stirrer started to mix after all aPP softened. Then, MAH (1.50 g, 0.015 mol) and DCP (0.075 g, 0.00028 mol) were added subsequently onto molten aPP. The medium was purged with N_2 gas for 10 minutes after the addition of DCP. The moment when all DCP had been added was accepted as the reaction start time, and the set reaction time was 30 minutes. When the set reaction time elapsed, the reactor was removed from the oil bath, and the fluid product was poured onto a polytetrafluoroethylene (PTFE) surface and waited for a while to recover it in solid phase. 0.50 g solid was dissolved in 25 mL toluene at 110 °C and precipitated in

125 mL ethanol after cooling down to room temperature. The solutions containing precipitates were placed aside and filtered next day. The products obtained were dried under vacuum for 24 h at room temperature prior to analyze.

Maleic anhydride grafting reactions in melt were abbreviated as MAG, and varying ratios of reactants for specific MAG reactions were given in Table 3.2. The numbers following '"MAG_" specify the used amounts of MAH and DCP in parts per hundred resin (phr) in that particular reaction, respectively. For instance, MAG_10/0.5 means that 100 phr aPP is reacted with 10 phr MAH in the presence of 0.5 phr DCP.

Table 3.2. Varying ratios of reactants for grafting reactions in melt.

Experiment Code	aPP: MAH: DCP (phr)
MAG_10/0.5	100: 10: 0.5
MAG_10/1	100: 10: 1
MAG_10/2	100: 10: 2
MAG_10/3	100: 10: 3
MAG_20/1	100: 20: 1

3.1.2.2. Modified MAH Grafting onto aPP in Melt. Modified MAH (mMAH) grafting in melt was initiated by DCP. In a typical experimental procedure, aPP (25 g) was placed in a glass reactor equipped with a mechanical stirrer and immersed in a silicone oil bath at T_1 °C. The mechanical stirrer started to mix after all aPP melted. Then, mMAH (2.5 g) and DCP (0.75 g) were added subsequently onto molten aPP. The medium was purged with N_2 gas for t_0+10 minutes after the addition of DCP. The moment when all DCP had been added was accepted as the reaction start time. When the set reaction time had elapsed, the reactor was removed from the oil bath. Next, the fluid product was poured onto a PTFE surface and waited for a while to recover it in solid phase. mMAH grafting reactions in melt were abbreviated as MEG, and details of them were given in Table 3.3. The numbers following "MEG_" specify the used amounts of mMAH and DCP in phr and reaction time respectively,

and reaction temperature was specified as T_1 or T_1+5. For instance, MEG_10/3_10_T_1 means that 100 phr aPP is reacted with 10 phr mMAH in the presence of 3 phr DCP for t_0+10 min at T_1 °C.

Control Experiments: Five different control experiments were carried.

The control experiments coded as Blank_aPP_T_1 and Blank_aPP_T_1+5 were performed to evaluate degradation of aPP at T_1 °C and T_1+5 °C, respectively, for t_0+30 min in the absence of mMAH and DCP. In a typical experimental procedure, aPP (25 g) was placed in a glass reactor equipped with a mechanical stirrer and immersed in a silicone oil bath at T_1 °C. The mechanical stirrer started to mix after all aPP melted. Then, the medium was purged with N_2 gas for 10 minutes. The moment when all aPP melted was accepted as the reaction start time. When the set reaction time had elapsed, the reactor was removed from the oil bath. Next, the fluid product was poured onto a PTFE surface and waited for a while to recover it in solid phase.

The control experiments coded as Blank_DCP_T_1 and Blank_DCP_T_1+5 were performed to evaluate peroxide-induced degradation of aPP at T_1 °C and T_1+5 °C, respectively, for t_0+30 min in the absence of mMAH. In a typical experimental procedure, aPP (25 g) was placed in a glass reactor equipped with a mechanical stirrer and immersed in a silicone oil bath at T_1 °C. The mechanical stirrer started to mix after all aPP melted. Then, DCP (0.75 g) were added onto molten aPP. The medium was purged with N_2 gas for 10 minutes after the addition of DCP. The moment when all DCP had been added was accepted as the reaction start time. When the set reaction time had elapsed, the reactor was removed from the oil bath. Next, the fluid product was poured onto a PTFE surface and waited for a while to recover it in solid phase.

The control experiment coded as Blank_mMAH_T_1 was performed to examine whether grafting occurs in the absence of DCP. Atactic PP (25 g) was placed in a glass reactor equipped with a mechanical stirrer and immersed in a silicone oil bath at T_1 °C. The mechanical stirrer started to mix after all aPP melted. Then, mMAH (2.5 g) was added onto molten aPP. The medium was purged with N_2 gas for 10 minutes after the addition of mMAH. The moment when all mMAH had been added was accepted as the reaction start time. When the set reaction time had elapsed, the reactor was removed from the oil bath.

Next, the fluid product was poured onto a PTFE surface and waited for a while to recover it in solid phase.

Table 3.3. Reaction conditions to graft mMAH onto aPP in melt.

Experiment Code	aPP: mMAH: DCP (phr)	Reaction conditions
Blank_aPP_T_1	100: -: -	T_1 °C, t_0+30 min
Blank_DCP_T_1	100: -: 3	T_1 °C, t_0+30 min
Blank_mMAH_T_1	100: 10: -	T_1 °C, t_0+30 min
Blank_aPP_T_1+5	100: -: -	T_1+5 °C, t_0+30 min
Blank_DCP_T_1+5	100: -: 3	T_1+5 °C, t_0+30 min
MEG_10/3_10_T_1	100: 10: 3	T_1 °C, t_0+10 min
MEG_10/3_20_T_1	100: 10: 3	T_1 °C, t_0+20 min
MEG_10/3_30_T_1	100: 10: 3	T_1 °C, t_0+30 min
MEG_10/3_45_T_1	100: 10: 3	T_1 °C, t_0+45 min
MEG_10/3_60_T_1	100: 10: 3	T_1 °C, t_0+60 min
MEG_10/1_30_T_1	100: 10: 1	T_1 °C, t_0+30 min
MEG_10/5_30_T_1	100: 10: 5	T_1 °C, t_0+30 min
MEG_10/5_45_T_1	100: 10: 5	T_1 °C, t_0+45 min
MEG_10/5_60_T_1	100: 10: 5	T_1 °C, t_0+60 min
MEG_5/1_30_T_1	100: 5: 1	T_1 °C, t_0+30 min
MEG_5/3_30_T_1	100: 5: 3	T_1 °C, t_0+30 min
MEG_5/5__30_T_1	100: 5: 5	T_1 °C, t_0+30 min
MEG_15/1_30_T_1	100: 15: 1	T_1 °C, t_0+30 min
MEG_15/3_30_T_1	100: 15: 3	T_1 °C, t_0+30 min
MEG_15/5_30_T_1	100: 15: 5	T_1 °C, t_0+30 min
MEG_10/3_10_T_1+5	100: 10: 3	T_1+5 °C, t_0+10 min
MEG_10/3_20_T_1+5	100: 10: 3	T_1+5 °C, t_0+20 min
MEG_10/3_30_T_1+5	100: 10: 3	T_1+5 °C, t_0+30 min
MEG_10/3_45_T_1+5	100: 10: 3	T_1+5 °C, t_0+45 min

Table 3.3. Reaction conditions to graft mMAH onto aPP in melt. (cont.)

MEG_10/3_60_T_1+5	100: 10: 3	T_1+5 °C, t_0+60 min
MEG_10/1_30_T_1+5	100: 10: 1	T_1+5 °C, t_0+30 min
MEG-10/5_30_T_1+5	100: 10: 5	T_1+5 °C, t_0+30 min
MEG_5/1_30_T_1+5	100: 5: 1	T_1+5 °C, t_0+30 min
MEG_5/3_30_T_1+5	100: 5: 3	T_1+5 °C, t_0+30 min
MEG_5/5_30_T_1+5	100: 5: 5	T_1+5 °C, t_0+30 min
MEG_15/1_30_T_1+5	100: 15: 1	T_1+5 °C, t_0+30 min
MEG_15/3_30_T_1+5	100: 15: 3	T_1+5 °C, t_0+30 min
MEG_15/5_30_T_1+5	100: 15: 5	T_1+5 °C, t_0+30 min

3.2. Analysis

3.2.1. FTIR Analysis

The samples were analyzed *via* Thermo Fisher Scientific Nicolet 380 FTIR spectroscopy with ATR accessory. A spectrum resolution was 4 cm^{-1}, and 32 scans were applied.

3.2.2. DSC Analysis

Thermal analyses of samples were done *via* Exstar SII DSC 7020 instrument with the method shown in Table 3.4.

Table 3.4. DSC run method.

Initial T (°C)	Final T (°C)	Rate (°C/min)	Hold Time (min)
-60	180	10	3
180	-60	10	2
-60	180	10	2

3.2.3. Volumetric Titration

The amount of MAH in purified samples were determined by a hot volumetric titration method. 50.0 mg sample was dissolved in 25 mL xylene at 110 °C. Next, two drops of distilled water were added to the solution to hydrolyze anhydride groups and heated for 10 minutes. Two drops of phenolphthalein solution in ethanol were added, and the solution was titrated against 0.005 M ethanolic KOH. During titration, the flask was in contact with hot silicon oil to inhibit precipitation of the polymer. The point where the pale pink color was persistent was noted as the end point. Each sample was titrated following the same procedure three times, and the results were expressed as an average.

Following equation was used to calculate grafted MAH wt. % in purified samples:

$$MAH\ \% = \frac{V_{KOH} \times M_{KOH}}{2 \times m_{polymer}} \times 98.06 \times 100\ \% \quad (3.1)$$

where V_{KOH} is the volume of KOH in mL at the end point, M_{KOH} is the molar concentration of titrant KOH in mol/L and $m_{polymer}$ is the amount of purified polymer which is titrated. Grafted MAH forms two carboxylic acid groups upon hydrolysis as shown in Figure 3.1 so the denominator in the Equation 3.1 involves two, and 98.06 g/mol is molar mass of MAH.

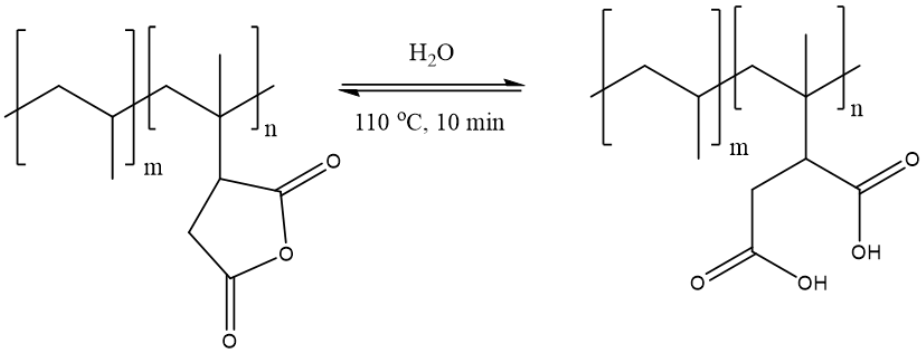


Figure 3.1. Hydrolysis of grafted MAH in titration conditions.

3.2.4. NMR Analysis

Varian Gemini 400 MHz NMR spectrometer was used in chloroform-d_1 at room temperature. On the other hand, Bruker 400 MHz NMR spectrometer was used in toluene-d_8 at room temperature or 80 °C.

4. RESULTS AND DISCUSSION

Within the scope of the thesis, modification of atactic polypropylene (aPP) was attempted by free radical grafting. In the first place, free radical grafting of maleic anhydride (MAH) onto aPP was carried out in solution. Next, melt grafting as a more facile method for industrial applications were performed. However, sublimation of MAH and inhomogeneity between MAH, aPP and the peroxide type-initiator were faced during grafting in melt. Thus, MAH grafting in melt was not efficient in the presence of these problems. To overcome these problems during melt grafting, MAH was modified accordingly. The potential grafting mechanism of MAH is shown is Figure 4.1. The desired MAH grafting is accompanied by various side reactions including homopropagation of MAH, chain scission and crosslinking of PP macroradical.

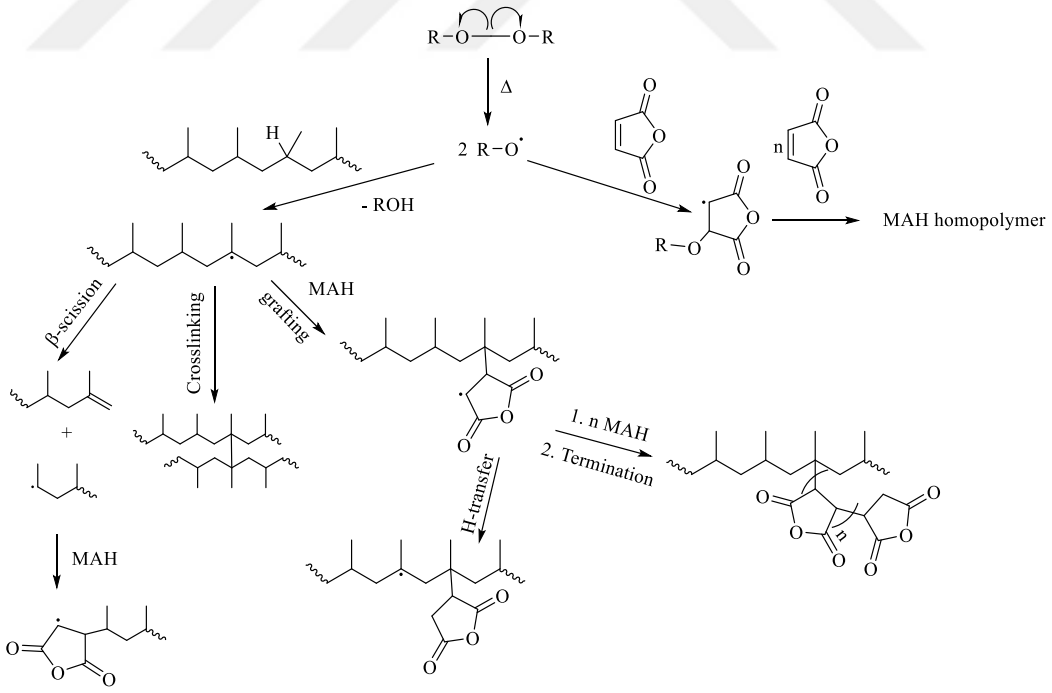


Figure 4.1. Possible free radical grafting mechanism and competing side reactions.

4.1. Analyses of Pristine Atactic Polypropylene Used in the Thesis

In this section, properties of aPP used in the study will be presented before giving results of grafting reactions. Atactic PP used in this study was obtained as a byproduct of iPP manufacturing. As formerly mentioned, this type of aPP is not fully amorphous because it is a blend of PPs with different tacticities and molecular weights [7]. The atactic PP was used without any treatments in grafting reactions. The atactic PP was characterized by means of DSC, FTIR, ^{1}H-NMR and ^{13}C-NMR. The results obtained from DSC analysis of aPP used are shown in Table 4.1. Although the pristine aPP had a single glass transition temperature (T_g) and crystallization temperature (T_c), it had two distinct melting temperatures (T_{m1} and T_{m2}). The crystalline forms are controlled by the inclusion of defects. In general, while short isotactic sequences favor the formation of the γ-form, long isotactic sequences are likely to favor the formation of the α-form [1]. The double melting characteristics might be due to the transition from metastable phase to thermodynamically stable phase. Additionally, the crystal form crystallizing at higher temperatures can initiate nucleation of the other crystal form, so single crystallization temperature can be observed [29]. However, DSC was not adequate to ascertain accurate crystalline structures in the aPP, and further crystallographic analysis techniques such as wide-angle X-ray diffraction were not applied in the scope of this study.

Table 4.1. Thermal properties of aPP used in the study.

T_g (°C)	T_c (°C)	ΔH_c (mJ/mg)	T_{m1} (°C)	ΔH_{m1} (mJ/mg)	T_{m2} (°C)	ΔH_{m2} (mJ/mg)
-30.7	82.8	17.1	109	3.36	149	0.99

FTIR analysis of polypropylene supplies significant information about conformational structures since some FTIR bands are sensitive to stereoregularity. The band at 973 cm^{-1} corresponds to successive five repeat units in an isotactic helix, and it can be attributed to both crystalline and amorphous chains. Furthermore, the FTIR bands at 998 and 841 cm^{-1}

correspond to isotactic helices with 11-12 and 13-14 successive repeat units, and these bands are commonly used for calibrating isotacticity [1]. In Figure 4.2, FTIR spectrum of pristine aPP is shown. The FTIR bands at 997.33 and 841.24 cm^{-1} indicate that aPP contains locally stereoregular sequences. In contrast to fully amorphous aPP, aPP used in the study was not readily soluble in toluene and xylene at room temperature, so ultrasonic waves or heat was required to obtain a clear solution. Once aPP had dissolved, it did not precipitate for a couple of days, but when it was cooled and filtered, insoluble residue was obtained. FTIR spectrum of xylene insoluble part of aPP is shown in Figure 4.2, as well. The peaks at 1167, 997 and 841 cm^{-1} in the spectrum of xylene insoluble part of aPP got sharper when compared to those of pristine aPP. The similar changes in narrowness and sharpness of the peaks were also observed by Garcia *et al*., and Quyn *et al.* showed linear correlation between narrowness and crystallinity of PP [30]. This means that xylene insoluble part was rich in isotactic sequences.

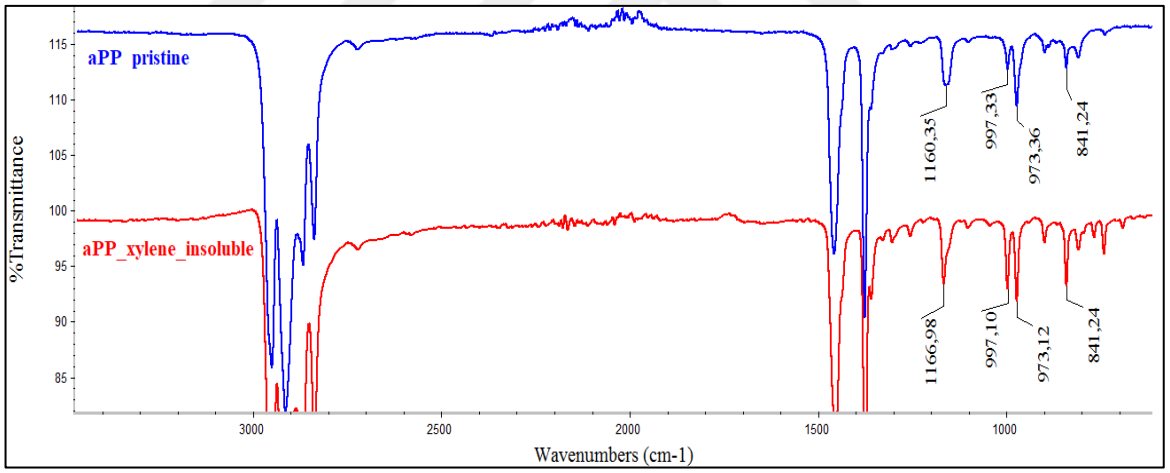


Figure 4.2. FTIR spectra of pristine aPP (top) and xylene insoluble fraction of aPP (bottom).

^{1}H-NMR and ^{13}C-NMR spectra of pristine aPP dissolved in toluene-d_8 are shown in Figure 4.3 and 4.4, respectively. The resolution of ^{1}H-NMR is limited because methyl, methylene and methine protons are chemically similar. The integration of methylene resonance corresponding to *meso* (0.90 and 1.25 ppm) and *racemo* (1.05 ppm) diads allows to recognize predominant tacticity of PP samples [31]. Since these peaks were not well-

resolved in ^{1}H-NMR spectrum of pristine aPP, the overall isotacticity was not determined *via* ^{1}H-NMR. On the other hand, the peaks in the range of 3.27- 6.09 ppm and 0.69 ppm cannot be related to the aPP, but they can belong to co-catalysts. The ^{13}C chemical shifts of methyl, methylene and methine carbons spread over greater range, and consequently ^{13}C-NMR is more sensitive to local structural details. The methyl region of ^{13}C-NMR spectrum is generally preferred for tacticity analysis. FTIR bands already exhibited that the pristine aPP had local isotactic sequences, and the presence of a distinct peak at 21.78 ppm corresponding to mmmm pentad configuration supported the isotactic sequences in the aPP [1], [31].

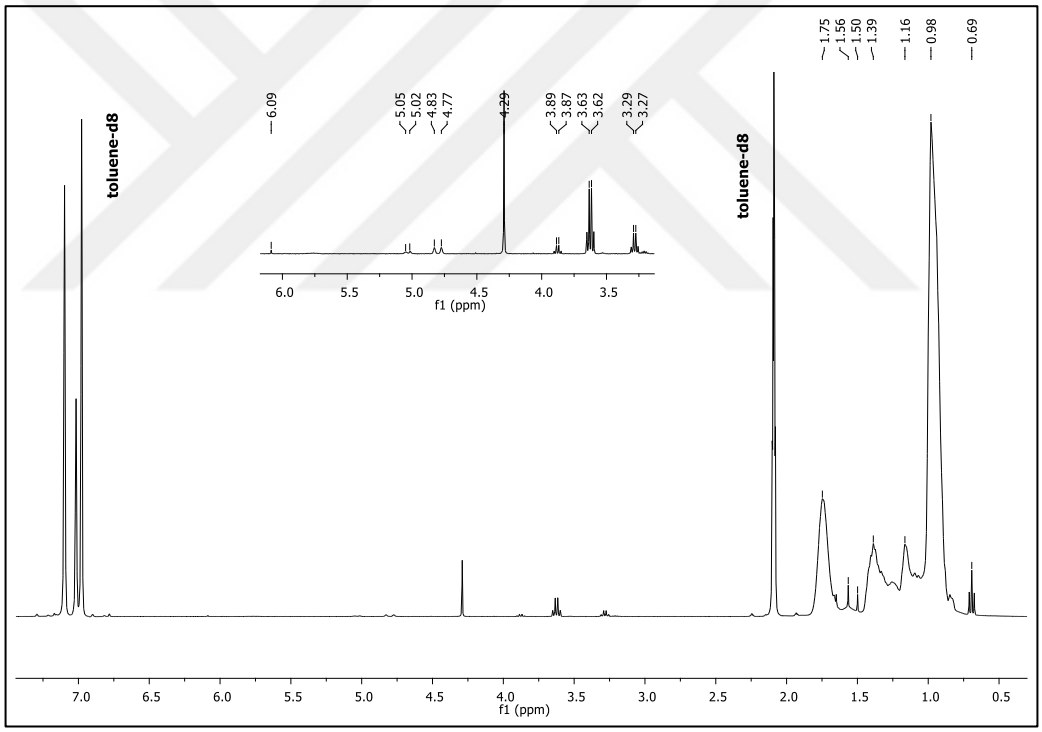


Figure 4.3. ^{1}H-NMR spectrum of aPP used in the study in toluene-d_8.

In Figure 4.5, ^{1}H-NMR spectrum of xylene soluble aPP washed with acetone is shown. The peaks in the range of 3.54- 5.45 ppm were still present. That is, purification steps did not remove completely the catalyst impurities.

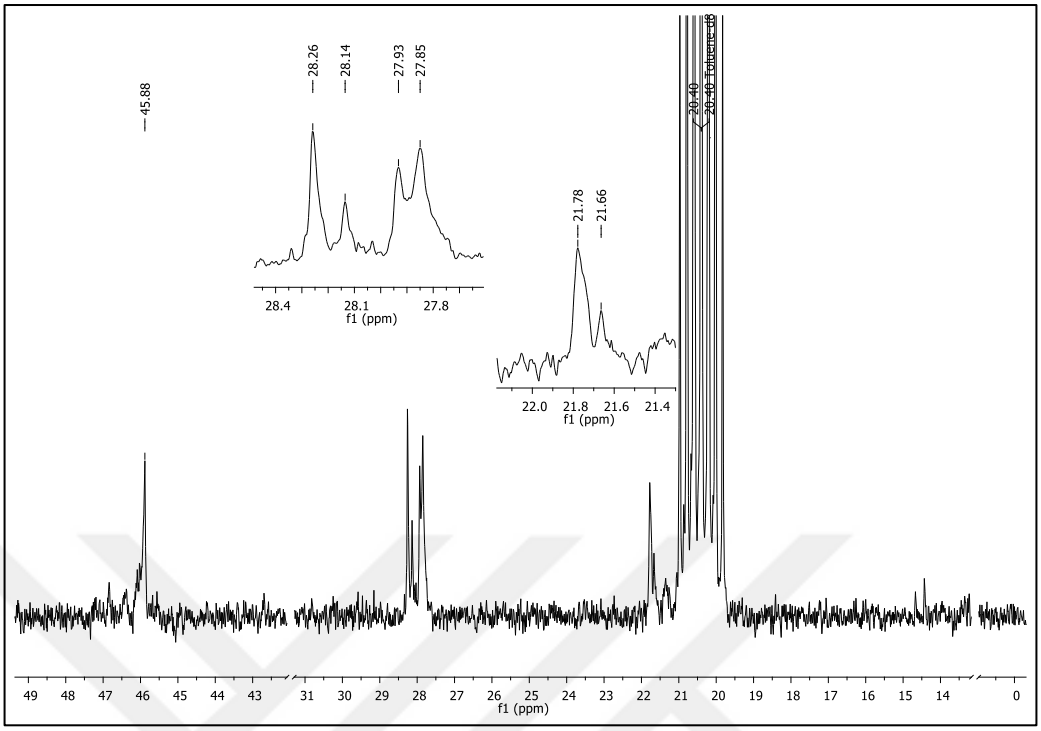


Figure 4.4. ^{13}C-NMR spectrum of aPP used in the study in toluene-d_8.

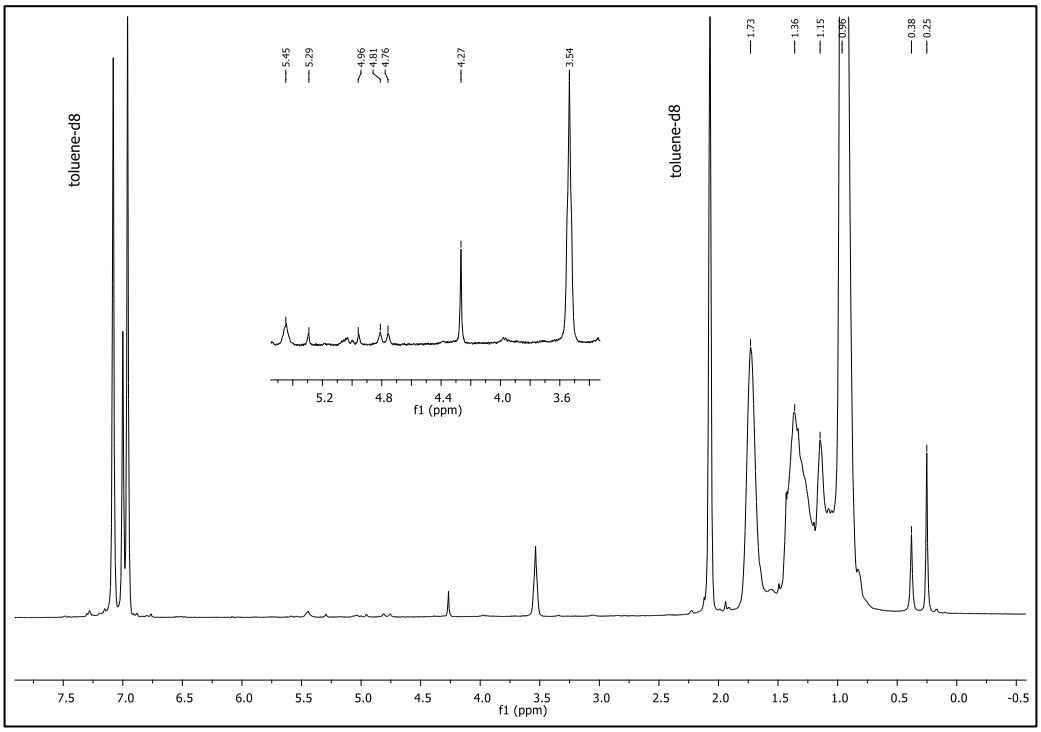


Figure 4.5. ^{1}H- NMR spectrum of acetone washed, xylene soluble aPP in toluene-d_8.

4.2. Free Radical Grafting of MAH onto aPP in Solution

Maleic anhydride grafting onto aPP was performed in solution by changing the reactant ratios at 110 °C for four hours. Results of solution reactions will be presented under two separate titles as control experiments and grafting experiments.

4.2.1. Control Experiments in Solution

Apart from MAH grafting onto aPP, reaction conditions and purification steps can influence properties of the pristine aPP. The atactic PP can undergo chain scission or crosslinking in the presence of peroxides and/or thermal energy. In addition, purification operations performed to get rid of free MAH or MAH oligomers can lead to fractionation of the pristine aPP. Thus, control experiments in solution were carried out to resolve better the effect of grafting.

The modification of aPP was carried out under nitrogen atmosphere to minimize its thermo- and photo-oxidative degradation. While thermo-oxidative degradation of aPP at 110 °C in the absence of the peroxide was evaluated in reaction Blank_aPP, the peroxide-induced degradation of the aPP at 110 °C was evaluated in reaction Blank_aPP+BPO. The presence of peroxide could potentially cause degradation, and thus result in severe molecular weight decrease in aPP. However, both blank reaction products were recovered with almost the same amount (~83%) as shown in Table 4.2 (Entries 2-3). Nearly 17% reactant mixture being probably PP oligomers was soluble in ethanol-toluene solution during purification. Both Blank_aPP and Blank_aPP+BPO had higher T_g, T_c and T_{m1} values than pristine aPP. The removal of oligomers acting like plasticizers and narrower MWD owing to ethanol precipitation can account for higher values measured for the blank reaction products. Nevertheless, there was a decrease in ΔH_c pointing out a decrease in crystalline content, most probably due to the fast precipitation process. Whereas Blank_aPP had higher T_{m2} value than pristine aPP, T_{m2} of Blank_aPP+BPO was considerably lower than that of pristine aPP.

Benzoyl peroxide initiator may induce degradation in regions which are responsible for formation of crystalline phase at T_{m2}.

Table 4.2. Thermal transition values of purified control samples.

Entry No	Experiment Code	T_g (°C)	T_c (°C)	ΔH_c (mJ/mg)	T_{m1} (°C)	T_{m2} (°C)	Recovery (wt. %)
1	Pristine aPP	-30.7	82.8	17.1	109	149	
2	Blank_aPP	-23.4	94.4	16.2	116	151	83.4%
3	Blank_aPP+BPO	-24.0	93.8	14.0	117	147	82.7%
4	Blank_aPP+MAH	-23.4	94.9	16.1	117	151	84.4%

In Figure 4.6, FTIR spectra of pristine aPP, Blank_aPP and Blank_aPP+BPO are shown. Even though blanks had different thermal characteristics from the aPP, there were no major differences among spectra which clarify the change in thermal behavior of the blanks.

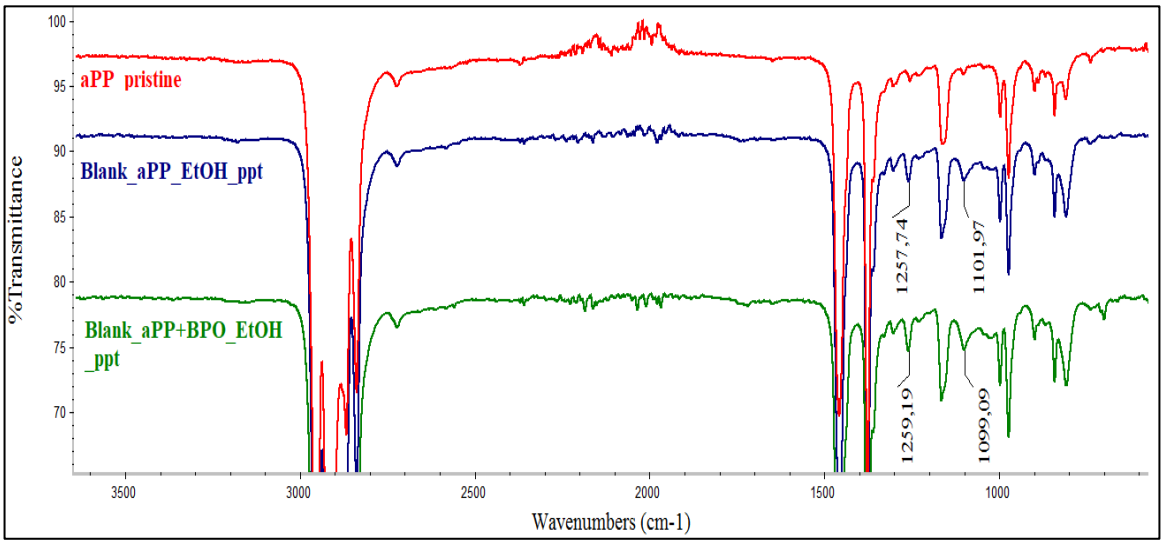


Figure 4.6. FTIR spectra of pristine aPP (top), Blank_aPP (middle) and Blank_aPP+BPO (bottom).

In Figure 4.7, FTIR spectrum of MAH is shown. It had characteristic =C-H stretch at 3128 cm^{-1}, anhydride asymmetrical stretch at 1855 cm^{-1} and anhydride symmetrical stretch at 1775 cm^{-1}, C=C stretch at 1633 cm^{-1}, cis- C=C wag at 698 cm^{-1} [32].

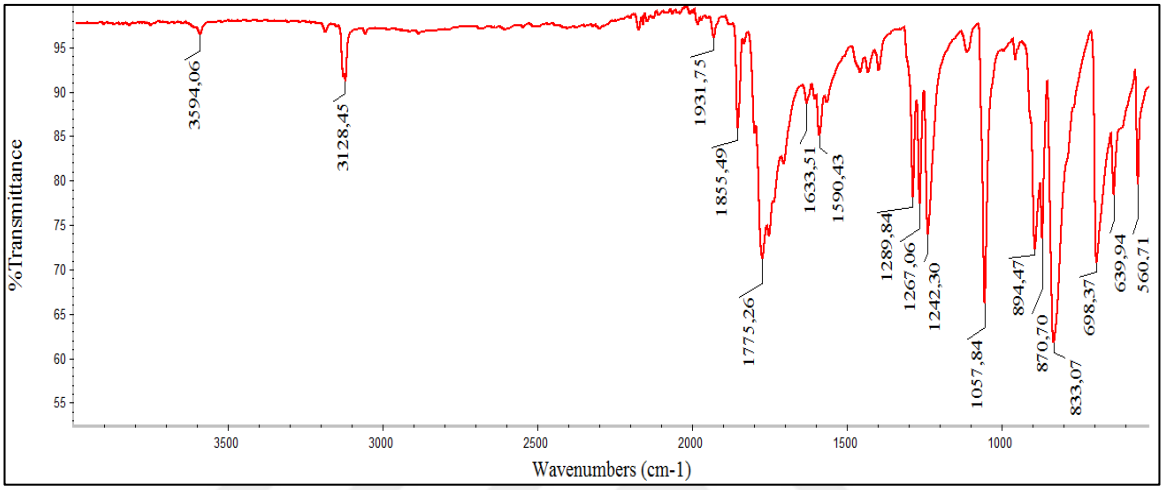


Figure 4.7. FTIR spectrum of MAH.

In Blank_aPP+MAH, MAH was reacted with aPP at 110 °C in the absence of peroxide. This reaction was carried out to learn whether thermo-mechanically induced radicals can initiate MAH grafting onto aPP. Thermomechanically induced radicals are thought as minor source for grafting [12]. Our observations also showed that in the absence of peroxide initiator, MAH grafting onto aPP was not detectable by means of FTIR spectroscopy. The FTIR spectrum of related reaction product is shown in Figure 4.8. The residue obtained from the first precipitation of Blank_aPP+MAH mixture in ethanol had peaks in carbonyl region in FTIR spectrum. Yet, when this residue was washed with ethanol further, peaks in the carbonyl region disappeared. Moreover, there were no peaks associated with anhydride groups in the spectrum, because anhydride groups can react with ethanol to form mono ethyl maleate during ethanol precipitation (Figure 4.9) [32]. The peak at 1739 cm^{-1} was assigned to ester group of mono ethyl maleate, whereas the peak at 1708 cm^{-1} was assigned to carboxylic acid group of mono ethyl maleate. Additionally, the C=C bond in MAH was intact during Blank_aPP+MAH reaction and purification process, so the peak at 1633 cm^{-1} was present. According to thermal transition values of Blank_aPP+MAH shown in Table

4.2, they were comparable with those of Blank_aPP. As a result, the presence of a peak at around 1630 cm^{-1} and the disappearance of peaks in the carbonyl region upon further ethanol wash enabled us to differentiate free MAH which did not chemically bound to aPP backbone.

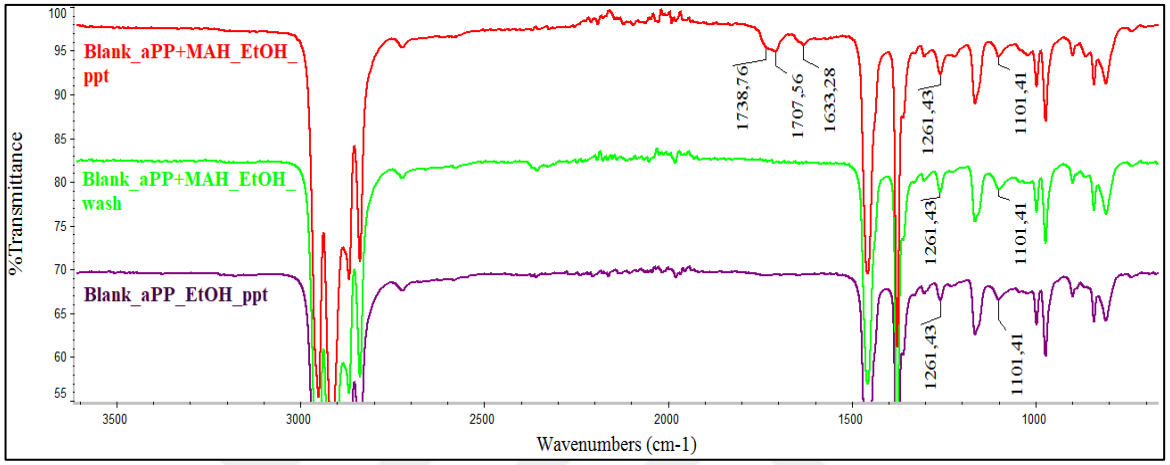


Figure 4.8. FTIR spectra of Blank_aPP+MAH (top), its ethanol wash (middle) and Blank_aPP (bottom).

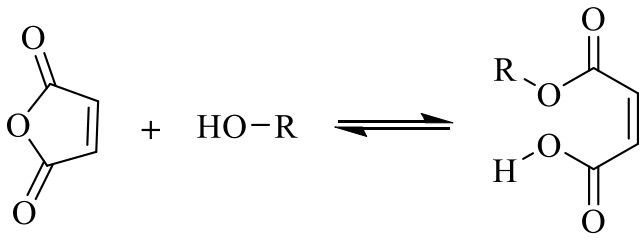


Figure 4.9. Mono-ester formation from MAH during the precipitation into ethanol.

In Blank_MAH+BPO, MAH was reacted with BPO at 110 °C, in the absence of aPP to investigate the homopolymerization potential/extent of MAH. As described in the synthesis section, there were burgundy particles adhered at the bottom of the reaction flask, and they were collected by dissolving in acetone. Upon evaporation of the solvent, brittle burgundy solid was obtained. This product was insoluble in hexane, xylene and toluene but soluble in acetone and tetrahydrofuran. This product when left at ambient conditions for

couple of weeks, got tackier. FTIR spectra of this product and its aged form are shown in Figure 4.10. Blank_MAH+BPO had IR bands at 1852 and 1776 cm^{-1} attributed to anhydride group, and the peak at 1705 cm^{-1} attributed to carboxylic acid group. The product of Blank_MAH+BPO differentiates from MAH because of its appearance and solubility properties despite the presence of common peaks at around 1850, 1770 and 698 cm^{-1}. On the other hand, the aged form had peak at 1705 cm^{-1}, and there was distinct broadness which was attributed to carboxylic acid groups. Thus, most likely, some oligomeric poly (maleic anhydride) was formed and upon aging anhydride groups opened to carboxylic acid groups due to the moisture in air. Ceiling temperature of poly (maleic anhydride) has been reported as 145 °C for 5 M MAH in benzene and 50 °C for 0.1 M MAH in benzene [22]. On the other hand, De Roover *et al*. has shown that MAH can homopolymerize in the absence of solvents at 190 °C [33]. Therefore, Blank_MAH+BPO product could be MAH oligomers because of its appearance and solubility properties.

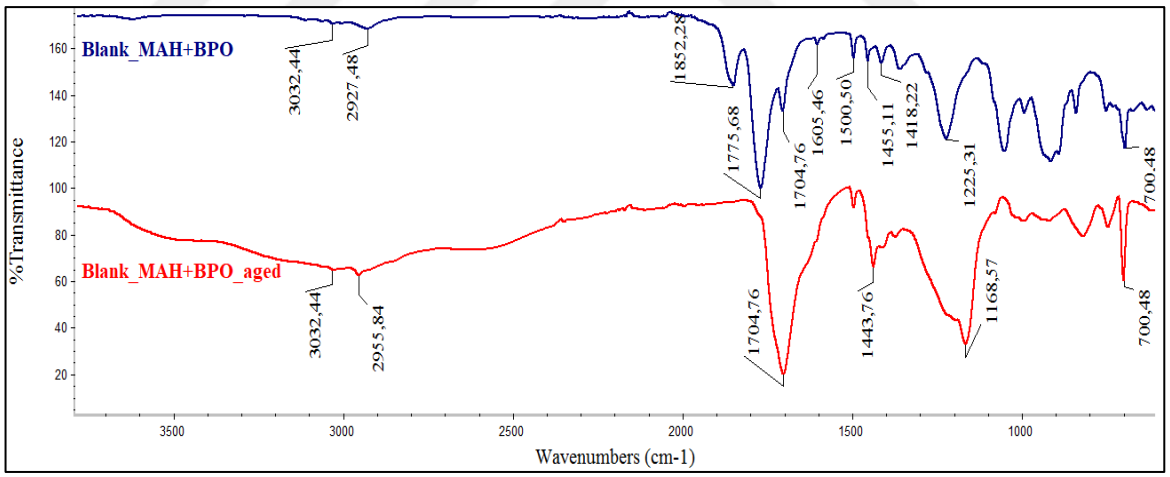


Figure 4.10. FTIR spectra of Blank_MAH+BPO (top) and its aged sample (bottom).

The control experiments in solution showed that:

- Purification steps enabled increase in thermal transition values.
- There was a noticeable decrease in T_{m2} and ΔH_c values in the presence of peroxide initiator.

- In the absence of the peroxide initiator, MAH grafting did not take place, and the presence of the peaks in carbonyl region and around 1630 cm^{-1} in FTIR spectrum indicated the presence of free MAH.
- Upon homopropagation of MAH in the presence of the peroxide, MAH oligomers could form. MAH oligomers could be distinguished by its appearance and solubility behavior.

The control experiments were followed by MAH grafting experiments in solution. The results of grafting reactions will be presented in the next section in the consideration of the outcomes of control experiments.

4.2.2. Maleic Anhydride Grafting Experiments in Solution

The reactions in Table 4.3 were conducted to examine the effect of MAH and BPO reactant ratios on grafting efficiency. Benzoyl peroxide initiated grafting reactions in solution were designated as BIG, and the numbers following BIG code represented the mole ratio of reactant MAH and BPO, respectively. Entries 1-4 show the effect of increasing amount of MAH when BPO mole ratio is kept constant at 0.037. Entries 5 -7 show the effect of increasing amount of MAH when BPO mole ratio is kept constant (approximately 0.07).

In Figure 4.11 FTIR spectra of BIG_0.70/0.037 and its ethanol wash are shown. The residue obtained from ethanol precipitation had a very small peak at around 1637 cm^{-1} which is attributed to double bond of unreacted MAH. This indicates purification was not fully efficient. When this residue washed with ethanol further, the peak at around 1637 cm^{-1} disappeared. Moreover, the area of carbonyl region was diminished because contribution of unbound MAH (or mono ethyl maleate) was lost. Single ethanol precipitation was not enough to get rid of unreacted MAH. Hence, before titrations and DSC analyses all ethanol precipitates were washed thoroughly with ethanol.

Table 4.3. Grafted MAH amounts in purified samples determined by hot titration method.

Entry No	Experiment Code	aPP: MAH: BPO (mole ratio)	$MAH_{grafted}$ (wt. %)
1	BIG_0.30/0.037	1: 0.30: 0.037	2.39
2	BIG_0.50/0.037	1: 0.50: 0.037	2.07
3	BIG_0.70/0.037	1: 0.70: 0.037	1.93
4	BIG_0.90/0.037	1: 0.90: 0.037	1.97
5	BIG_0.30/0.075	1: 0.30: 0.075	2.16
6	BIG_0.49/0.074	1: 0.49: 0.074	2.48
7	BIG-0.90/0.075	1: 0.90: 0.075	2.58

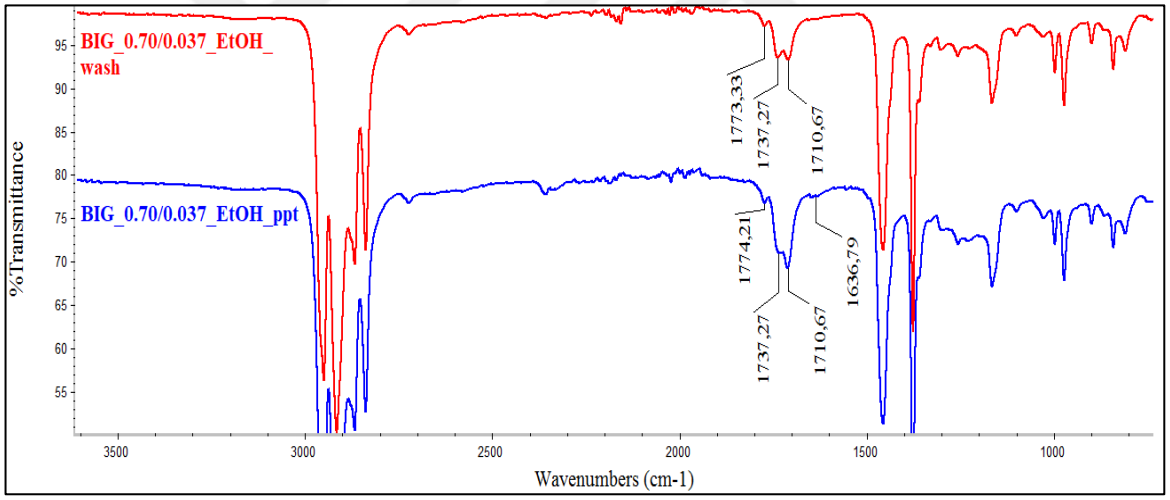


Figure 4.11. FTIR spectra of ethanol precipitate of BIG_0.70/0.037 (bottom) and its ethanol wash (top).

The possible structures of grafted MAH are shown in Figure 4.12. Maleic anhydride grafts can be either single succinic anhydride (SA) or poly (maleic anhydride) as shown in Figure 4.12a and Figure 4.12b, respectively. Some literature studies suggested that poly (maleic anhydride) type grafts had symmetrical C=O stretch at 1784 cm^{-1}, whereas single SA type grafts had symmetrical C=O stretch at 1792 cm^{-1} [34], [35]. However, the products of the present thesis study had an IR band at around 1773 cm^{-1} which can be attributed to

anhydride group coming from grafted MAH. Similarly, commercially available maleic anhydride grafted polypropylene (PP-g-MAH, Product No: 427845) purchased from Sigma-Aldrich had IR bands at 1771 and 1712 cm^{-1} which can be assigned to an anhydride and a carboxylic acid group, respectively (Figure 4.13). The presence of a peak associated with carboxylic acid group can be due to hydrolysis of grafted succinic anhydride to form 1,4-dicarboxylic acid (Figure 4.12c). Additionally, MAH grafted onto aPP can react with ethanol during precipitation to form ethyl hydrogen succinate which has both carboxylic acid and ester groups (Figure 4.12d). In the FTIR spectrum of purified BIG_0.70/0.037 sample, the peaks at 1737 and 1711 cm^{-1} were attributed to ester and carboxylic acid group of ethyl hydrogen succinate grafted onto aPP.

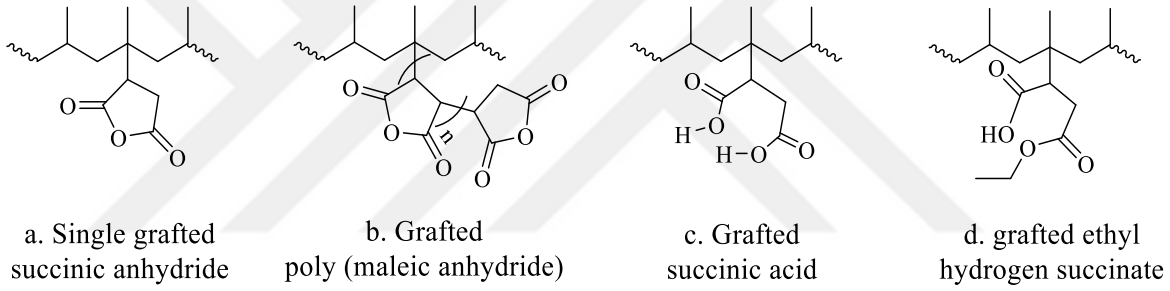


Figure 4.12. Possible structures of MAH grafted onto aPP.

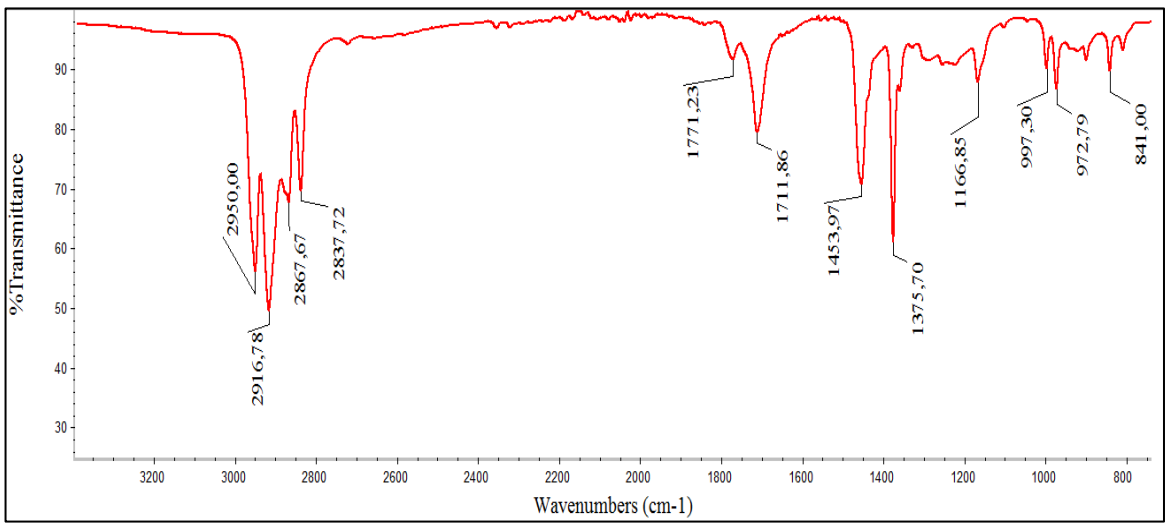


Figure 4.13. FTIR spectrum of commercial PP-g-MAH.

After all reaction mixtures were precipitated in ethanol, their filtrates were saved and evaporated under vacuum at 40 °C to get rid of solvent. As a result, sticky and yellowish products were obtained. In Figure 4.14, FTIR spectrum of ethanol filtrate of BIG_0.70/0.037 sample is shown. This spectrum was very similar to spectrum of Blank_MAH+BPO but the spectrum of the filtrate had also a distinct peak at 1633 cm^{-1}, probably coming from intact double bound of unreacted MAH. Hence, we can conclude that MAH grafting onto aPP were accompanied by MAH homopolymerization.

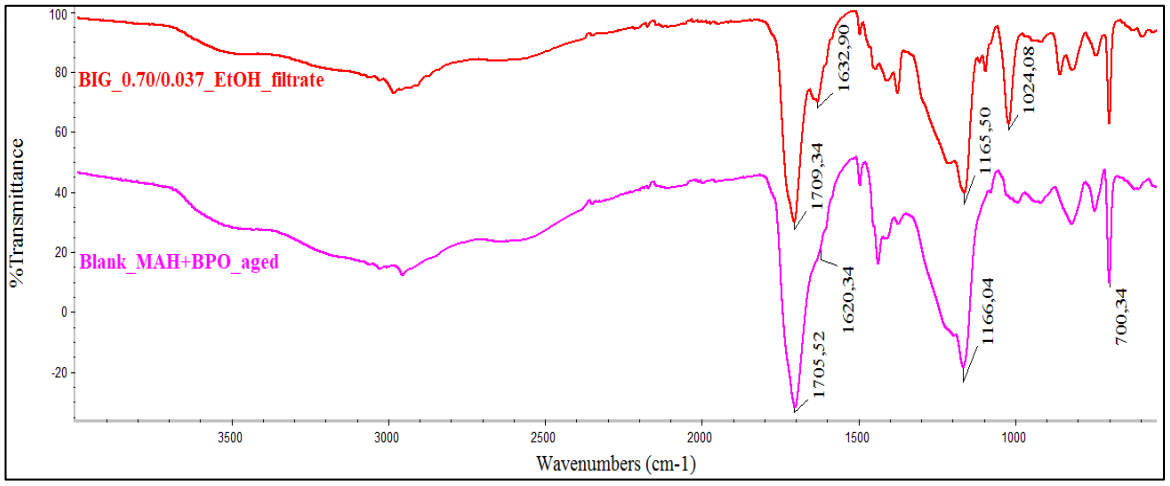


Figure 4.14. FTIR spectra of BIG_0.70/0.037 ethanol filtrate and Blank_MAH+BPO aged form.

In order to quantify the concentration of MAH grafted onto PP, acid-base titration can be performed, or FTIR spectroscopy can be used as a quantitative tool. When FTIR spectroscopy is chosen as quantification method, the construction of a calibration curve is necessary. Since single succinic anhydride type grafts or poly (maleic anhydride) type grafts can be generated upon MAH grafting, various concentrations of succinic anhydride and poly (maleic anhydride) are physically mixed within molten PP to build a calibration curve. However, instead of succinic anhydride, succinic anhydride bound to hydrocarbon chain such as n-octadecyl succinic anhydride is used due to sublimation problem of succinic anhydride at high temperatures [34], [36]. Moreover, all the grafted MAH should be in the anhydride state to simplify FTIR spectrum. The cyclization of dicarboxylic acid groups

(Figure 4.12c) and ester-carboxylic acid groups (Figure 4.12d) can be achieved by keeping under vacuum at elevated temperatures (110 °C, 24 h). Sclavons *et al.* also showed that longer heat treatment times under vacuum (100 °C, 60 h) led to thermo-oxidative degradation of the sample and the appearance of FTIR bands at around 1715-1720 cm^{-1}, so milder conditions should be applied to accomplish cyclization [35]. Due to these complications this method was not used in the present study.

On the other hand, since acid-base titration does not necessitate using standards, hot titration method was applied to quantify concentration of grafted MAH in purified samples in the current study. Obtained results are shown in Table 4.3. When BPO mole ratio was 0.037, increase in MAH load did not increase grafting yield, and BIG_0.30/0.037 gave the maximum grafting. However, when BPO mole ratio was increased to 0.07, grafted MAH increased with increasing MAH load and BIG_0.90/0.075 gave the maximum grafting. When BPO mole ratio was 0.037, the reaction mixture became reddish or burgundy particles stuck on walls of the flask with increasing MAH load. These observations support that increasing MAH load favored oligomerization of excess MAH, because there were not enough aPP macroradicals to react with MAH when BPO concentration was low. On the other hand, when BPO concentration was high, more aPP macroradicals could be generated to react with MAH, so MAH grafting competed with MAH oligomerization. However, it is important to state that our work showed that acid-base titration method may not be reliable because precipitate formation by the addition of titrant ethanolic KOH was observed during the titrations. Hot aromatic solvents necessary for polyolefin solubilization can lead to precipitation of mineral base (KOH) and acid (HCl) during titration. In addition, acidic and basic solutions are prepared in ethanol instead of water, because water and aromatic solvents (toluene and xylene) are immiscible. Hence, addition of ethanol into polymer solution can transform carboxylic acid groups to ester, and this leads to incorrect results. Likely, ethanol is a bad solvent for polypropylene, and this also leads to precipitation of polymer during titration. Sclavons *et al.* showed that the use of organic base (tetra-butylammonium hydroxide) as titrant gives reproducible results for quantification of MAH grafted onto PP [35]. However, titrations by using organic base as titrant were not tried within the time limit of this thesis. In contrast to pristine aPP, purified BIG samples were not soluble in toluene or xylene at ambient temperatures, but they were soluble at high temperatures. Nevertheless, their NMR spectra performed at 80 °C in toluene-d_8 were not resolved enough to use NMR

as a quantitative tool. Therefore, optimization of the quantification methods can be subject of future studies.

Table 4.4. Thermal properties of purified samples determined by DSC.

Entry No	Experiment Code	T_g (°C)	T_c (°C)	ΔH_c (mJ/mg)	T_{m1} (°C)	T_{m2} (°C)
1	Pristine aPP	-30.7	82.8	17.1	109	149
2	Blank_aPP	-23.4	94.4	16.2	116	151
3	Blank_aPP+BPO	-24.0	93.8	14.0	117	147
4	BIG_0.30/0.037	-22.1	91.9	17.1	115	145
5	BIG_0.50/0.037	-21.6	91.7	17.4	116	144
6	BIG_0.70/0.037	-20.2	94.0	15.2	118	145
7	BIG_0.90/0.037	-20.4	95.1	13.5	118	145
8	BIG_0.30/0.075	-20.6	90.7	15.5	113	142
9	BIG_0.49/0.074	-27.4	89.3	12.9	115	140
10	BIG_0.70/0.075	-19.1	89.4	19.6	114	141
11	BIG_0.90/0.075	-21.1	92.8	13.8	117	141

DSC analyses of purified samples were performed to understand the impact of grafting on thermal properties. Free radical grafting of aPP competes against chain scission. Severe chain scission leading to decrease in molecular weight can affect thermal properties of grafted aPP adversely. Decrease in molecular weight due to chain scission can lead to decrease in T_g, T_c and T_m values. Nonetheless, grafted MAH can increase intermolecular forces among polymer chains, and T_g can increase. Or, grafting in crystalline regions of aPP can decrease T_c and T_m since it can prevent lamellar packing. Hence, the interpretation of thermal properties is complicated by only means of DSC. Moreover, the unreliable MAH grafting degree determined by titration obstructed to establish a correlation between thermal properties and degree of MAH grafting. Table 4.4. shows the results obtained from the DSC analyses. These samples had higher T_g, T_c and T_{m1} values when compared to pristine aPP. Yet, to investigate MAH grafting and reaction conditions on aPP, these samples should be

compared with blanks. When BPO mole ratio was 0.037, all samples had higher T_g than blanks. While discussing T_g increase in blanks, it was associated with removal of oligomers and narrower MWD. The further increase in T_g in these grafted samples may arise from increased intermolecular forces among chains owing to polar MAH incorporation. On the other hand, these samples had lower T_{m2} values than Blank_aPP+DCP although they contained the same amount of BPO. This additional decrease in T_{m2} value may take place because grafted moieties can disrupt lamellar packing. When BPO mole ratio was 0.07, all samples had higher T_g than blanks except BIG_0.49/0.074 sample. Also, when BPO mole ratio was 0.07, there was drastic decrease in T_{m2} value, which may be originated from pronounced chain scission.

4.3. Free Radical Grafting of MAH onto aPP in Melt

Although MAH grafting onto aPP in solution may be carried out more efficiently than in melt due to better homogeneity, the use of large volume of solvent does not make grafting in solution convenient for industrial applications. Therefore, MAH grafting onto aPP was attempted in melt conditions. Bulk reactions were initiated by dicumyl peroxide (DCP) instead of BPO. The thermal decomposition of BPO which is highly exothermic is accompanied by the evolution of CO_2 (Figure 4.15). Hence, the lack of heat dissipation and pressure can lead to explosions in the closed melt system [37]. Pristine aPP which had two melting points at 109 and 149 °C was viscous enough at 130 °C. Increasing reaction temperature above T_{m2} not only enables effective mixing and decomposition of the initiator but also increases sublimation of MAH. Therefore, free radical grafting of MAH in melt was carried out at 130 °C. However, when the reaction was carried out for 30 minutes at 130 °C, purified samples *via* ethanol precipitation did not have any peaks at carbonyl region in their FTIR spectra (Figure 4.16). Furthermore, grafted MAH amounts determined by titration were negligible (Table 4.5). Details about these analyses are given in the next paragraph.

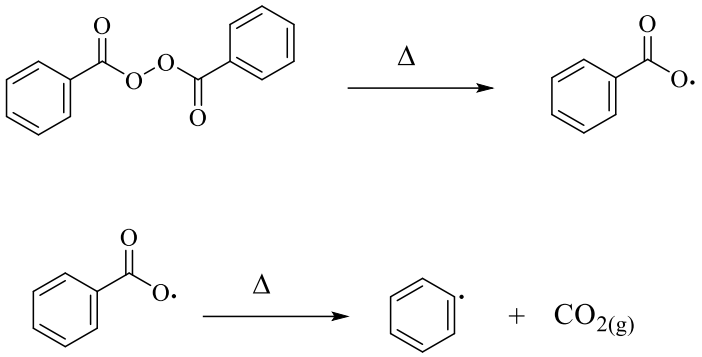


Figure 4.15. Mechanism of BPO decomposition.

Table 4.5. Details of melt reactions and grafted MAH amounts determined by hot titration.

Entry No	Experiment Code	aPP: MAH: DCP (phr)	$MAH_{grafted}$ (wt. %)
1	MAG_10/0.5	100: 10: 0.5	0.30
2	MAG_10/1	100: 10: 1	0.24
3	MAG_10/2	100: 10: 2	0.32
4	MAG_10/3	100: 10: 3	0.49
5	MAG_20/1	100: 20: 1	0.23

The spectrum of MAG_10/0.5 had peaks at around 1854 and 1783 cm^{-1} which were attributed to an anhydride group, but the residue obtained after purification did not have any peaks in carbonyl region. That is, MAH grafting did not happen or MAH grafted aPP was in filtrate, so the filtrates of MAG reactions were examined by FTIR spectroscopy. MAG_10/0.5_EtOH_filtrate had a broad peak in carbonyl region (1720 cm^{-1}) but it had also a peak at 1634 cm^{-1} which belonged to C=C stretching of MAH (Figure 4.16). The presence of a peak at around 1630 cm^{-1} attributed to C=C stretching of unbound MAH (or MAH ester formed upon ethanol precipitation) indicates that ethanol filtrates of MAG reactions could be physical blend of aPP and MAH (or MAH ester). Also, since FTIR bands of MAG filtrates could not attributed to MAH oligomers, it can be said that DCP did not initiate MAH homopropagation at melt conditions. The reason for not detecting both homopolymerization and grafting of MAH could be low decomposition rate of DCP at 130 °C in 30 min. The

half-life of BPO at 91 °C is one hour whereas the half-life of DCP at 135 °C is one hour. Since the half-life of a peroxide does not depend on its concentration, decomposition rate can be accelerated by increasing reaction temperature. However, increasing reaction temperature increases MAH sublimation as well. Therefore, melt reactions were continued with modified MAH at higher temperatures.

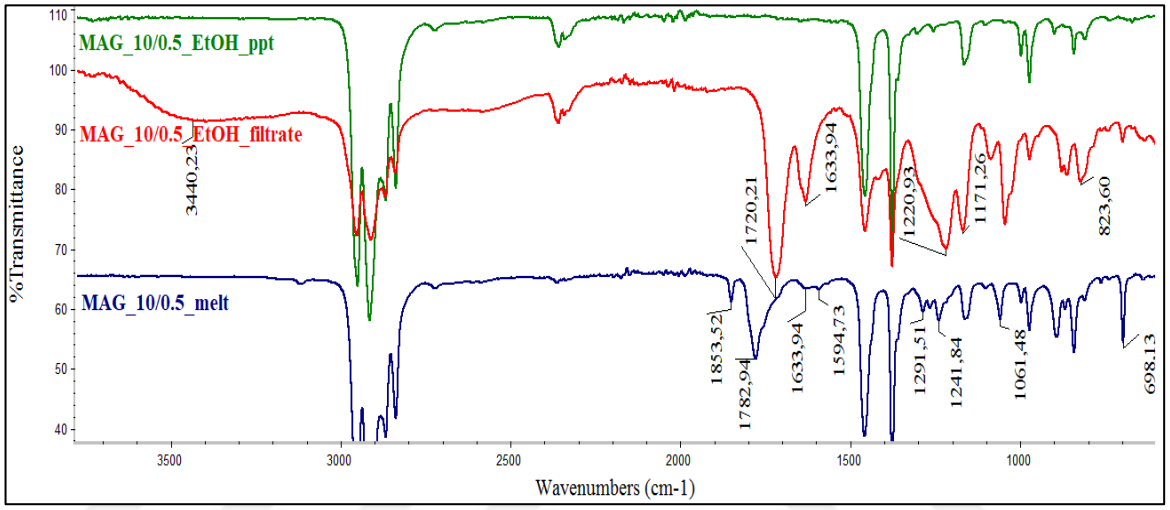


Figure 4.16. FTIR spectra of ethanol precipitate (top), ethanol filtrate (middle) of MAG_10/0.5 and itself (bottom).

4.4. Free Radical Grafting of mMAH onto aPP in Melt

Maleic anhydride grafting in melt was not efficient due to the immiscibility of MAH in aPP, low decomposition rate of DCP at 130 °C and MAH sublimation. To overcome sublimation problem and to make it compatible with molten aPP, MAH was modified. X, Y and Z locations of MAH are prone to various reactions to modify it for melt grafting reactions (Figure 4.17). In this study, modified MAH was designated as mMAH formed upon one of the possible reactions.

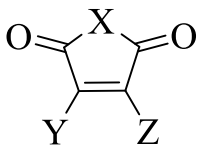


Figure 4.17. Reactive locations of MAH.

4.4.1. Control Experiments for mMAH Grafting in Melt

Sublimation problem of MAH was overcome thanks to modification of MAH. In this way, melt grafting reactions could be carried out at elevated temperatures. However, increase in temperature can affect properties of pristine aPP, so control experiments in the presence and absence of peroxide were carried out. Thermal properties of purified control samples are shown in Table 4.7. Except Blank_mMAH_T_1, the rest was purified with ethanol precipitation. Blank_mMAH_T_1 was purified with Soxhlet extraction with acetone. aPP_2nd batch was not purified.

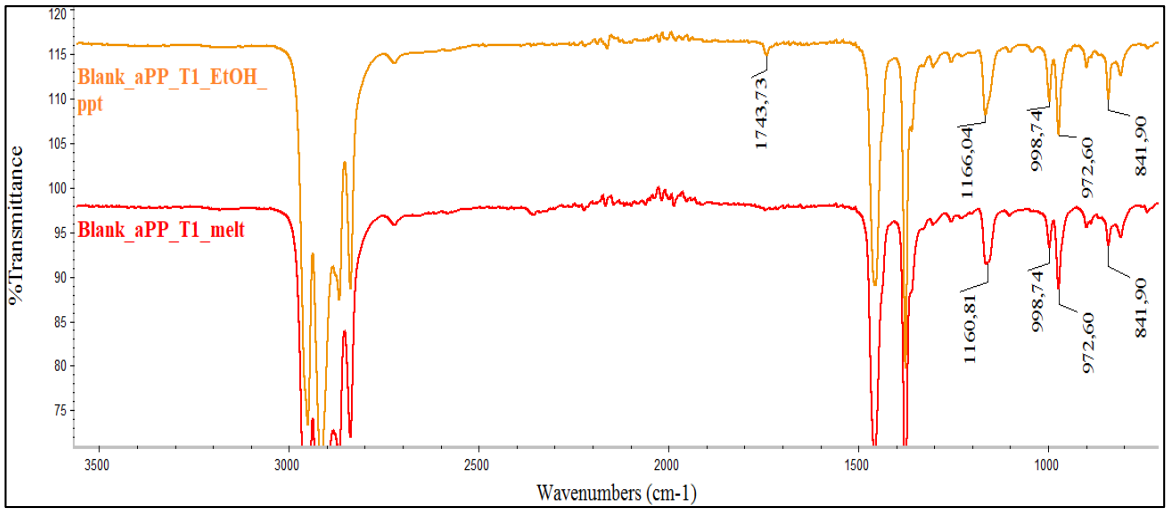


Figure 4.18. FTIR spectra of purified (top) and unpurified (bottom) Blank_ aPP_T_1.

Table 4.6. Thermal properties of purified control samples.

Entry No	Experiment Code	T_g (°C)	T_c (°C)	ΔH_c (mJ/mg)	T_{m1} (°C)	T_{m2} (°C)	Recovery (wt. %)
1	aPP_2nd batch	-34.2	83.5	17.1	112	148	
2	Blank_aPP_T_1	-20.0	95.6	20.0	119	151	66.7
3	Blank_DCP_T_1	-20.2	95.0	18.3	118	150	61.5
4	Blank_mMAH_T_1	-34.5	83.1	20.8	111	143	61.4
5	Blank_aPP_T_1+5	-20.8	93.3	19.7	118	152	58.3
6	Blank_DCP_T_1+5	-20.3	94.8	17.8	118	150	62.5

In reaction Blank_aPP_T_1, aPP was heated alone at T_1 °C. This reaction mixture was recovered with 66.7 % yield. This yield was lower than that of solution blanks. The decrease in recovery yield might arise from aPP thermal degradation. Moreover, another factor affecting decrease in recovery yield can be aPP used could be already decomposed because of atmospheric conditions (air, light, and heat). aPP used in modified MAH grafting reactions was yellowish, but its FTIR spectrum was the same as the first batch although its T_g was lower (Table 4.6, entry 1). In Figure 4.18, FTIR spectra of purified and unpurified samples of Blank_aPP_T_1 are shown. Upon purification, the peaks at around 1166, 998, 973 and 841 cm^{-1} became sharper owing to increase in crystalline ratio. Also, a weak but distinct peak at about 1744 cm^{-1} was present. The presence of this peak can reveal thermo-oxidation of aPP despite N_2 purge. As showed in Table 4.7, thermal transition temperatures of purified Blank_aPP_T_1 were higher when compared to aPP_2nd batch. The same changes upon purification were common in spectra of Blank_aPP_T_1+5 sample. When compared to Blank_aPP_T_1, thermal transition values of Blank_aPP_T_1+5 were slightly lower.

The reactions of Blank_DCP_T_1 and Blank_DCP_T_1+5 were carried out to evaluate peroxide-induced degradation of aPP at T_1 °C and T_1+5 °C, respectively. When compared to blanks of Blank_aPP_T_1 and Blank_aPP_T_1+5, there was no correlation between the presence of DCP and recovery yields, but T_{m2} value was lower in blanks containing DCP, most probably due to the peroxide-induced chain scission. In contrary to melts of Blank_aPP_T_1 and Blank_aPP_T_1+5, DCP containing blanks had IR bands at 763 and 699

cm^{-1}, which were attributed to undecomposed DCP. Upon purification, the peak at about 1744 cm^{-1} appeared, and the peaks at 763 and 699 cm^{-1} disappeared (Figure 4.19).

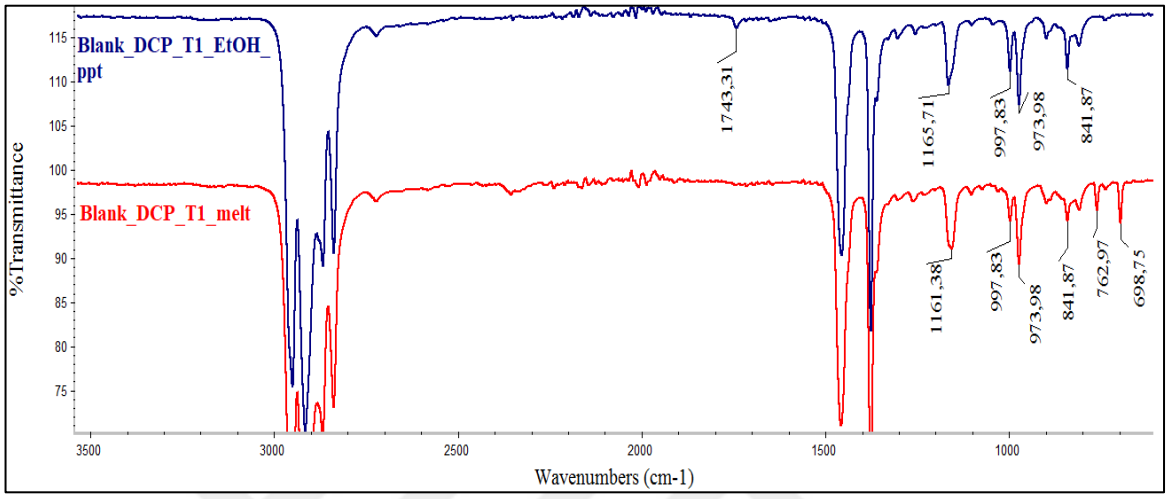


Figure 4.19. FTIR spectra of purified (top) and unpurified (bottom) samples of Blank_DCP_T_1

In reaction Blank_mMAH_T_1, aPP was mixed with mMAH in the absence of initiator. During mixing, no sublimation was observed. Blank_mMAH_T_1 dissolved in toluene did not precipitate well in ethanol so filtrate part was slightly blurry. Thus, to get rid of unreacted mMAH, Soxhlet extraction with acetone was performed. In Figure 4.20, FTIR spectra of purified and unpurified samples of Blank_mMAH_T_1 were shown. In purified sample of Blank_mMAH_T_1 , there were no peaks in carbonyl region. This shows that mMAH does not add to aPP in the absence of a radical initiator.

Although mMAH was not chemically bound to aPP, the carbonyl peaks of unpurified Blank_mMAH_T_1 were different from mMAH. In the presence of unreacted mMAH, the peak at around 1166 cm^{-1} was sharp and intense (Figure 4.20). The shape of this peak can be distinctive in the determination of unbound mMAH in aPP. Thermal properties of purified Blank_mMAH_T_1 were appearently worse than aPP_2^{nd} batch as shown in Table 4.7. Since purification might not be accomplished by means of Soxhlet extraction, and impurities which

cannot be detected by FTIR spectroscopy, were present in the analyzed sample. Thus, Blank_mMAH_T_1 purified sample had lower thermal transition values.

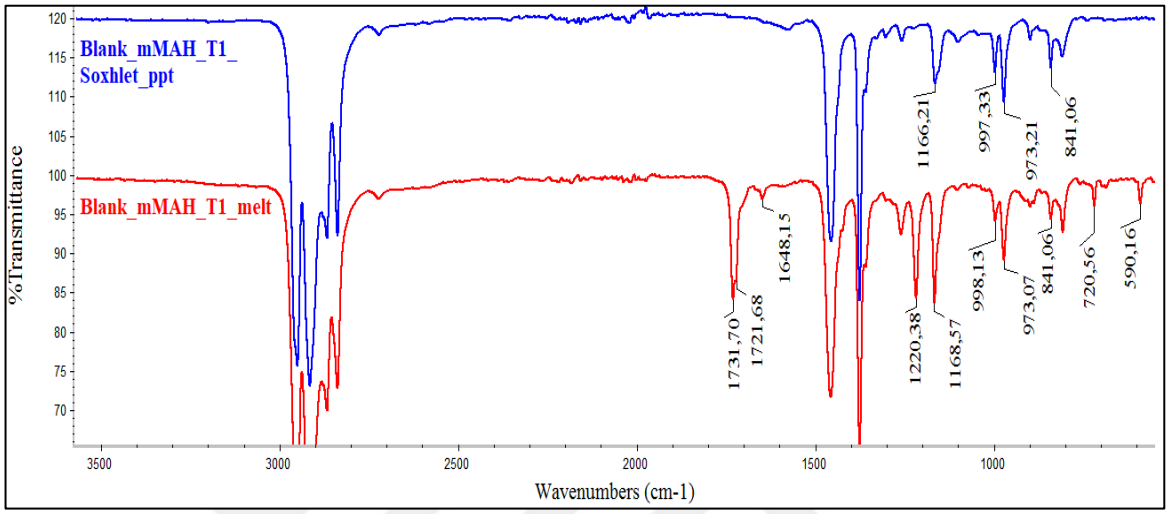


Figure 4.20. FTIR spectra of purified (top) and unpurified (bottom) samples of Blank_mMAH_T_1.

Experiments shown in Table 3.3 were carried out to investigate the effect of reaction time, temperature and reactant ratio on mMAH grafting onto aPP. As opposed to the direct MAH grafting reactions in solution and in melt, melts of mMAH grafting reactions dissolved in hot xylene (or toluene) but did suspend in ethanol, so the precipitation step was not efficient. We believe that noticeable chain scission during grafting leading to shorter polymer chains, high grafting degree leading to increased hydrophilicity, or combination of both can be reasons for the formation of suspension during purification. Analyses by means of GPC or MFR were required to characterize chain scission but they were not performed in this study. Therefore, the effect of reaction parameters on grafting was investigated based on FTIR spectra of unpurified samples.

4.4.2. Effect of Time on mMAH Grafting in Melt

To examine the effect of reaction time on grafting at T_1 ºC, reactions with duration of t_0+10 min, t_0+20 min, t_0+30 min, t_0+45 min and t_0+60 min were carried out where other parameters were held constant. In Figure 4.21, FTIR spectra of the melts of t_0+10 min, t_0+30 min and t_0+60 min reactions are shown. Comparisons between IR bands revealed that optimum reaction time was t_0+30 min when mMAH concentration was 10 phr and DCP concentration was 3 phr at T_1 °C. When reaction time was short (i.e t_0+10 min), unreacted mMAH peaks were dominant, which were sharp and strong peaks at 1732 cm^{-1}, 1222 cm^{-1} and 1167 cm^{-1}, and distinct peaks at around 720 cm^{-1} and 590 cm^{-1}. Also, the presence of the peak at about 1648 cm^{-1} implied unreacted mMAH. As reaction time increases, the peaks related to unreacted mMAH disappeares. Grafted mMAH shows peaks at around 1770 cm^{-1}, 1735 cm^{-1} and 1710 cm^{-1}. There were no apparent differences between FTIR spectra belonging to t_0+30 min and t_0+60 min reactions and thus, t_0+30 min was considered as an optimum reaction time at the specified reaction conditions.

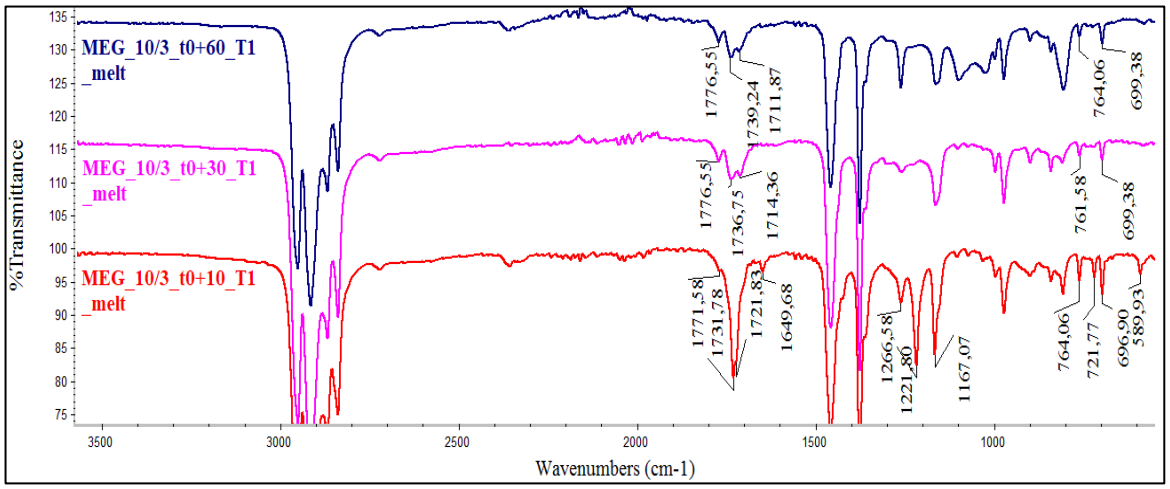


Figure 4.21. FTIR spectra of MEG_10/3_t_0+60_T_1 (top), MEG_10/3_t_0+30_T_1 (middle), MEG_10/3_t_0+10_T_1 (bottom).

When reaction temperature was changed to T_1+5 °C, again reactions with duration of t_0+10 min, t_0+20 min, t_0+30 min, t_0+45 min and t_0+60 min were carried out where other parameters were held constant. In Figure 4.22, FTIR spectra of the melts of t_0+10 min, t_0+30 min and t_0+60 min reactions are shown. When reaction time was t_0+10 min, mMAH peaks were very strong. As reaction time increased, carbonyl region became more like grafted mMAH. The distinct difference between t_0+30 min and t_0+60 min reactions was the disappearance of undecomposed DCP peaks as reaction time increased. Yet, there was no distinct difference between carbonyl regions. Thus, there was no need to increase reaction time since it can lead to undesirable side reactions and degradation. Comparisons between IR bands revealed that optimum reaction time was t_0+30 min when mMAH concentration was 10 phr and DCP concentration was 3 phr at T_1+5 °C.

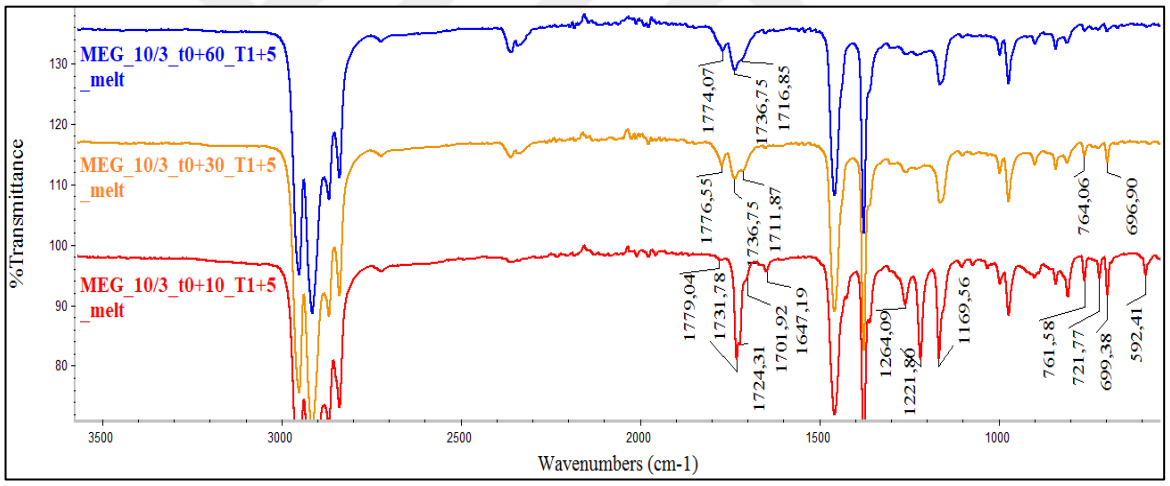


Figure 4.22. FTIR spectra of MEG_10/3_t_0+60_T_1+5 (top), MEG_10/3_t_0+30_T_1+5 (middle), MEG_10/3_t_0+10_T_1+5 (bottom).

4.4.3. Effect of Initiator Concentration on mMAH Grafting in Melt

To optimize DCP concentration at T_1 °C, reactions with DCP concentration of 1 phr, 3 phr and 5 phr were carried out. In Figure 4.23, FTIR spectra of the melts of corresponding reactions were shown. When DCP concentration was 1 phr, unreacted mMAH peaks were

strong. That is, when mMAH concentration was 10 phr, this amount of DCP did not provide enough radical concentration to graft mMAH. When DCP concentration was 5 phr, there were peaks related to undecomposed DCP, which were at around 760 cm^{-1} and 699 cm^{-1}. Therefore, the optimum DCP concentration at T_1 °C was determined as 3 phr (MAH concentration was 10 phr and reaction time t_0+30 min).

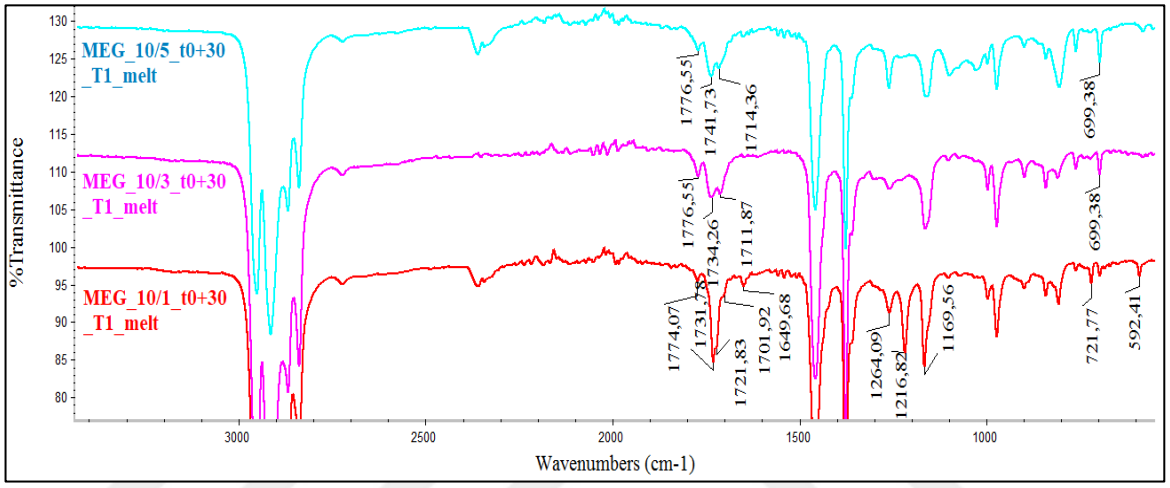


Figure 4.23. FTIR spectra of MEG_10/5_t_0+30_T_1 (top), MEG_10/3_t_0+30_T_1 (middle), MEG_10/1_t_0+30_T_1 (bottom).

Similarly, to optimize DCP concentration at T_1+5 °C, reactions with DCP concentration of 1 phr, 3 phr and 5 phr were carried out. In Figure 4.24, FTIR spectra of the melts of corresponding reactions were shown. When IR spectra were examined, the optimum DCP concentration at T_1+5 °C was found as 1 phr (when mMAH concentration was 10 phr and reaction time t_0+30 min). In contrast to equivalent reaction at T_1 °C, at T_1+5 °C with the DCP concentration of 1 phr, pattern of mMAH FTIR bands was like grafted. That is, increasing temperature by 5 °C , enabled grafting with less amount of DCP. On the other hand, when DCP concentration was increased, there were no explicit difference in carbonyl region, but there were peaks pointing out undecomposed DCP.

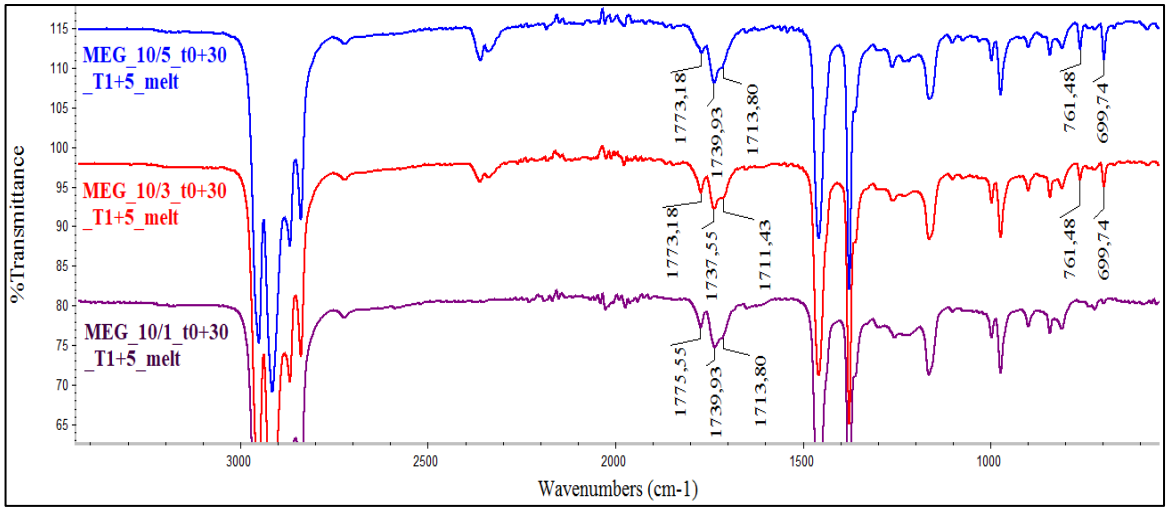


Figure 4.24. FTIR spectra of MEG_10/5_t_0+30_T_1+5 (top), MEG_10/3_t_0+30_T_1+5 (middle), MEG_10/1_t_0+30_T_1+5 (bottom).

4.4.4. Effect of mMAH concentration on mMAH Grafting in Melt

To optimize mMAH concentration at T_1 °C, reactions with mMAH concentration of 5 phr, 10 phr and 15 phr were carried where when other parameters were held constant. In Figure 4.25, FTIR spectra of the melts of corresponding reactions are shown. As mMAH concentration was increased, area of carbonyl region was increasing. In addition, the shape of the peaks was like grafted mMAH. However, when mMAH concentration was 15 phr, there was a peak at around 1648 cm^{-1} indicating the presence of unreacted mMAH. Therefore, when DCP concentration was 3 phr and reaction time t_0+30 min, the optimum mMAH concentration was determined as 10 phr at T_1 °C.

To determine optimum mMAH concentration at T_1+5 °C, reactions with MAE concentration of 5 phr, 10 phr and 15 phr were carried out. FTIR spectra of corresponding reactions were shown in Figure 4.26. The optimum mMAH concentration was found as 10 phr, when FTIR spectra were analyzed. When mMAH concentration was 15 phr, unreacted mMAH peaks were dominant. When mMAH concentration was 5 phr, the area of carbonyl region was small. Increasing mMAH concentration from 5 phr to 10 phr increased area of carbonyl region, and the pattern was like grafted mMAH.

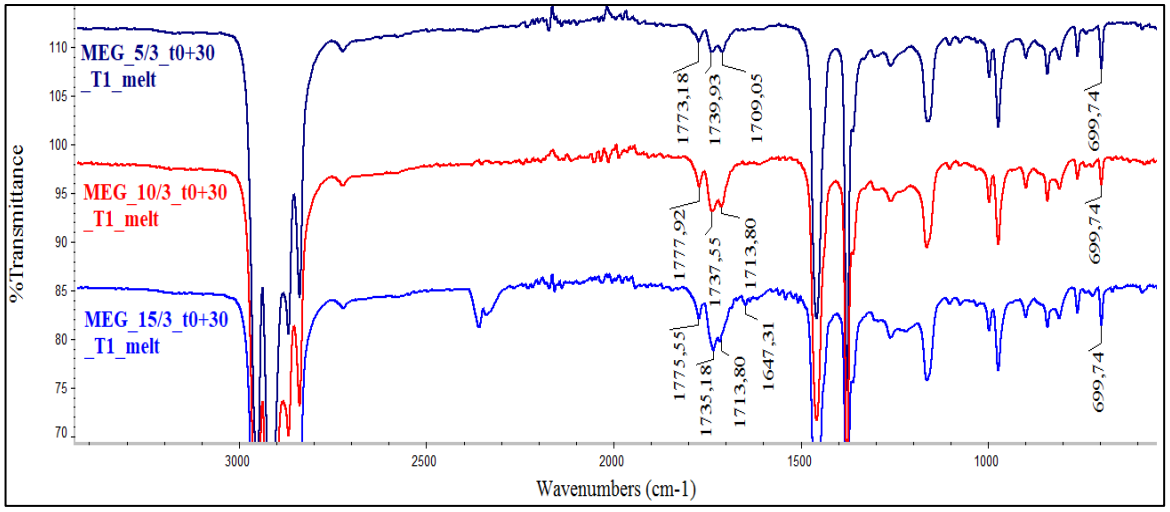


Figure 4.25. FTIR spectra of MEG_5/3_t_0+30_T_1 (top), MEG_10/3_t_0+30_T_1 (middle), MEG_15/3_t_0+30_T_1 (bottom).

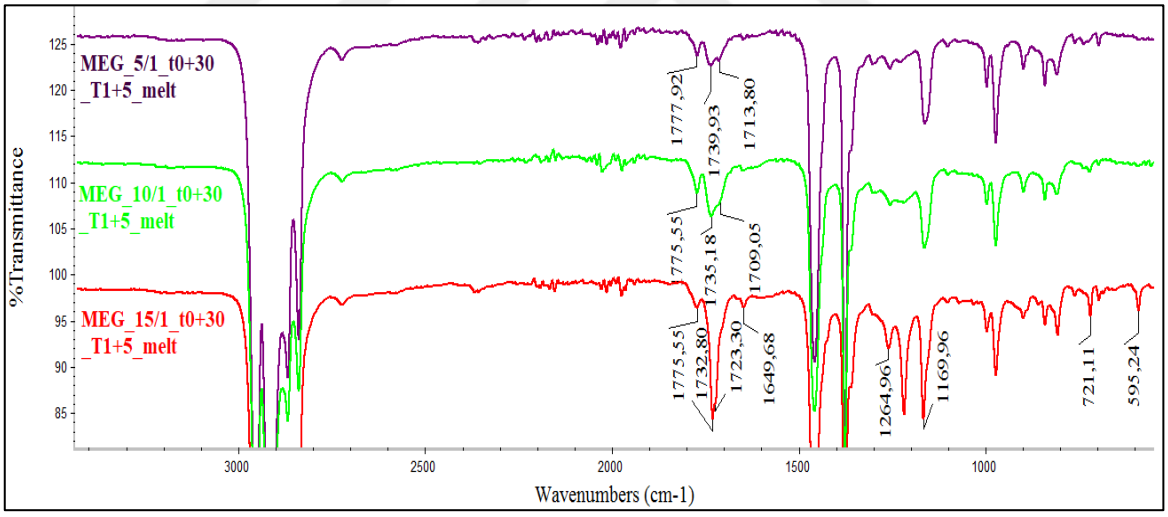


Figure 4.26. FTIR spectra of MEG_5/1_t_0+30_T_1+5 (top), MEG_10/1_t_0+30_T_1+5 (middle), MEG_15/1_t_0+30_T_1+5 (bottom).

5. CONCLUSION

Modification of atactic polypropylene was carried out by free radical grafting technique within the scope of this study. Maleic anhydride was selected as a comonomer to graft onto aPP. In the first place, MAH grafting reactions were conducted in toluene at 110 °C in the presence of benzoyl peroxide initiator. The grafting was ascertained by FTIR spectroscopy with the presence of the peaks at around 1770, 1735 and 1710 cm^{-1}. The exact structure and location of the grafts could be not determined. Upon grafting, the difference in solubility behavior was examined. Hot titration method was performed for quantification of MAH grafting, but the reliability of obtained results was questionable due to precipitate formation during titrations. Upon grafting, increase in T_g values was observed. However, with increasing amount of BPO, decrease in T_{m2} values was observed, as well. Additionally, homopropagation of MAH during grafting as a competing reaction was examined.

Secondly, MAH grafting onto aPP was tried at 130 °C in the presence of dicumyl peroxide initiator. Nonetheless, purified samples did not have any peak in carbonyl region in their FTIR spectra, confirming the accomplishment of grafting. During melt grafting, sublimation of MAH and its immiscibility within molten aPP were noted. Afterwards, MAH was modified to overcome the problems of sublimation and inhomogeneity. These problems were not faced in the modified MAH grafting rections carried out at higher temperatures. Yet, blank reactions conducted at these temperatures were recovered with lower yields. Thus, thermal degradation of aPP causing decrease in molecular weight may be pronounced at high reaction temperatures. Unlike MAH grafting reactions, the products of reactions with modified MAH did not precipitate in ethanol. This difference can be arise from severe chain scission, high grafting degree or contribution of both to some extent.

In conclusion, MAH grafting onto aPP was carried out successfully in solution and modification of MAH solved the problems faced during the melt grafting. Quantification by titration should be optimized, or alternative methods should be studied. Though FTIR spectroscopy and DSC are useful tools to determine grafting and its effect onto thermal properties, complementary tools such as high temperature GPC and High temperature NMR

are required to characterize chain scission and the structural analysis of the grafts are required.

REFERENCES

1. Karger-Kocsis, J. and T. Barany, *Polypropylene Handbook*, Springer, 2019.
2. Grandviewresearch, Polypropylene Market Size, Share & Trends Analysis Report By Type, By Process, By Application, By End Use and Segment Forecasts, https://www.grandviewresearch.com/industry-analysis/polypropylene-market, 2020.
3. Ravve, A., *Principles of Polymer Chemistry*, Springer+Business Media, LLC, 2012.
4. Odian, G., *Principles of Polymerization*, John Wiley & Sons, Inc., New Jersey, 2004.
5. Malpass, D. B., and E. I. Band, *Introduction to Industrial Polypropylene*, Scrivener Publishing LLC, Massachusetts, 2012.
6. Moore, E. P., *Polypropylene Handbook: Polymerization, Characterization, Properties, Processing, Applications*, Hanser/Gardner Publications, Inc., Cincinnati, USA, 1996.
7. Karger-Kocsis, J., *Polypropylene: An A-Z Reference*, Kluwer Academic Publishers, Dordrecht, The Netherlands, 1999.
8. Sauter, D. W., M. Taoufik, and C. Boisson, "Polyolefins, A Success Story", *Polymers (Basel)*, Vol. 9, No. 6, pp. 1–13, 2017.
9. Braun, D., H. Cherdron, and H. Ritter, *Polymer Synthesis: Theory and Practice*, Springer, Germany, 2001.
10. Zhang, Z., R. Zhang, Y. Huang, Y. Chen, J. Tang, and Z. Li, "Efficient Utilization of Atactic Polypropylene in Its Isotactic Polypropylene Blends via 'Structuring' Processing", *Industrial & Engineering Chemistry Research*, Vol. 53, No. 24, pp. 10144–10154, 2014.
11. Zhang, M., R. H. Colby, S. T. Milner, T. C. M. Chung, T. Huang, and W. deGroot, "Synthesis and Characterization of Maleic Anhydride Grafted Polypropylene with a Well-Defined Molecular Structure", *Macromolecules*, Vol. 46, No. 11, pp. 4313–4323, 2013.

12. Al-Malaika, S., *Reactive Modifiers for Polymers*, Chapman & Hall, London, UK, 1997.

13. Lindner, M., N. Rodler, M. Jesdinszki, M. Schmid, and S. Sängerlaub, "Surface Energy of Corona Treated PP, PE and PET Films, Its Alteration as Function of Storage Time and the Effect of Various Corona Dosages on Their Bond Strength After Lamination", *Journal of Applied Polymer Science*, Vol. 135, No. 11, pp. 1–9, 2018.

14. Beyer, G., and C. Hopmann, *Reactive Extrusion: Principles and Applications*, Wiley-VCH, Weinheim, Germany, 2018.

15. Krause-Sammartino, L. E., J. C. Lucas, M. M. Reboredo, and M. I. Aranguren, "Maleic Anhydride Grafting of Polypropylene: Peroxide and Solvent Effects", *Plastics, Rubber and Composites*, Vol. 35, No. 3, pp. 117–123, 2006.

16. Russell, K. E., "Free Radical Graft Polymerization and Copolymerization at Higher Temperatures", *Progress in Polymer Science*, Vol. 27, No. 6, pp. 1007–1038, 2002.

17. García-Martínez, J. M., S. Areso, and E. P. Collar, "The Transient Nature of Maximum Maleic Anhydride Grafting of Polypropylene: A Mechanistic Approach Based on a Consecutive Reaction Model Part 1: Batch Solution Process", *Journal of Applied Polymer Science*, Vol. 102, No. 2, pp. 1182–1190, 2006.

18. Kučera, F., J. Petruš, P. Poláček, and J. Jančář, "Controlled Reactive Modification of Polypropylene with Maleic Anhydride via Solvent-Free Technique", *Polymer Degradation and Stability*, Vol. 168, pp. 2–9, 2019.

19. Cartier, H., and G. H. Hu, "Styrene-Assisted Melt Free Radical Grafting of Glycidyl Methacrylate onto Polypropylene", *Journal of Polymer Science Part A: Polymer Chemistry*, Vol. 36, No. 7, pp. 1053–1063, 1998.

20. Machado, A.V., J. A. Covas, and M. Van Duin, "Effect of Polyolefin Structure on Maleic Anhydride Grafting", *Polymer (Guildf)*, Vol. 42, No. 8, pp. 3649–3655, 2001.

21. Aburatani, R., S. Machida, H. Nakashima, and T. Fujimura, "Preparation of Modified Low-Melting Point Polypropylene: Effect of Tacticity for Modification", *Polymer Journal*, Vol. 41, No. 1, pp. 34–39, 2009.

22. K. E. Russell, “Grafting of Maleic Anhydride to Hydrocarbons below the Ceiling Temperature.”, *Journal of Polymer Science Part A: Polymer Chemistry*, Vol. 33, pp. 555-561, 1995.

23. Marco, C., E. P. Collar, S. Areso, and J. M. García-Martínez, “Thermal Studies on Polypropylene/Polyamide-6 Blends Modified by Succinic Anhydride and Succinyl Fluorescein Grafted Polypropylenes”, *Journal of Polymer Science Part B: Polymer Physics*, Vol. 40, No. 13, pp. 1307–1315, 2002.

24. Ching, T. Y., J. A. Solis, H. Yang, and W. A. Diecks, “Polypropylene-Graft-Acrylic Acid or Polypropylene-Graft-Maleic Anhydride in Oxygen Scavengine Tie Layers” WO 2004/103701 A1, Dec. 2, 2004.

25. Aranburu, N., and J. I. Eguiazábal, “Improved Mechanical Properties of Compatibilized Polypropylene/Polyamide-12 Blends”, *International Journal of Polymer Science*, Vol. 2015, 2015.

26. Gartner, C., M. Suarez, and B. L. Lopez, “Grafting of Maleic Anhydride on Polypropylene and Its Effect on Blending with Poly (ethylene terephthalate)”, *Polymer Engineering & Science*, Vol. 48, No: 10, pp. 1910-1916, 2008.

27. Rustal, C., *Functionalization of PP for the Enhancement of Adhesion between Polypropylene and Polyamide Layers*, Ph.D. Thesis, University of Stuttgart, 2009.

28. Poletto, M., “Polypropylene-Based Wood-Plastic Composites: Effect of Using a Coupling Agent Derived From a Renewable Resource”, *Maderas, Ciencia y Tecnologia*, Vol. 19, No. 3, pp. 265–272, 2017.

29. Mai, K., K. Wang, and H. Zeng, “Multiple Melting Behavior of Nucleated Polypropylene,” *Journal of Applied Polymer Science*, Vol. 88, No. 6, pp. 1608–1611, 2003.

30. García-Martínez, J. M., O. Laguna, S. Areso, and E. P. Collar, “FTIR Quantitative Characterization of Chemically Modified Polypropylenes Containing Succinic Grafted Groups”, *Journal of Applied Polymer Science*, Vol. 73, No. 14, pp. 2837–2847, 1999.

31. Busico, V., and R. Cipullo, “Microstructure of Polypropylene”, *Progress in Polymer*

Science, Vol. 26, No. 3, pp. 443–533, 2001.

32. Musa, O. M., *Handbook of Maleic Anhydride Based Materials*, Springer International Publishing, Switzerland, 2016.

33. De Roover, B., J. Devaux, and R. Legras, "Maleic Anhydride Homopolymerization during Melt Functionalization of Isotactic Polypropylene", *Journal of Polymer Science Part A: Polymer Chemistry*, Vol. 34, pp. 1195-1202, 1996.

34. De Roover, B., M. Sclavons, V. Carlier, J. Devaux, R. Legras, and A. Momtaz, "Molecular Characterization of Maleic Anhydride-Functionalized Polypropylene", *Journal of Polymer Science Part A: Polymer Chemistry*, Vol. 33, No. 5, pp. 829–842, 1995.

35. Sclavons, M., P. Franquinet, V. Carlier, G. Verfaillie, I. Fallais, R. Legras, M. Laurent, and F. C. Thyrion, "Quantification of the Maleic Anhydride Grafted onto Polypropylene by Chemical and Viscosimetric Titrations, and FTIR Spectroscopy", *Polymer (Guildf)*, Vol. 41, No. 6, pp. 1989–1999, 2000.

36. Bettini, S. H. P., and J. A. M. Agnelli, "Evaluation of Methods Used for Analysing Maleic Anhydride Grafted onto Polypropylene by Reactive Processing", *Polymer Testing*, Vol.19, pp. 3-15, 2000.

37. Lee, M. H., J. R. Chen, G. Y. Shiue, Y. F. Lin, and C. M. Shu, "Simulation Approach to Benzoyl Peroxide Decomposition Kinetics by Thermal Calorimetric Technique", *Journal of the Taiwan Institute of Chemical Engineers*, Vol. 45, No. 1, pp. 115–120, 2014.

APPENDIX A: SPECTROSCOPY DATA

FTIR spectra and DSC thermograms of analyzed samples are presented.

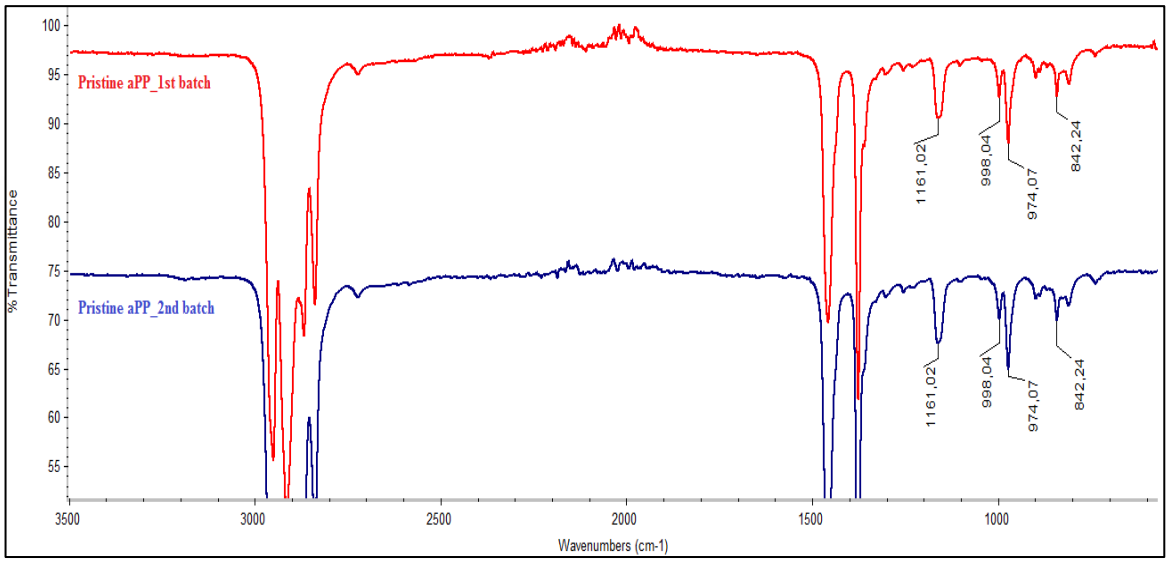


Figure A.1. FTIR spectra of 1st batch (top) and 2nd batch of pristine aPP.

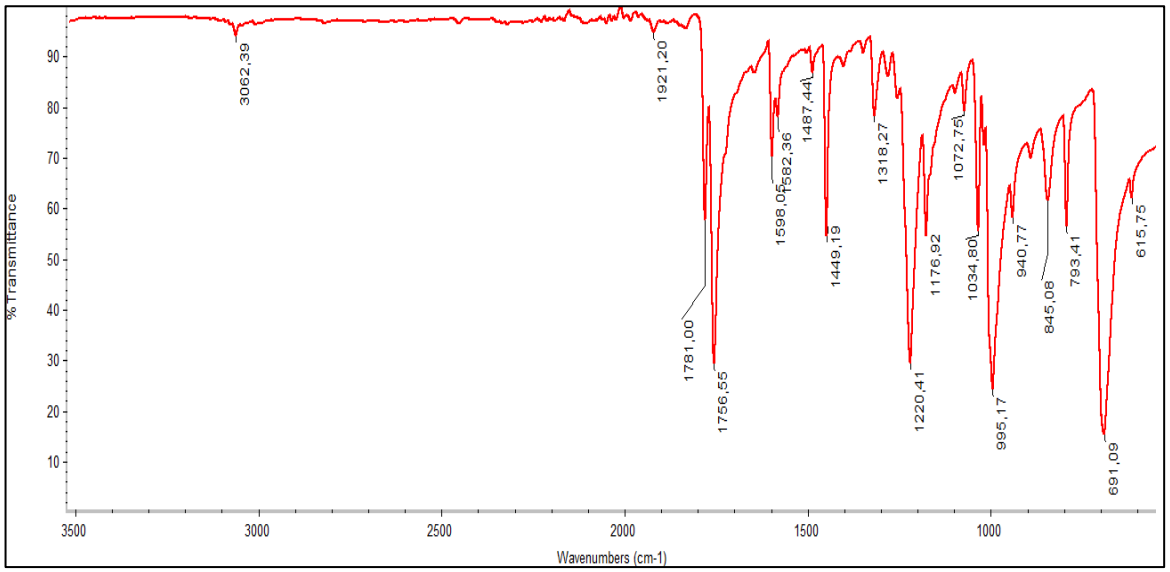


Figure A.2. FTIR spectrum of BPO.

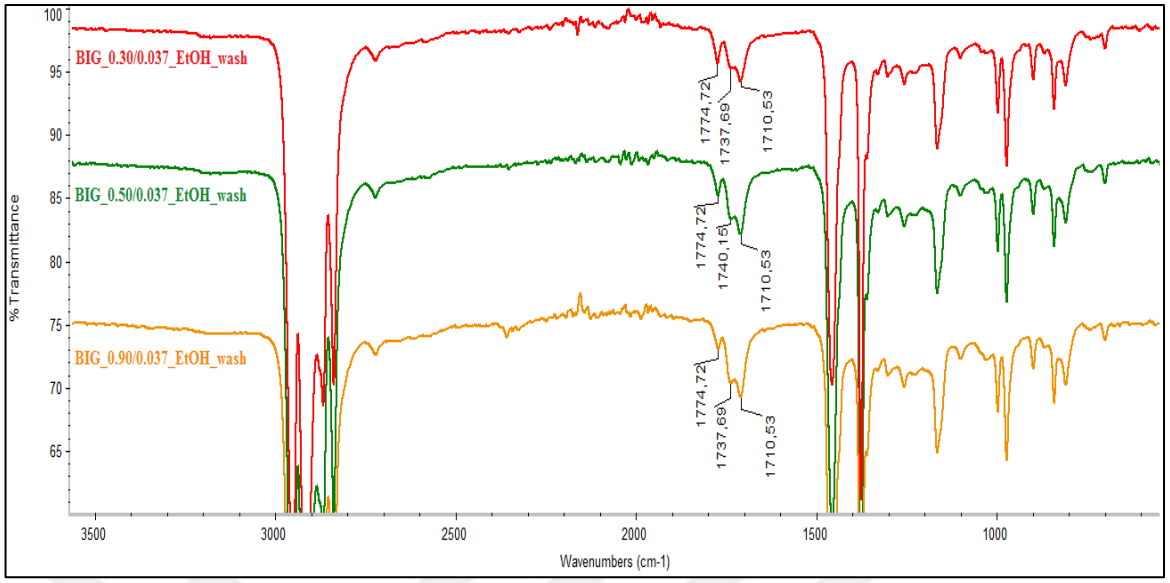


Figure A.3. FTIR spectra of EtOH washes of BIG_0.30/0.037 (top), BIG_0.50/0.037 (middle), BIG_0.90/0.037 (bottom).

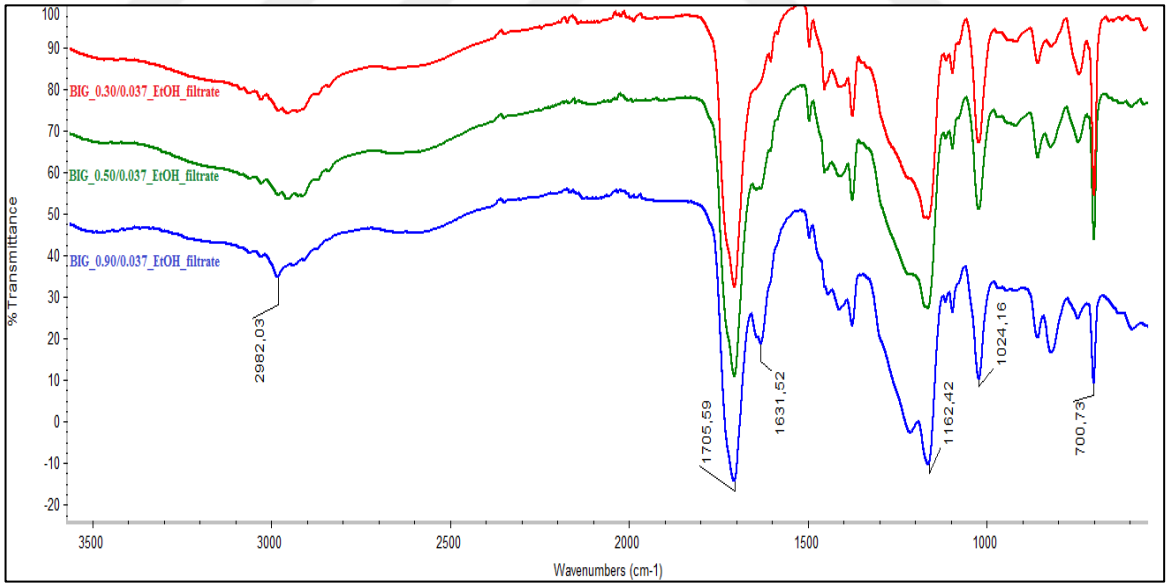


Figure A.4. FTIR spectra of EtOH filtrates of BIG_0.30/0.037 (top), BIG_0.50/0.037 (middle), BIG_0.90/0.037 (bottom).

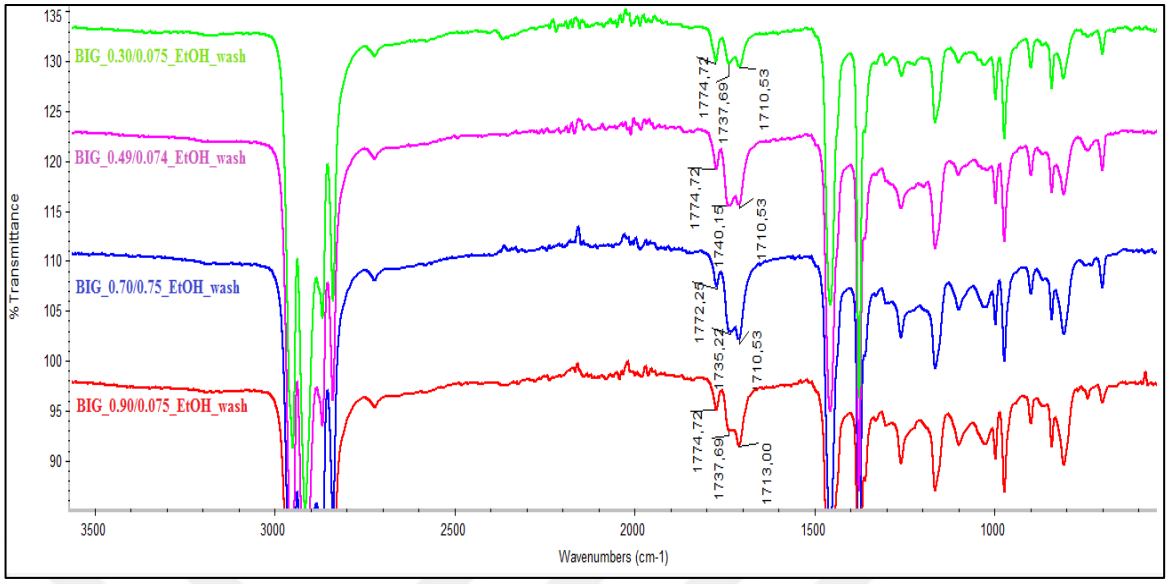


Figure A.5. FTIR spectra of EtOH washes of BIG_0.30/0.075 (pale green), BIG_0.49/0.074 (pink), BIG_0.70/0.075 (blue), BIG_0.90/0.075 (red).

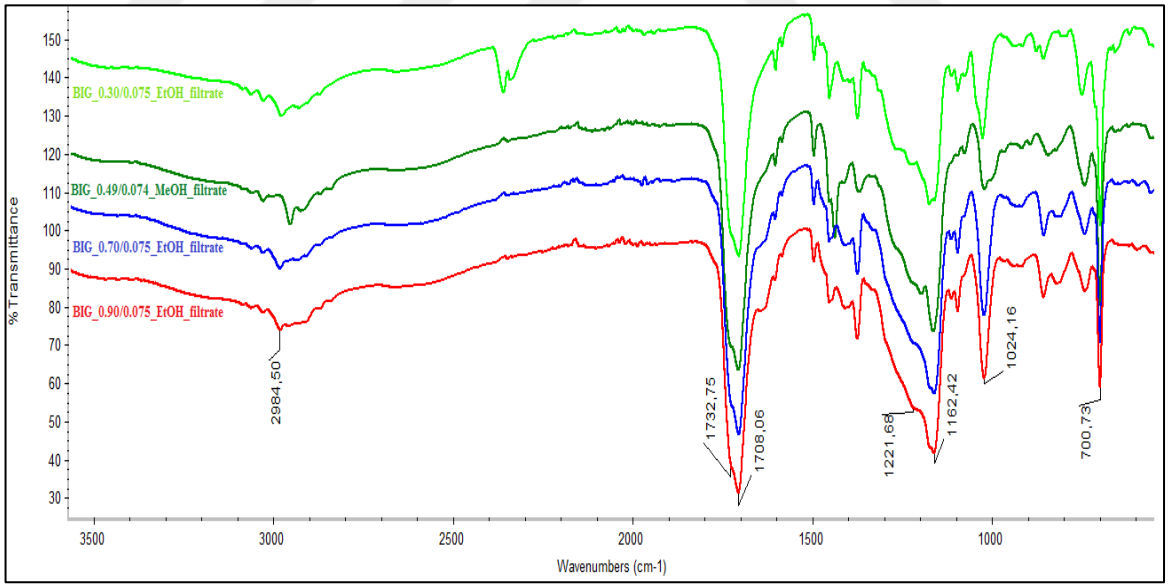


Figure A.6. FTIR spectra of EtOH filtrates of BIG_0.30/0.075 (pale green), BIG_0.49/0.074 (dark green), BIG_0.70/0.075 (blue), BIG_0.90/0.075 (red).

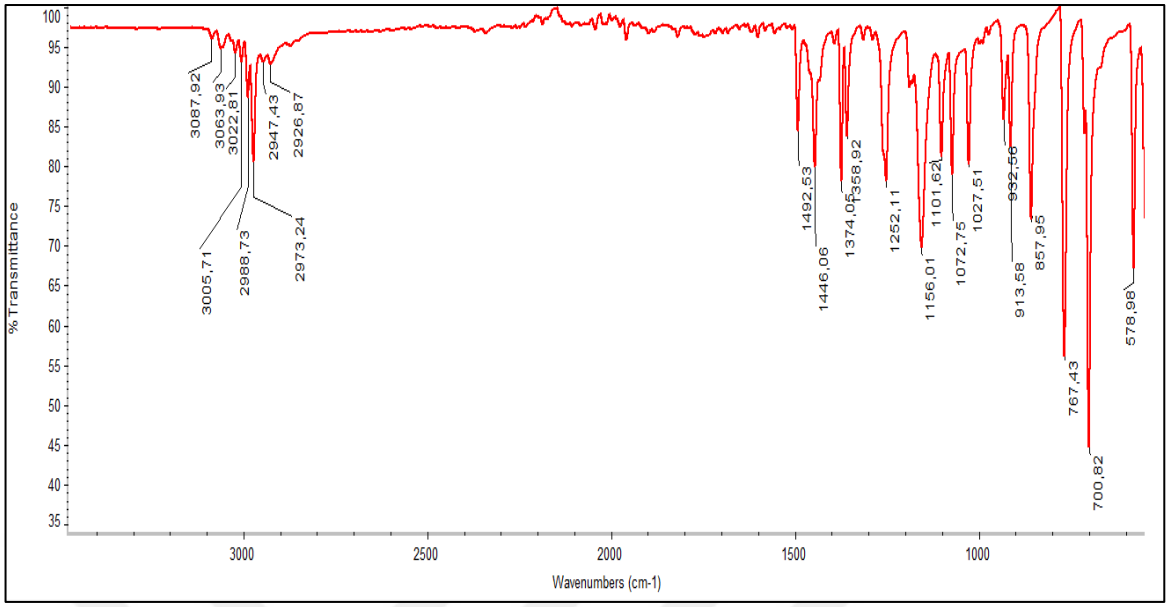


Figure A.7. FTIR spectrum of DCP.

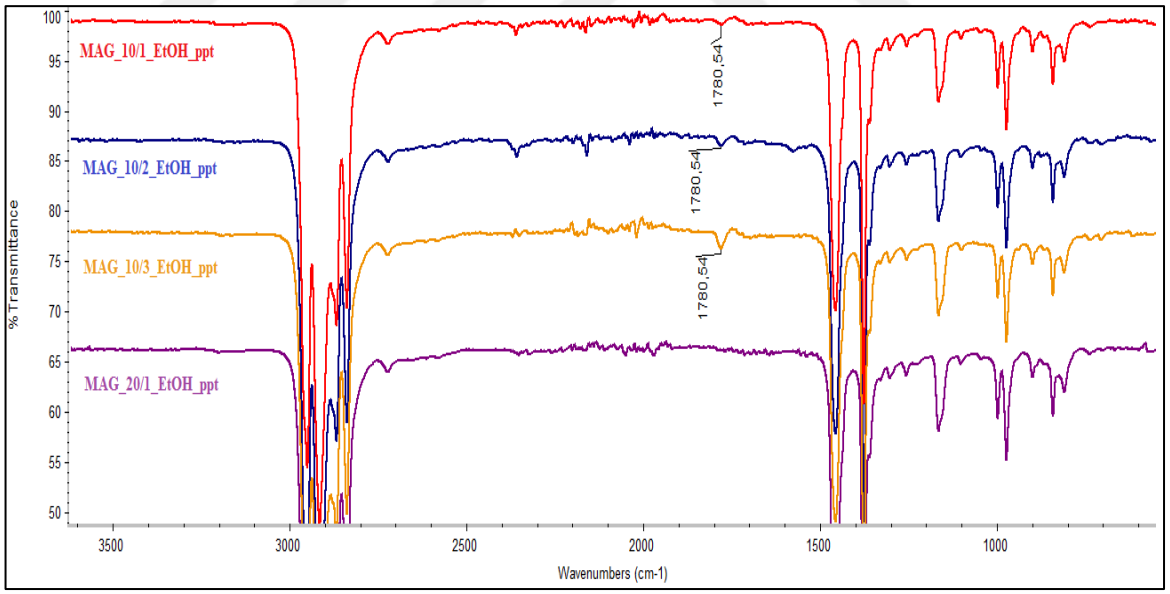


Figure A.8. FTIR spectra of purified MAG_10/1 (red), MAG_10/2 (blue), MAG_10/3 (yellow), MAG_20/1 (purple).

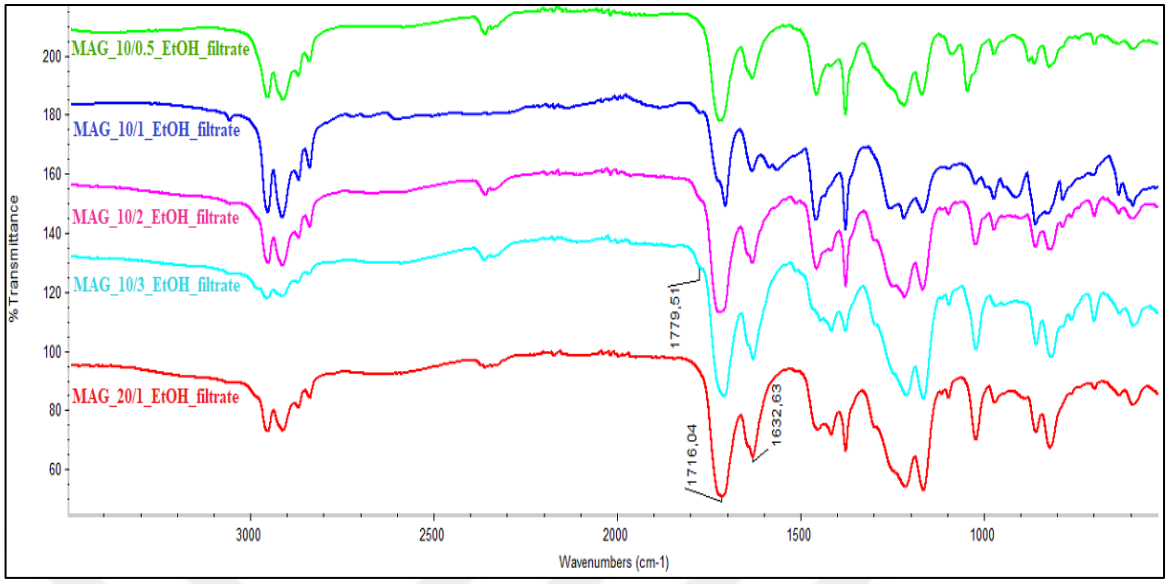


Figure A.9. FTIR spectra of filtrates of MAG reactions.

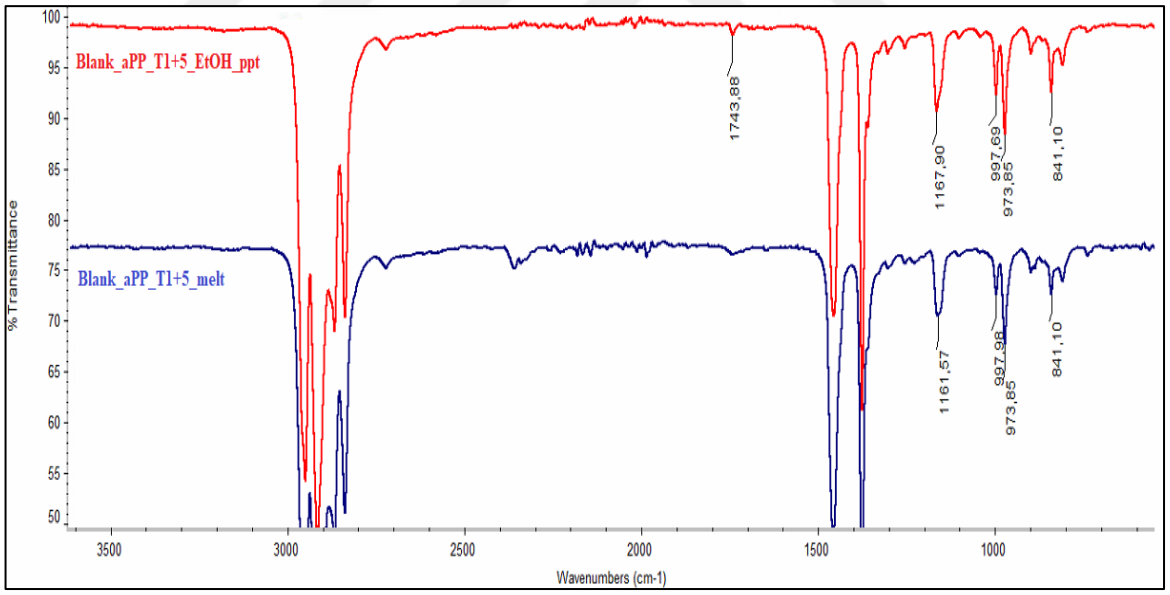


Figure A.10. FTIR spectra of purified (top) and unpurified (bottom) Blank_aPP_T_1+5.

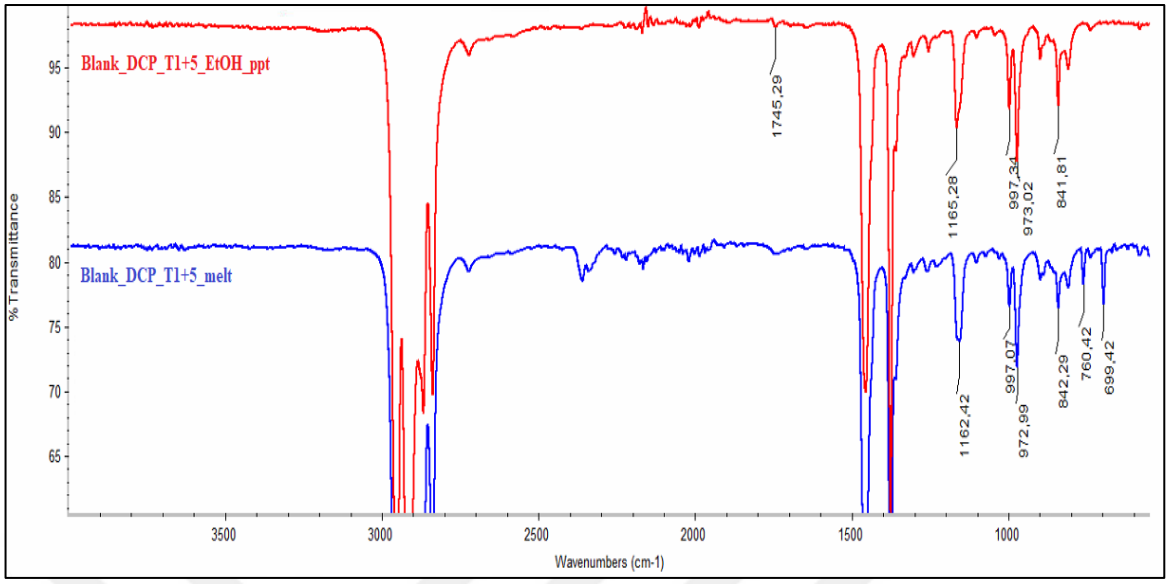


Figure A.11. FTIR spectra of purified (top) and unpurified (bottom) Blank_DCP_T_1+5.

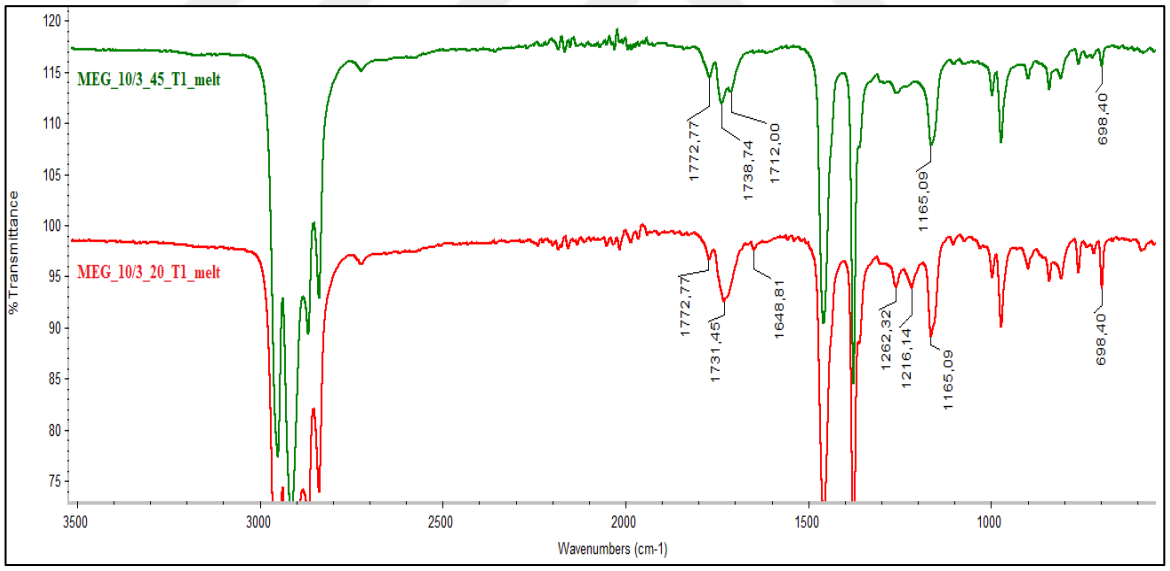


Figure A.12. FTIR spectra of MEG_10/3_45_T_1 (top) and MEG_10/3_20_T_1 (bottom).

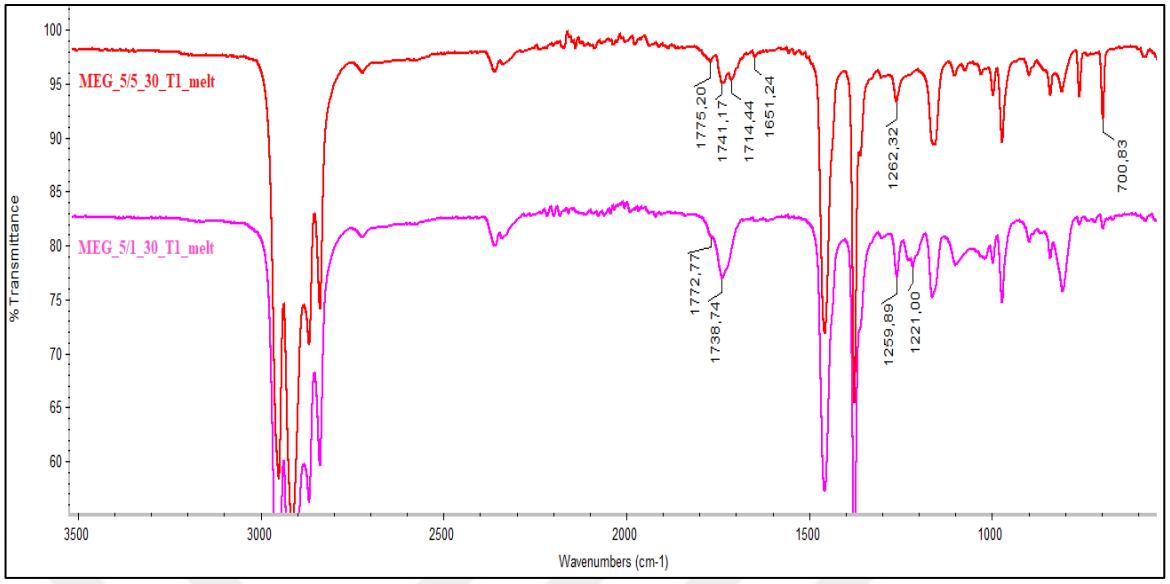


Figure A.13. FTIR spectra of MEG_5/5_30_T_1 (top) and MEG_5/1_30_T_1 (bottom).

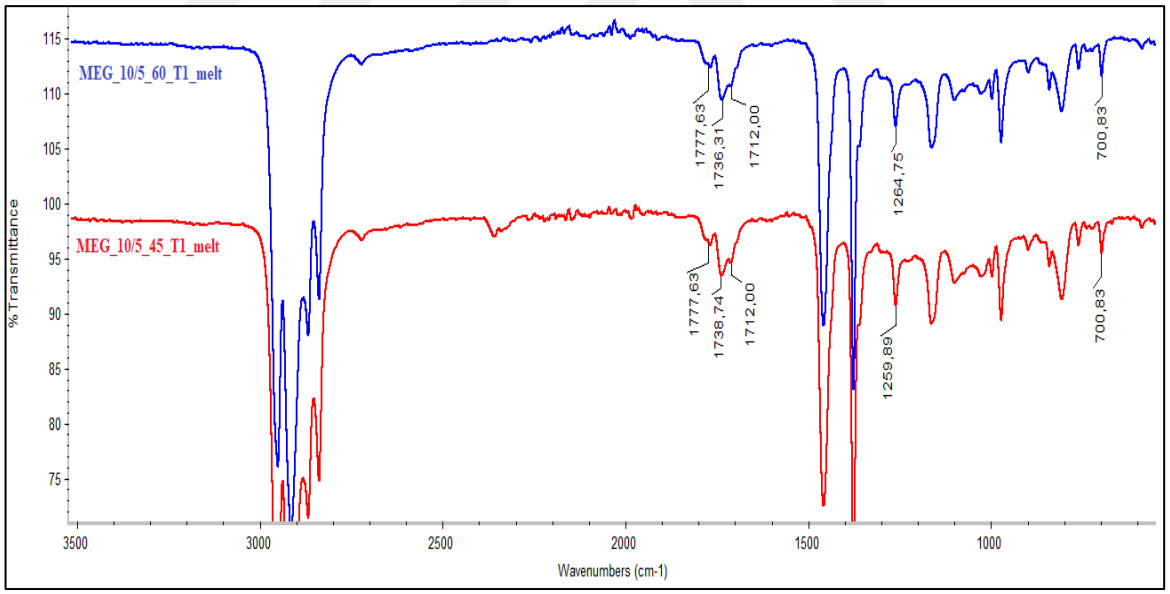


Figure A.14. FTIR spectra of MEG_10/5_60_T_1 (top) and MEG_10/5_45_T_1 (bottom).

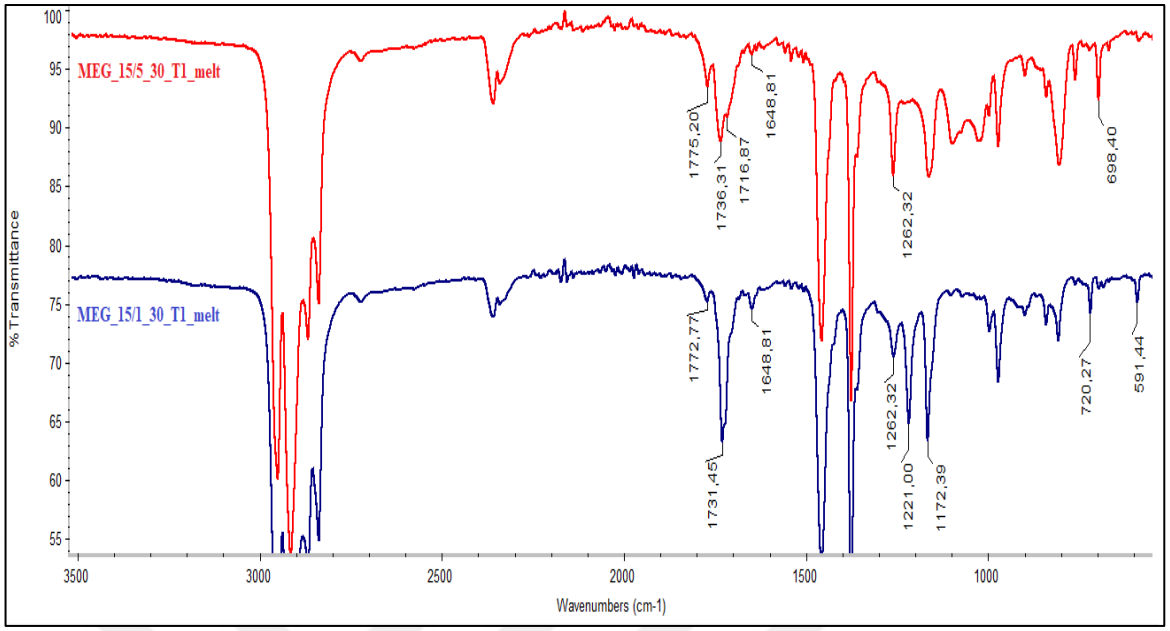


Figure A.15. FTIR spectra of MEG_15/5_30_T_1 (top) and MEG_15/1_30_T_1 (bottom).

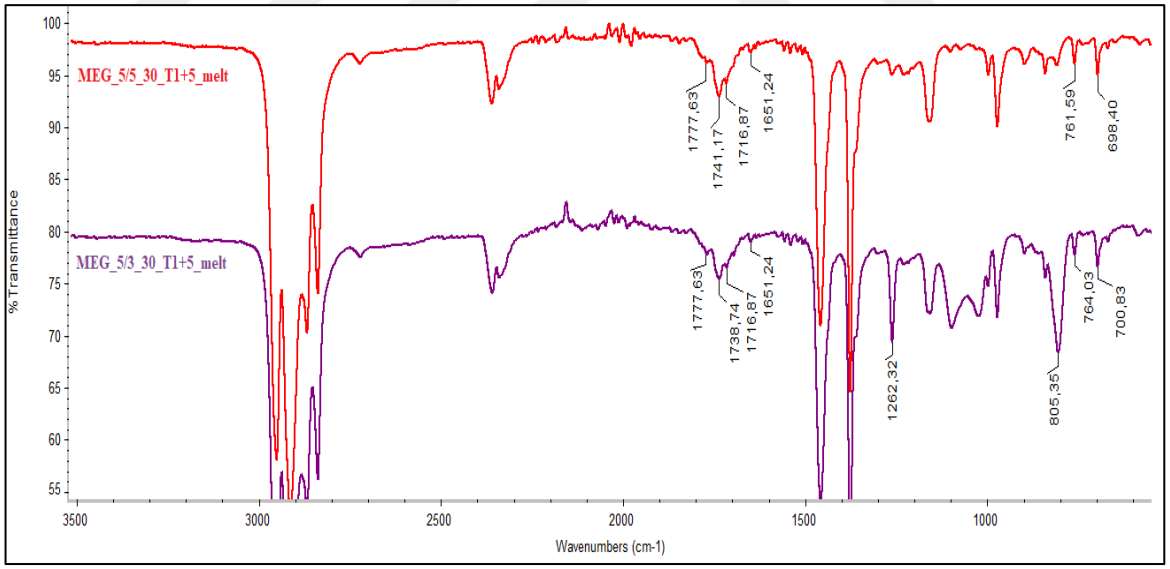


Figure A.16. FTIR spectra of MEG_5/5_30_T_1+5 (top) and MEG_5/3_30_T_1+5 (bottom).

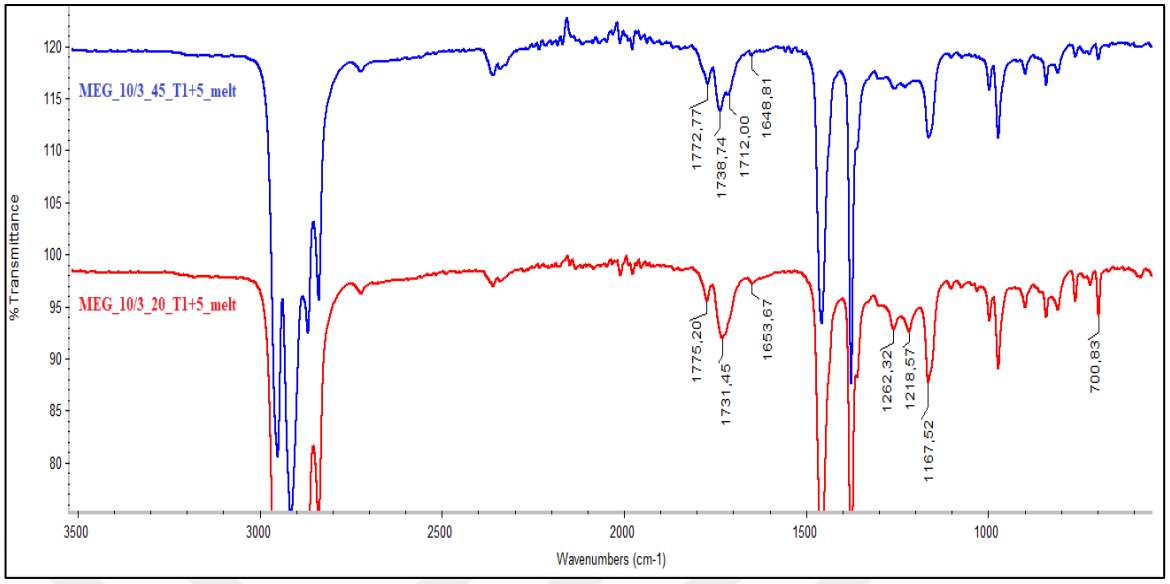


Figure A.17. FTIR spectra of MEG_10/3_45_T_1+5 (top) and MEG_10/3_20_T_1+5 (bottom).

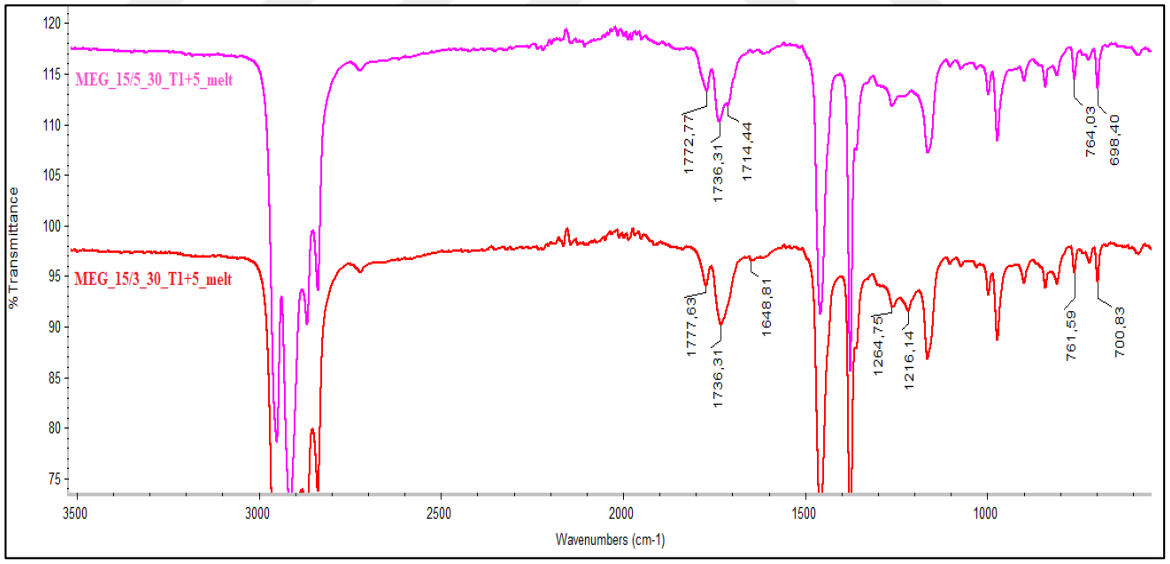


Figure A.18. FTIR spectra of MEG_15/5_30_T_1+5 (top) and MEG_15/3_30_T_1+5 (bottom).

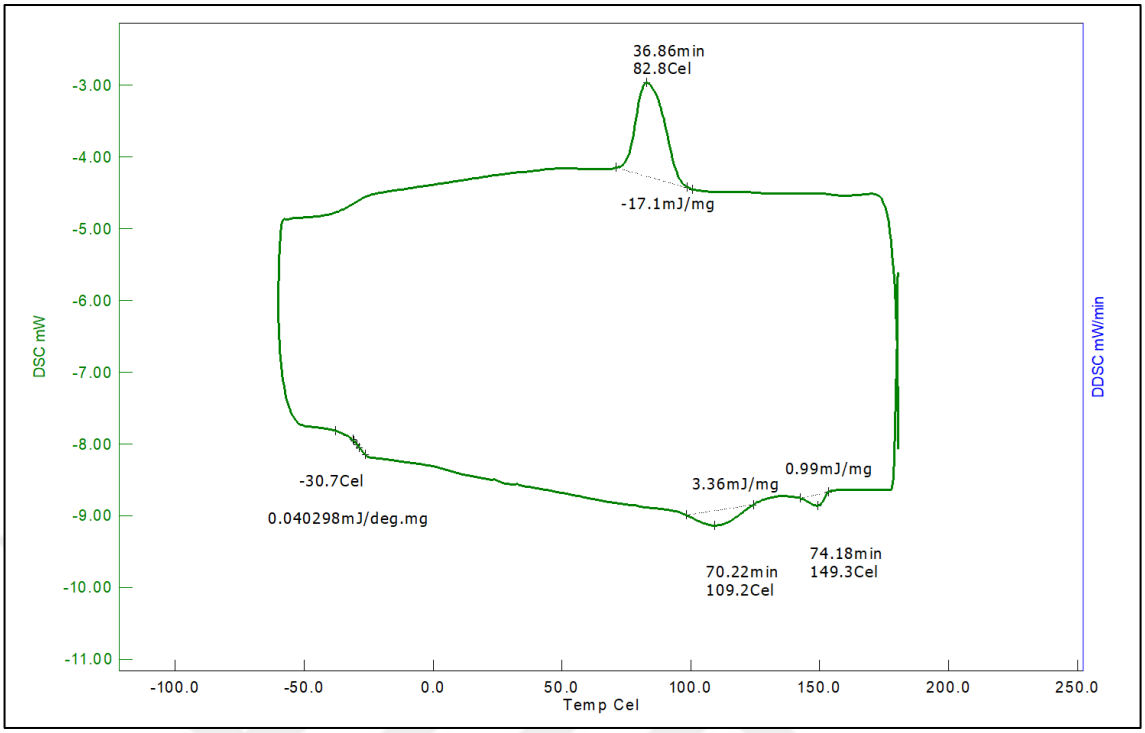


Figure A.19. DSC thermogram of pristine aPP used in the study.

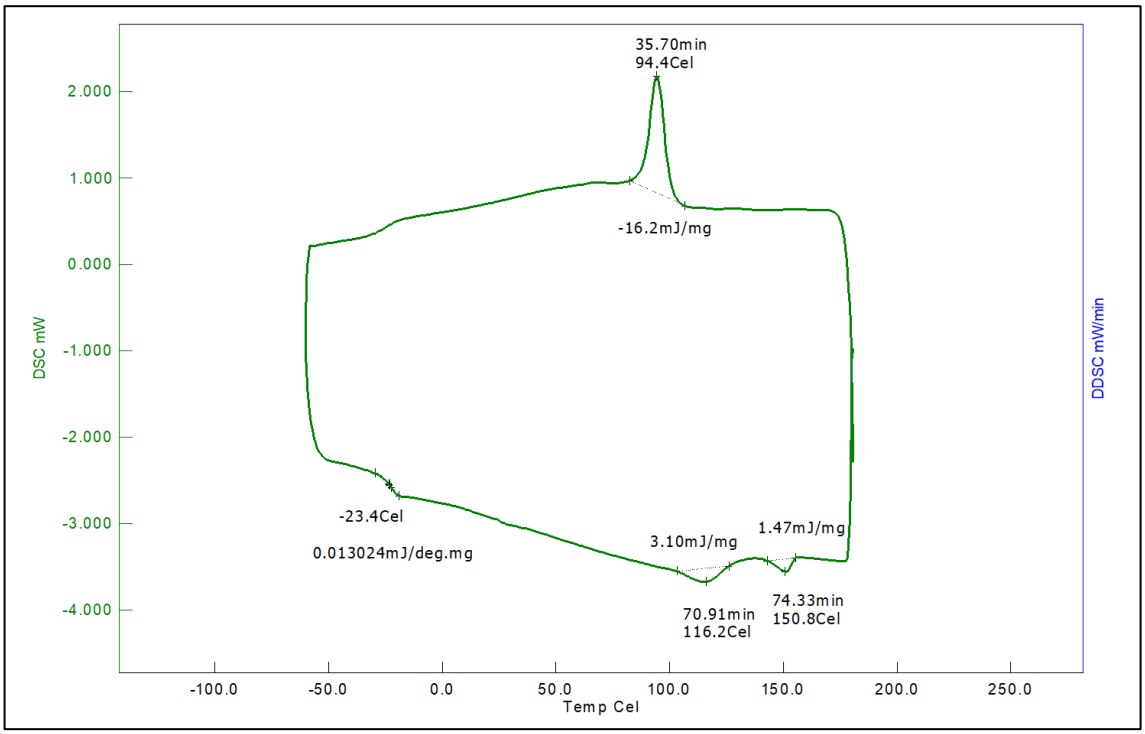


Figure A.20. DSC thermogram of Blank_aPP.

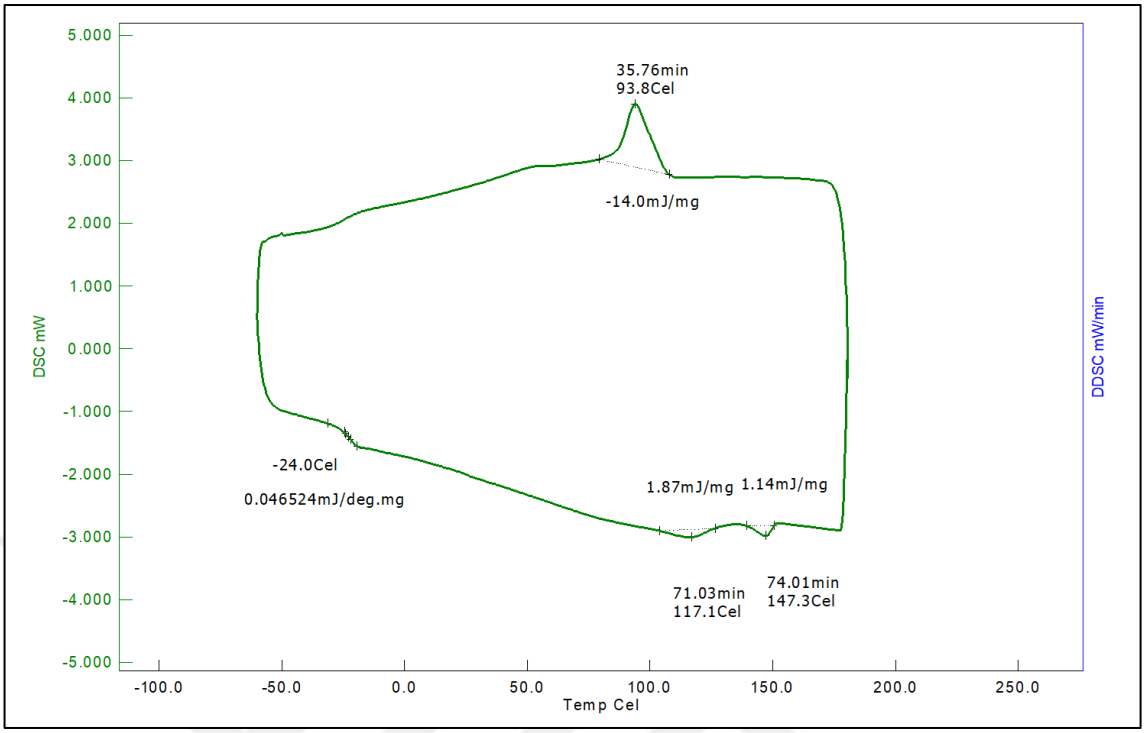


Figure A.21. DSC thermogram of Blank_aPP+BPO.

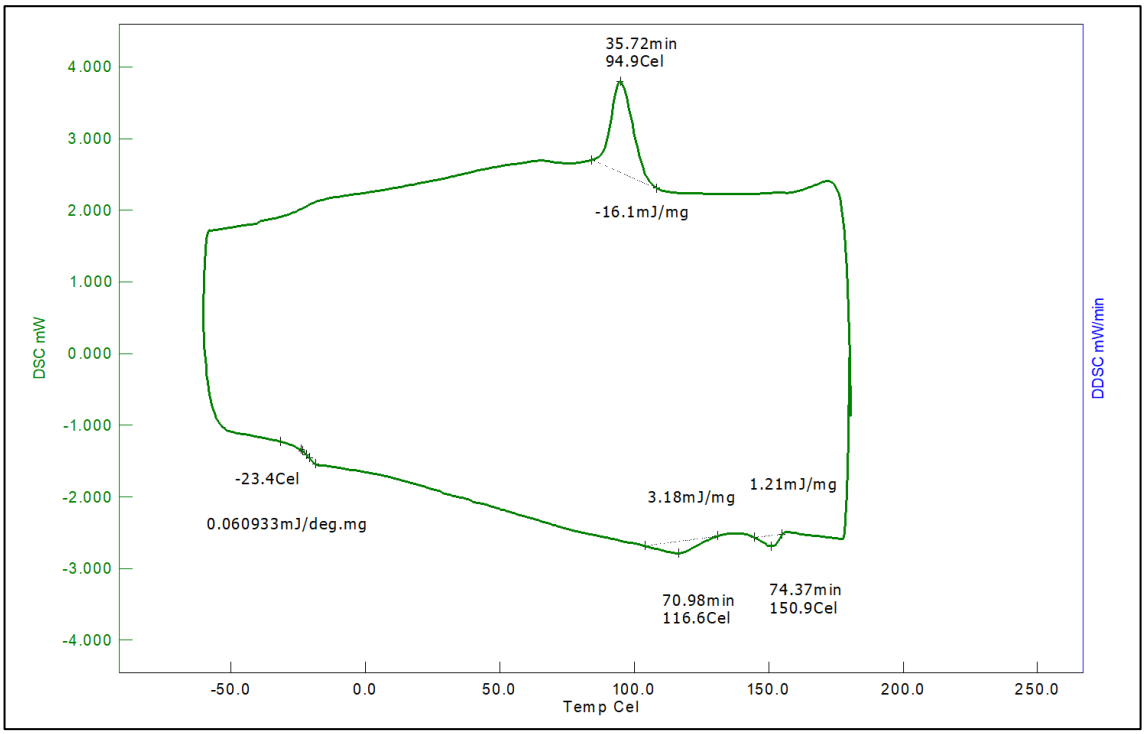


Figure A.22. DSC thermogram of Blank_aPP+MAH.

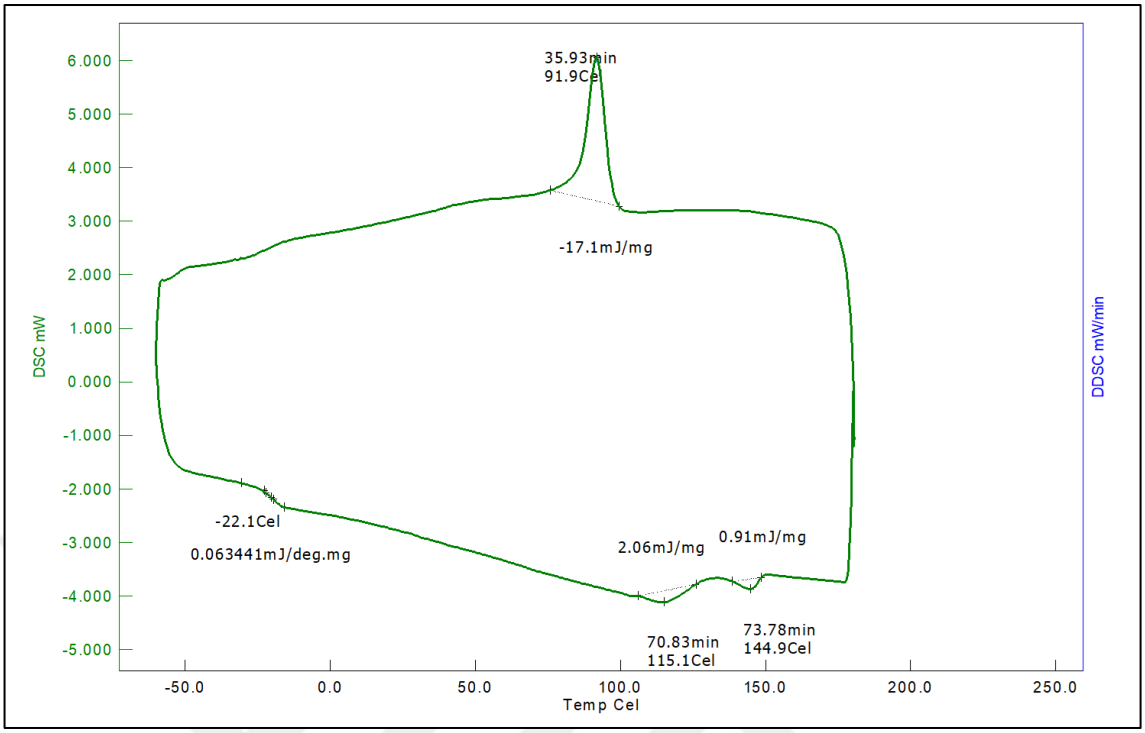


Figure A.23. DSC thermogram of BIG_0.30/0.037_EtOH_wash.

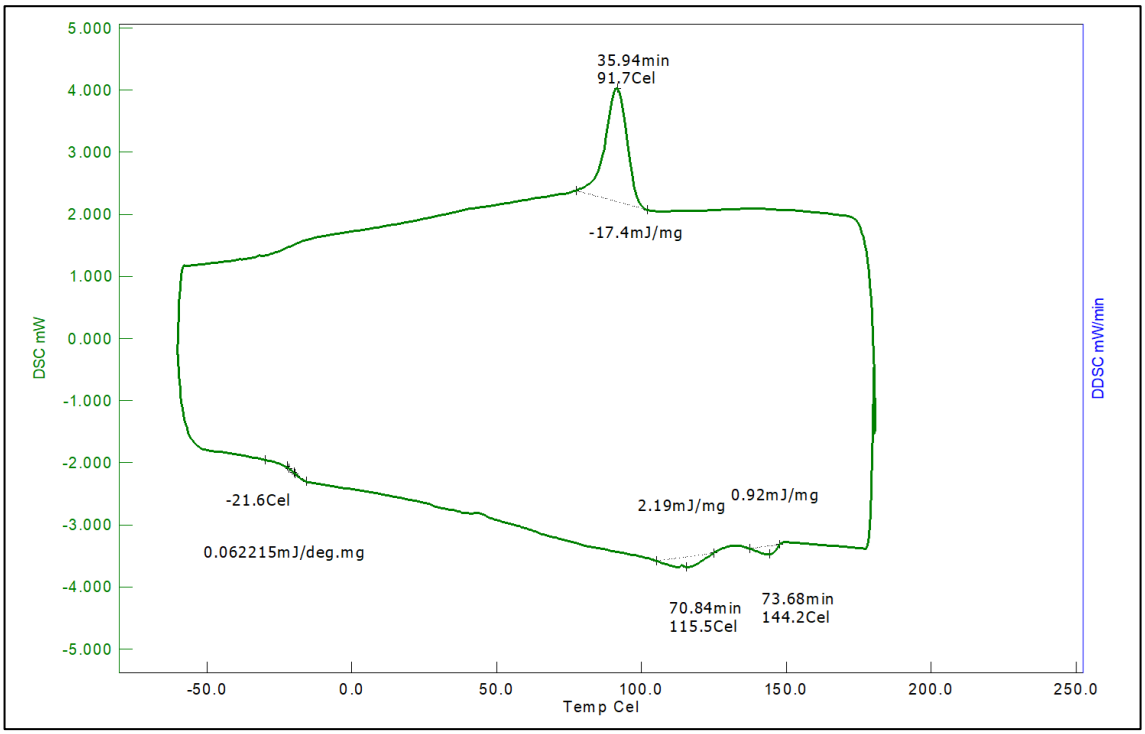


Figure A.24. DSC thermogram of BIG_0.50/0.037_EtOH_wash.

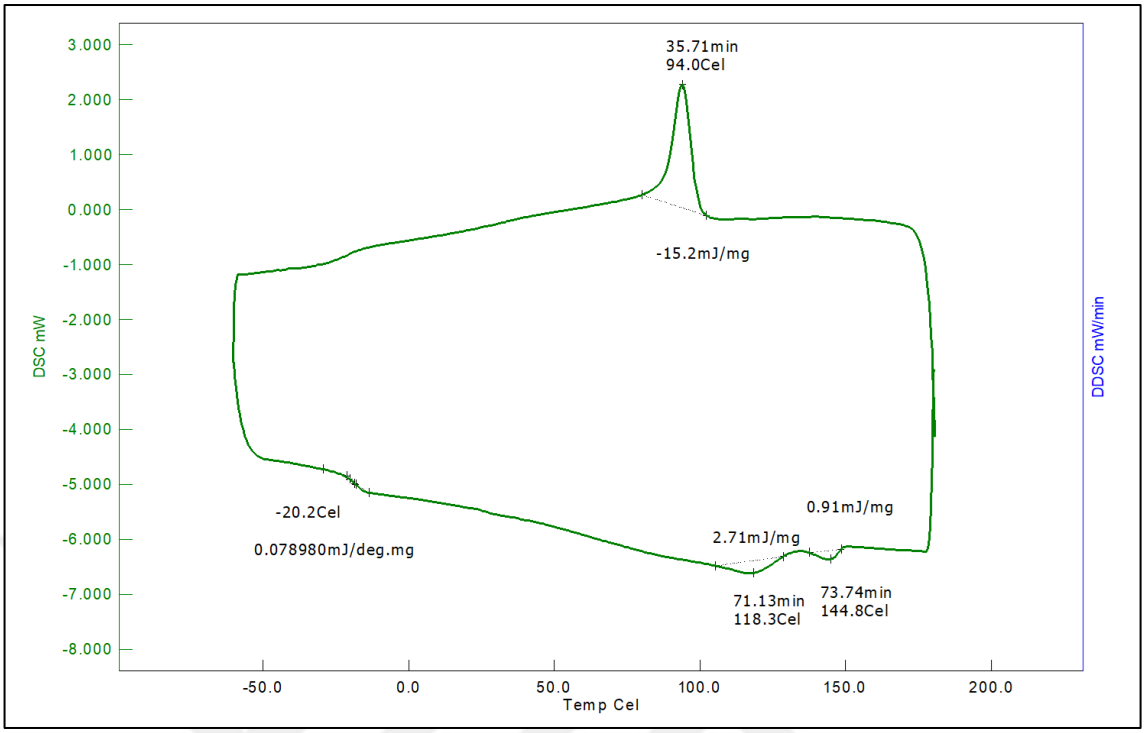


Figure A.25. DSC thermogram of BIG_0.70/0.037_EtOH_wash.

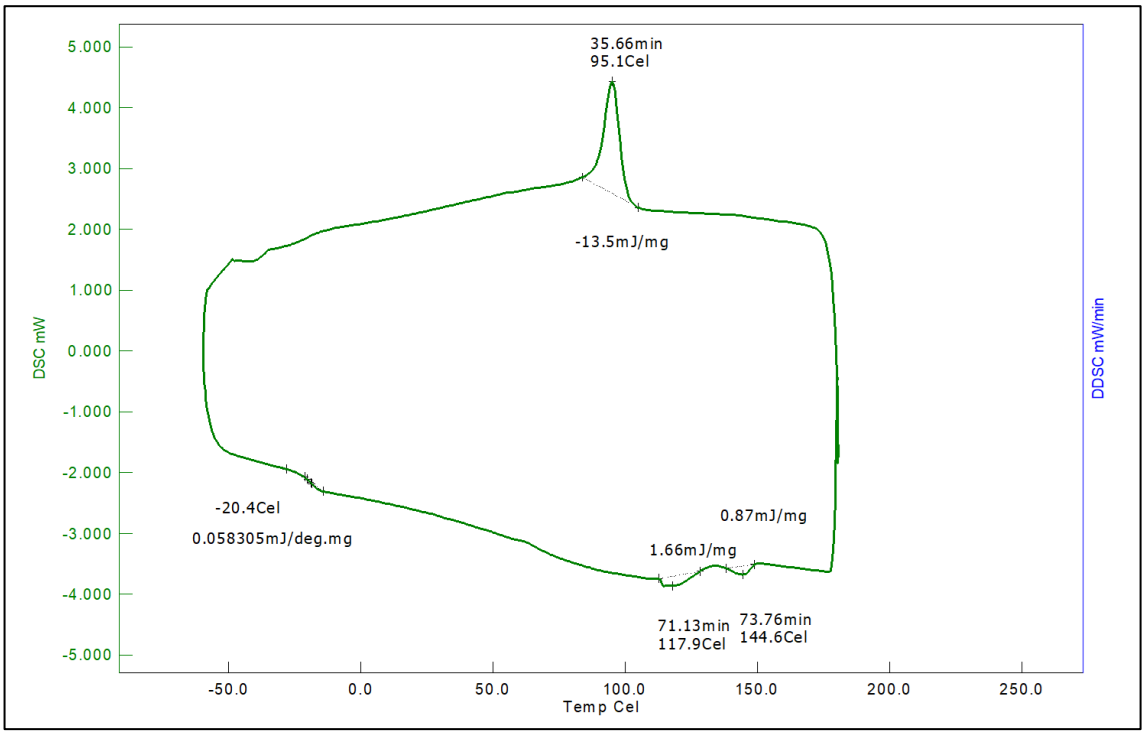


Figure A.26. DSC thermogram of BIG_0.90/0.037_EtOH_wash.

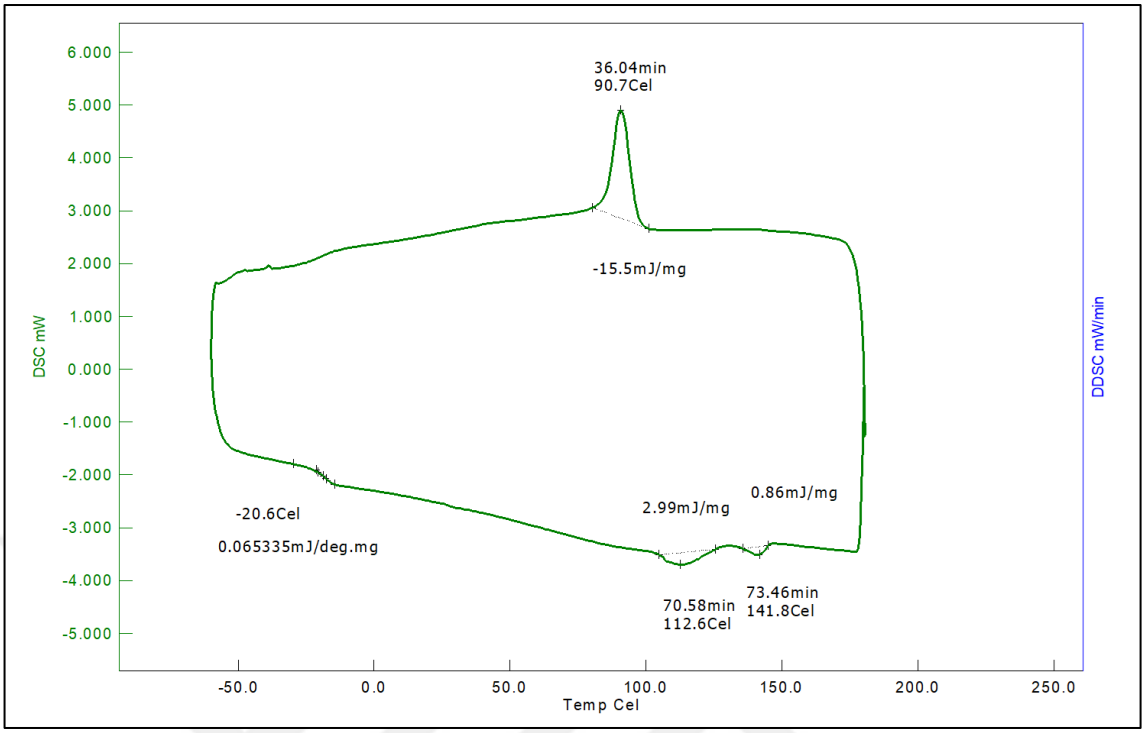


Figure A.27. DSC thermogram of BIG_0.30/0.075_EtOH_wash.

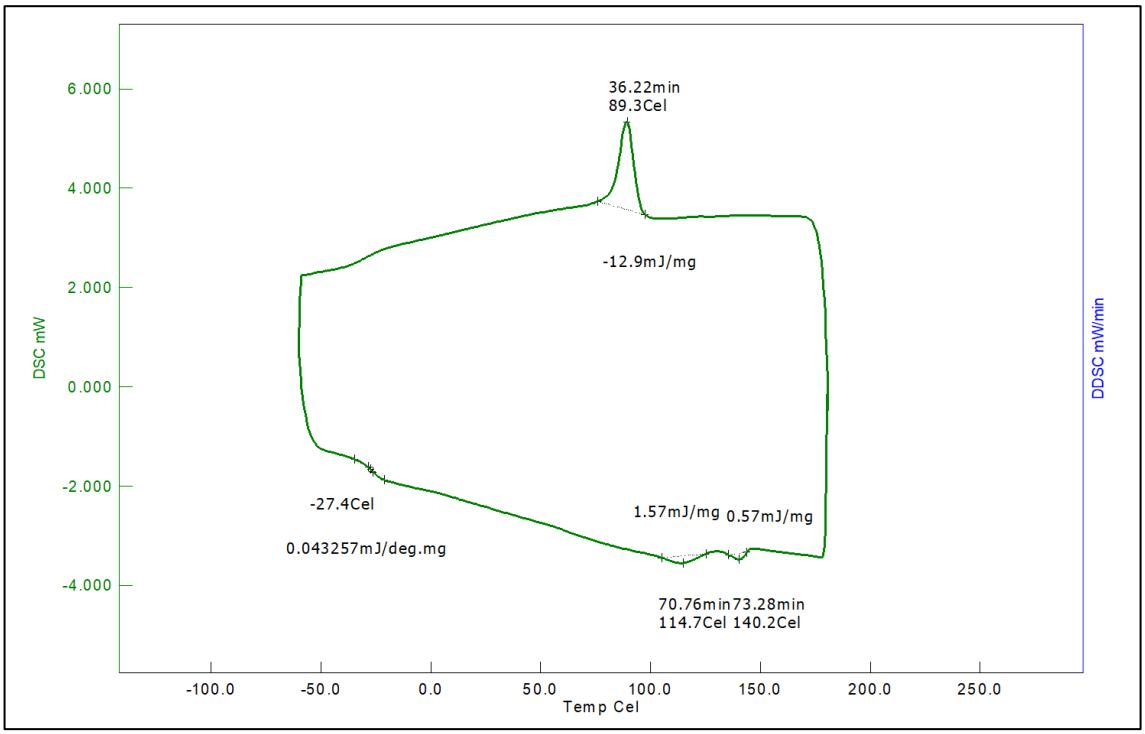


Figure A.28. DSC thermogram of BIG_0.49/0.074_EtOH_wash.

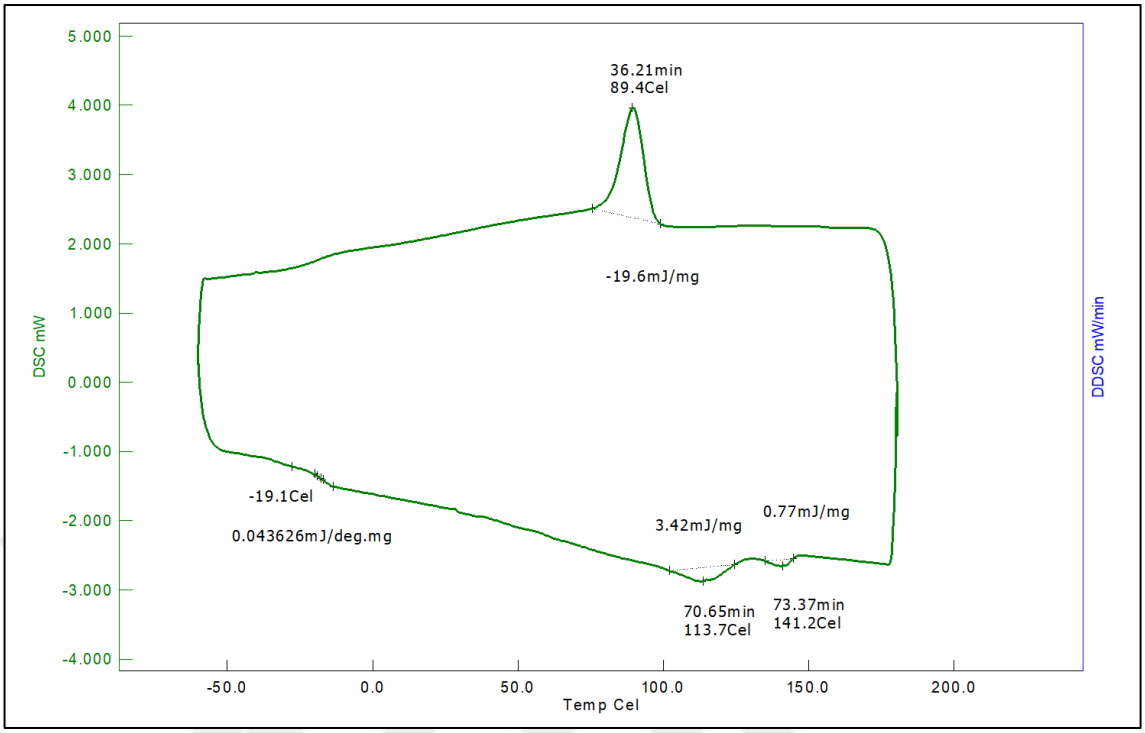


Figure A.29. DSC thermogram of BIG_0.70/0.075_EtOH_wash.

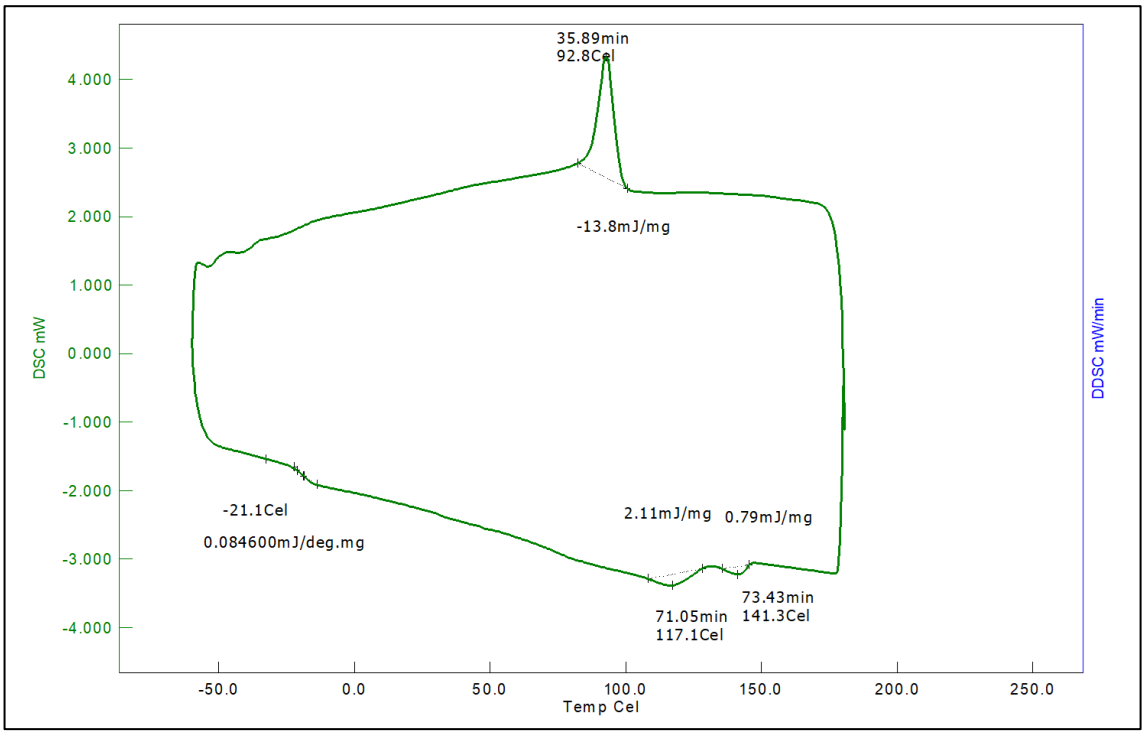


Figure A.30. DSC thermogram of BIG_0.90/0.075_EtOH_wash.

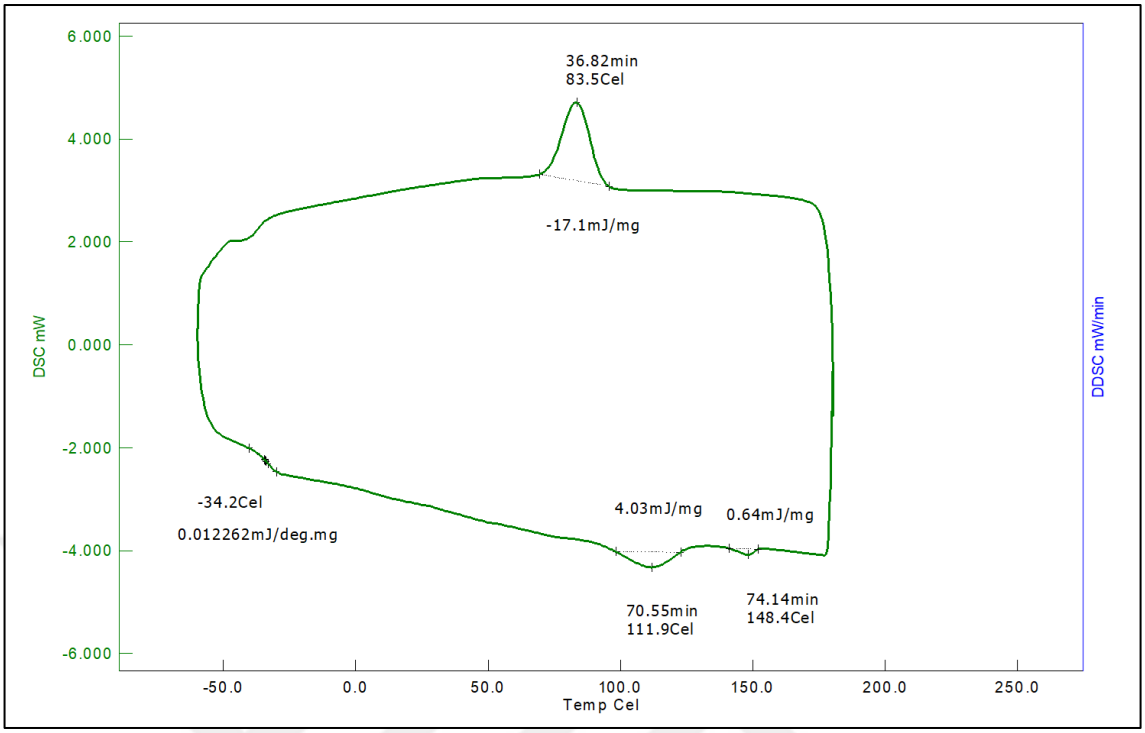


Figure A.31. DSC thermogram of aPP_2nd batch.

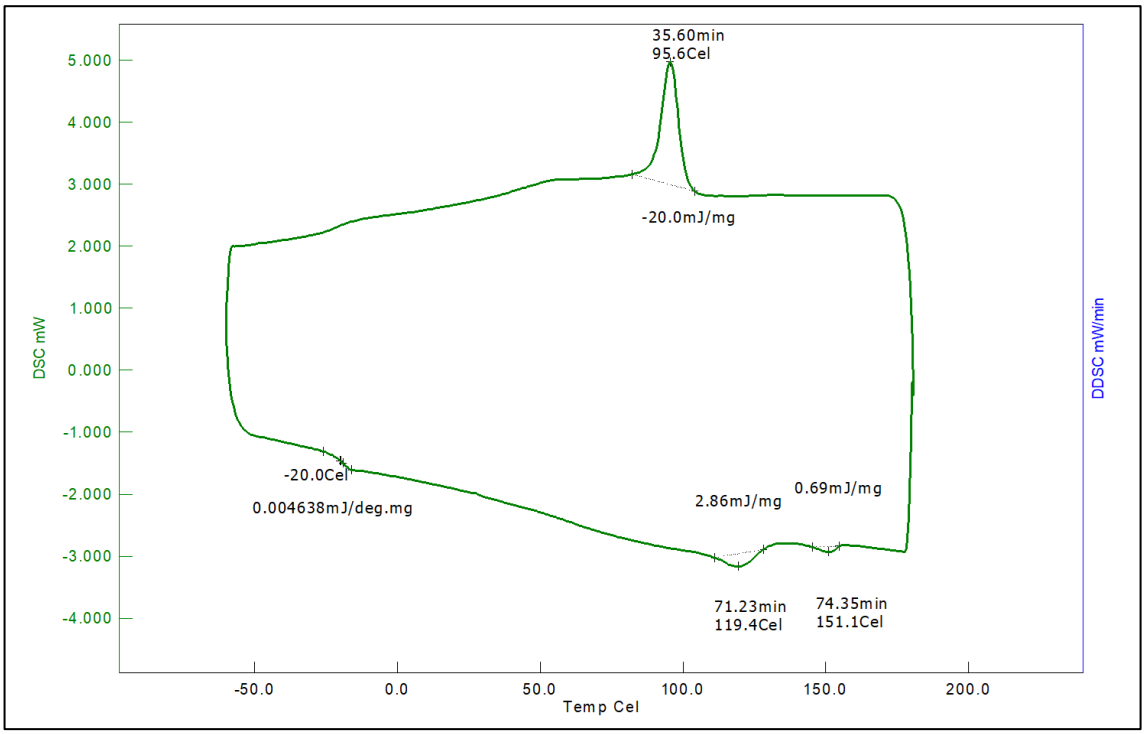


Figure A.32. DSC thermogram of purified Blank_aPP_T1.

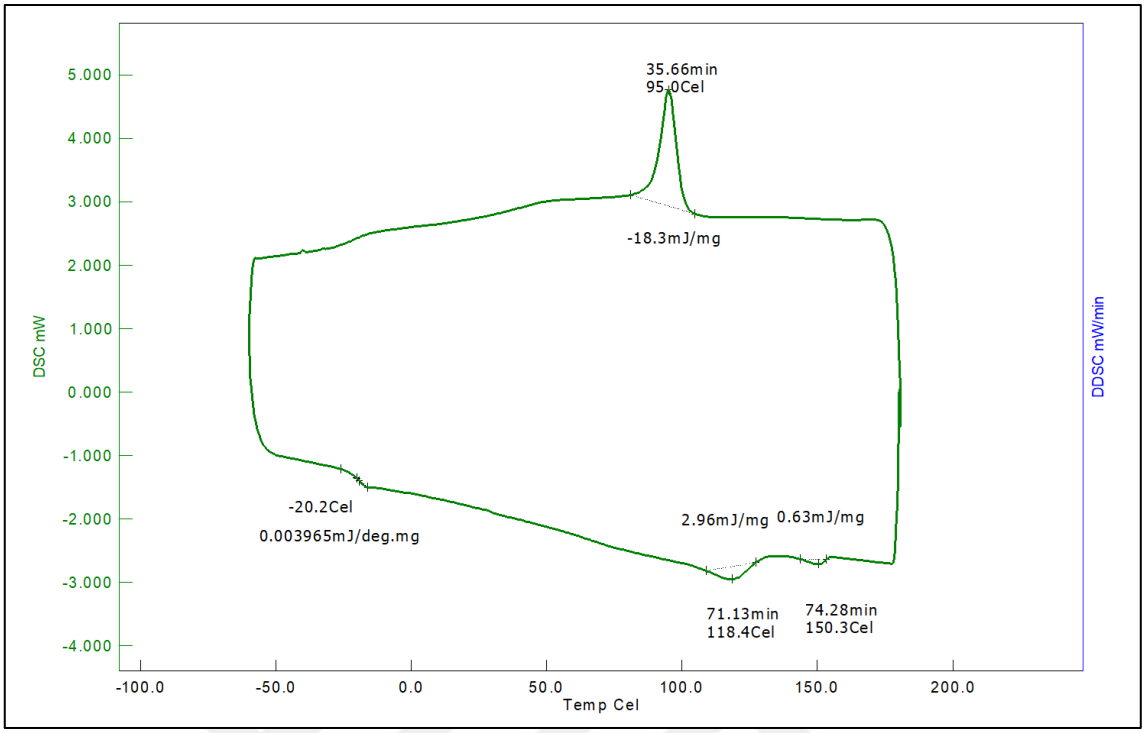


Figure A.33. DSC thermogram of purified Blank_DCP_T_1.

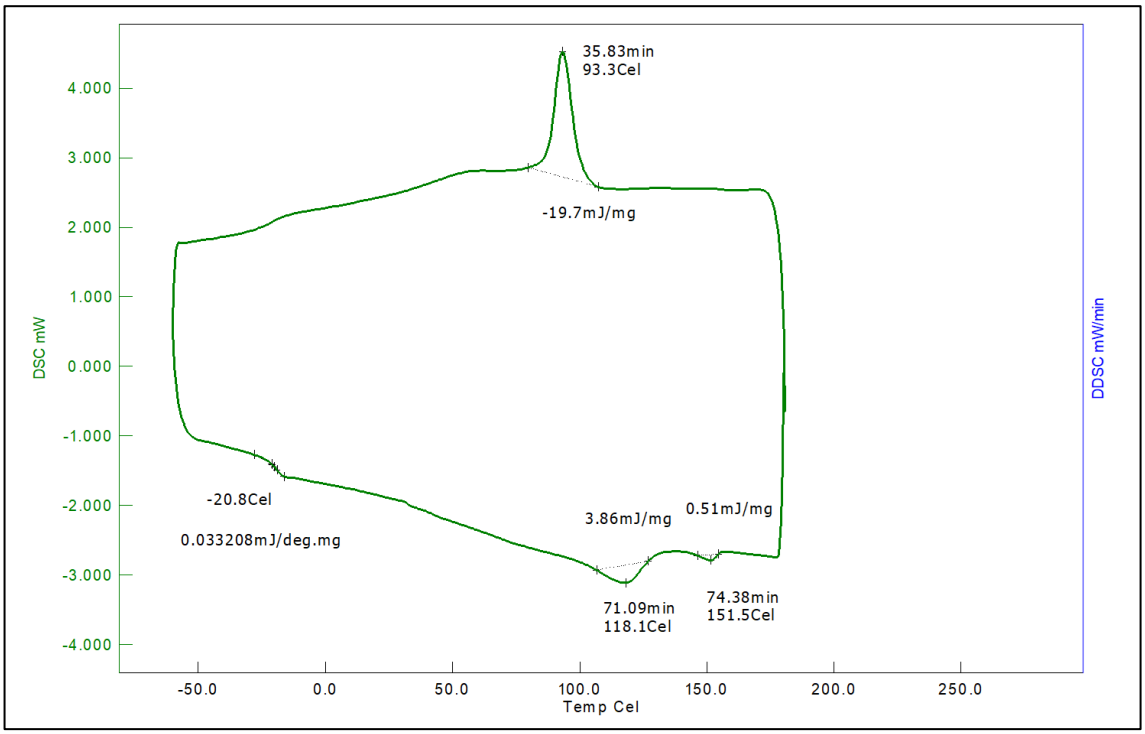


Figure A.34. DSC thermogram of purified Blank_aPP_T_1+5.

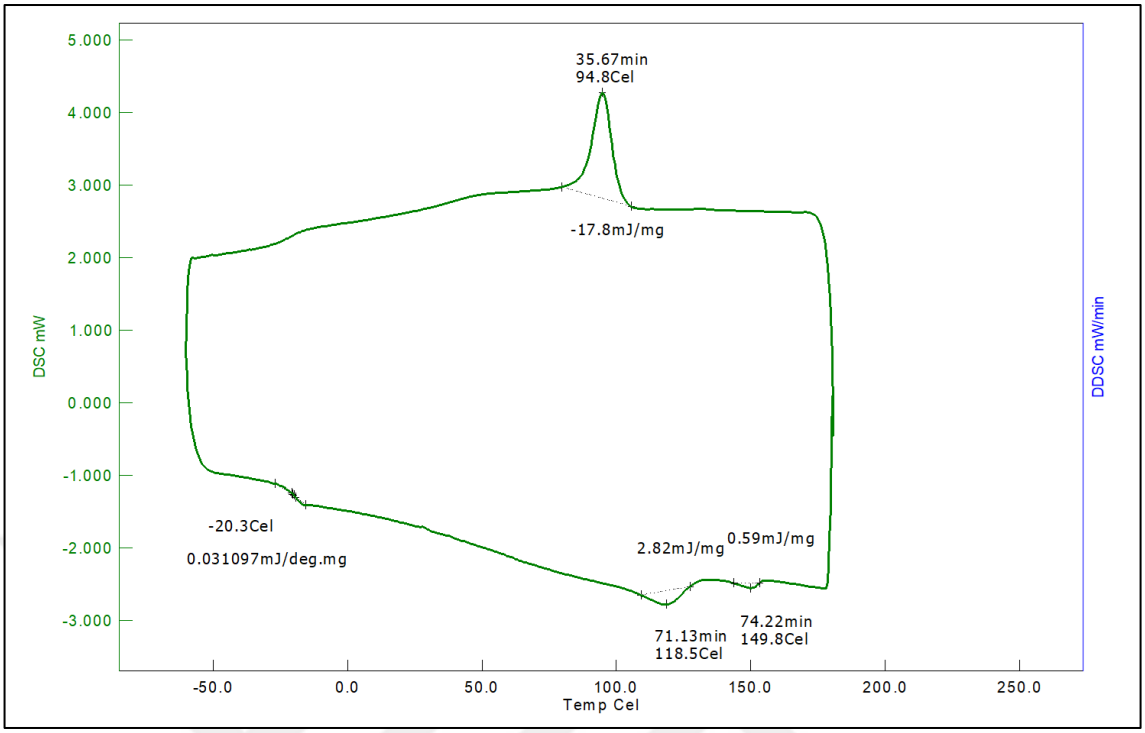


Figure A.35. DSC thermogram of purified Blank_DCP_T_1+5.

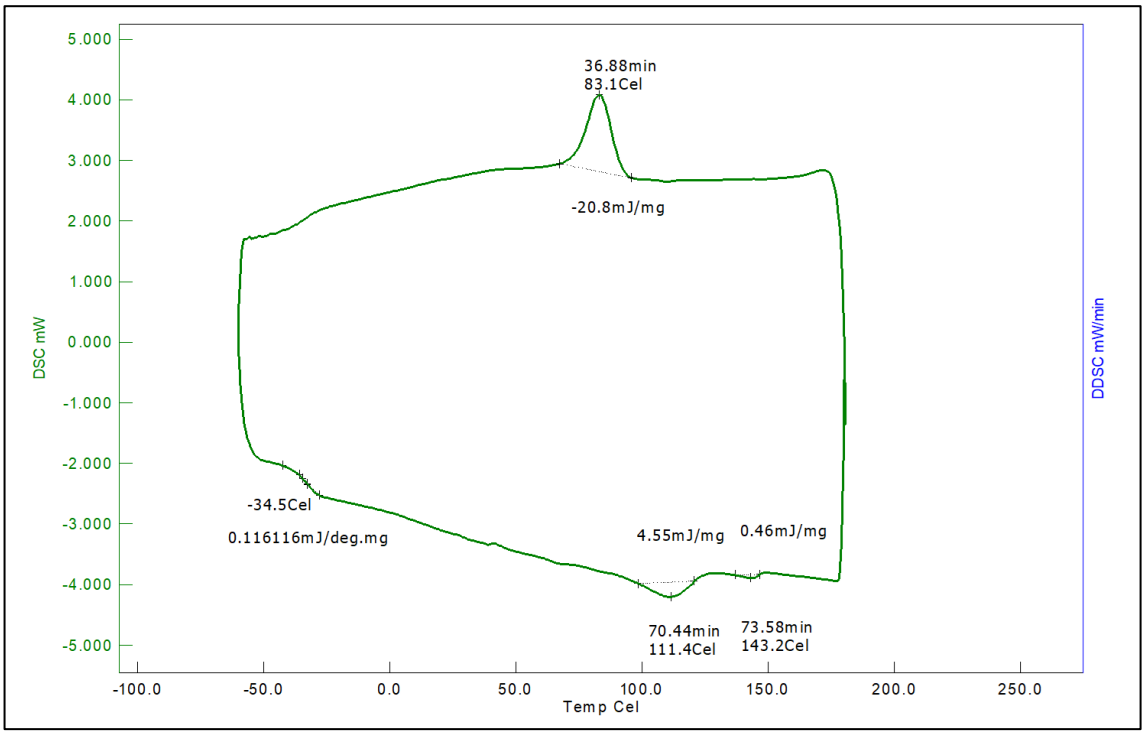


Figure A.36. DSC thermogram of purified Blank_mMAH_T_1.